The Dissertation Committee for JinGyu Ock Certifies that this is the approved version of the following dissertation:

Development of a Laser Foaming Process for High Throughput Three-dimensional Tissue Model Devices

Committee:

Wei Li, Supervisor

Ronald E Barr

Adela Ben-Yakar

Carolyn C. Seepersad

Laura J. Suggs

Development of a Laser Foaming Process for High Throughput Three-dimensional Tissue Model Devices

by

JinGyu Ock

Dissertation

Presented to the Faculty of the Graduate School of

The University of Texas at Austin

in Partial Fulfillment

of the Requirements

for the Degree of

Doctor of Philosophy

The University of Texas at Austin

August 2017

Dedication

To my mother and sister and to my father in heaven

Acknowledgements

I would first like to express my sincere gratitude to my advisor and Ph.D. committee chair Dr. Wei Li for his expert guidance and support. He has been a great mentor both academically and professionally throughout the course of this research. He led me on the way to complete my doctoral program with the right balance of critical advice and encouragement.

I would also like to express my sincere appreciation to Dr. Ronald E Barr, Dr. Adela Ben-Yakar, Dr. Carolyn C Seepersad, and Dr. Laura J Suggs for serving on my doctoral committee. I appreciate their valuable advice and suggestions to improve my Ph.D. works.

I would like to thank my colleagues in the Nano- and Bio- Materials Processing and Manufacturing Lab: Dr. Liang Ma, Dr. Wei Jiang, Hao Xin, Russell Borduin, and Daniel Justiss for constructive discussions and their helpful inputs to this work. I would also like to thank undergraduate students: Byan Philpott and Jenny Zhan for collaboration with them.

Finally, I would like to thank my mother, sister and to my father in heaven for their support and love from Korea. I'm thankful to my friends from Austin for their support. I would also like to thank my best friend, Hangil Kim.

Development of a Laser Foaming Process for High Throughput Three-dimensional Tissue Model Devices

JinGyu Ock, Ph.D.

The University of Texas at Austin, 2017

Supervisor: Wei Li

A three-dimensional (3D) porous structure on biodegradable or biocompatible polymers have attracted tremendous attention in numerous bio-related areas including 3D cell culturing and tissue engineering because of their microenvironment similar to ones *in vivo*. In this study, a novel fabrication process, named selective laser foaming, was developed to create localized 3D porous structure on a polymer chip. The effects of laser power and lasing time on the porous structure were studied both experimentally and through finite element modeling. A high throughput two-chamber tissue model platform was developed using the proposed selective laser foaming process.

For comparison, cell culture studies were conducted with both selective laser foamed and unfoamed polylactic acid (PLA) samples using T98G cells. The results show that by laser foaming gas-impregnated polylactic acid it is possible to generate an array of inverse cone-shaped wells with porous walls. The size of the foamed region can be controlled with laser power and exposure time, while the pore size of the scaffold can be manipulated with the saturation pressure. The finite element modeling results showed good agreement with the experimental data; therefore, the model could be used to optimize and control the selective foaming process. T98G cells grew well in the foamed scaffolds, forming clusters that have not been observed in 2D cell cultures. Cells were more viable in

the 3D scaffolds than in the 2D cell culture cases, suggesting that the 3D porous microarray could be used for parallel studies of drug toxicity, guided stem cell differentiation, and DNA binding profiles.

As an example, a high-throughput two-chamber 3D tissue model platform driven by the centrifugal force was developed for drug screening. The selective laser foaming process was calibrated to fabricate 3D scaffold on a commercially available compact disc (CD) made of polycarbonate (PC). Laser foaming of gas saturated polycarbonate created inverse cone-shaped wells with micro-sized porous structure underneath the surface. The open pores were hundreds of micrometers in diameter and depth. The pore size of the underneath porous structure was several tens of micrometers. The size of the well was dependent on the laser power and laser exposure time. Two laser-foamed scaffolds were fabricated in tandem and two mechanically-machined chambers were placed adjacent to the scaffolds, respectively. All scaffolds and chambers were in line and all of them were connected with micro-channels. The surface was coated with polydopamine (PDA) in order to increase the hydrophilicity and biocompatibility. After sterilization, human glioblastoma multiforme (M059K) and hepatoblastoma (C3A sub28) were seeded in the two 3D scaffolds separately and cultured for up to four weeks. These cells grew well in the scaffolds and cell aggregates were observed, suggesting that the developed two-chamber tissue model array could be useful for high-throughput biochemical assays.

Table of Contents

List of Tables

List of Figures

Chapter 1. Introduction

1.1 Motivation of Research

The traditional two-dimensional (2D) cell culture is a rapid and convenient method for cellular studies in biomedical fields. On the other hand, cells *in vivo* are surrounded by three-dimensional (3D) structures known as the extracellular matrix (ECM). In this environment, cells conduct complex biochemical and physical signaling [1, 2], performing distinct tissue functionality that cannot be observed in 2D [3]. In traditional 2D cell cultures, cells grow on 2D substrates, such as Petri dishes, micro-well plates, and cell culture flasks. Cells inside the 3D ECM will form various types of structures and perform their own biological functions. For example, the surface properties of 3D adult stem cell niches will significantly affect the stem cell differentiation process [4]. Lacking of the complex and dynamic microenvironment of ECM-like structure could mislead cellular behavior by forcing the cells to form an artificial monolayer, which will alter the cellular metabolism and cause the cells to lose certain functionality. This is the main limitation of 2D cell cultures [3].

Porous polymers play an important role in many biomedical applications from drug release to tissue engineering [5-12]. For ECM-like structures, porous polymers have been studied and fabricated using various techniques. The concept of cell culture in 3D porous polymeric scaffolds are combined with the microfluidic channel to develop 3D perfused cell culture devices [13]. The 3D perfusion-based device can mimic not only multi-organ interaction, but also key physiological and pathological processes *in vivo.* It allows realistic 3D tissue model systems for various biomedical related studies, such as drug discovery.

Drug discovery is a lengthy and costly process. In the current drug discovery process, there are two major steps: tests on a number of 2D cell culture assays and animal

tests. At first, thousands of drug candidates are screened based on their efficiency and toxicity. Then only 3-5 lead compounds are chosen for animal tests in the next step [14]. Through these tests, the most effective and least toxic drug candidate is found for further clinical trials. However, the percentage of failures is high due to the lack of efficacy or undesired toxicity of those compounds that have passed the 2D cell culture tests. Moreover, animal models have intrinsic inaccuracy because of the physiological difference from human. They are also of high cost and with moral objections [15]. *In-vitro* 3D tissue model systems can be used to achieve more accurate test results via mimicking the *in vivo* functions of human organs. As an example, liver models have been employed to make quantitative and qualitative assessment of pharmacodynamics and pharmacokinetic properties of drug candidates [16, 17]. In order to reproduce dynamic process of absorption, distribution, metabolism and excretion (ADME), multi-organ tissue model system has been developed via combining tissue model systems and microfluidic devices [18, 19].

Recently Ma *et al.* developed a 3D two-chamber tissue model system for drug studies. The two chambers had liver and brain tumor cells, respectively. The culture medium was circulated from the chamber having liver cells to the one having tumor cells. Each cell line was cultured in a porous biodegradable polymer scaffold to provide a 3D environment for cell to reproduce *in vivo* tissue-like structures. It was demonstrated that the system can be used to study liver metabolism effects on cancer treatment drugs.

High throughput platforms draw significant interests from both academia and industry for drug testing. The 3D two chamber system developed by Ma *et al.* has certain limitations for the high throughput applications. The system has multiple components that need to be assembled. Each chamber is filled with a scaffold with a diameter of 13 mm and a thickness of 2.5 mm. The size of the system needs to be significantly reduced and multiple systems need to be fabricated on one platform to enable high throughput drug study.

Therefore, a radically different fabrication process and system design is needed to develop a high throughput tissue model platform for drug study.

1.2 RESEARCH OBJECTIVES

The goal of this research is to develop a novel 3D high throughput tissue model system through the development of an enabling fabrication process for localized and small-scale polymer tissue engineering scaffolds. The following objectives have been identified:

- To develop a scaffold fabrication method, named selective laser foaming, to control the scaffold size, shape, and porous structure,
- To understand the effect of process parameters of the laser foaming process through finite element modeling,
- To demonstrate the biocompatibility of the fabricated 3D porous structures for cell culture studies, and
- To design and fabricate a 3D high throughput tissue model device for drug screening using the selective laser foaming and micro-machining.

1.3 ORGANIZATION OF THIS DISSERTATION

This dissertation is organized into six chapters. Chapter 1 is a brief introduction followed by motivation and objectives of this research. Chapter 2 provides a literature review of the current state-of-the-art. Chapter 3 presents fabrication of 3D scaffolds using the selective laser foaming process and feasibility of using the foamed structure for cell cultures. Chapter 4 discusses a finite element model to investigate the effects of laser parameters on porous structures. Chapter 5 presents fabrication of a high throughput 3D two-chamber tissue model platform and its feasibility for drug study. Finally, Chapter 6 provides a summary of current research and recommendations for future work.

Chapter 2. Literature Review

2.1 The Need for 3D Cell Cultures

Scientists in biology and medicine often use 2D cell culture, which means culturing cells on flat bottom of micro-well plates, Petri dishes, or cell culture flask, for drug testing. 2D cell cultures have their own advantages, such as convenience, low cost, affluent nutrient and oxygen exchange, and high cell viability. However, the 2D cell culture has its intrinsic limitations. Cells *in vivo* are surrounded by an extracellular matrix (ECM). The ECM allows complex physical and biochemical signals by providing cell-cell or cell-matrix interactions. These signals are important to analyze essential cellular functions, such as cell adhesion and motility [20, 21]. In addition, different types of cells are situated in evidently different 3D environments and organize into diverse architectures [20]. For example, liver cells closely aggregate together and form hexagonal-shaped lobules, whereas white blood cells are suspended in the blood flow. Moreover, 2D cell culture forces different types of cells to form monolayer on a rigid and flat surface, so it has an influence on not only the cellular metabolism, but also other functionalities [3, 21], such as cell motility and cell differentiation. Three-dimensional (3D) cell cultures are suggested to overcome these shortcomings of 2D cell cultures. Highly porous 3D scaffolds can enhance cell growth, organization, and differentiation.

2.2 Fabrication of Three-Dimensional Tissue Engineering Scaffolds

Porous material is a solid matrix that has interconnected pores filled with liquid or gas. In medical fields, porous polymer materials have attracted continuous attention. These materials composed of repeating subunits can be classified into natural polymers or synthetic polymers. The polymers from nature are honey comb, extra cellular matrix, bone, and so on. In addition, DNA and protein, examples of natural polymers, are considered as

the most important biology function carriers and executors in human body [22]. The ones synthesized in the laboratory consist of plastic, synthetic fibers, and synthetic rubbers. Porous polymers play an important role in biomedical applications because of their unique structures and biocompatibility, for example controlled drug release [5, 6], bio-chemical sensor [7], and tissue engineering scaffolds [8-12].

Among natural and synthetic porous polymers, the natural ones have been preferred in biomedical applications. However, researchers have investigated the use of synthetic polymers in terms of mass production for clinical applications. Existing fabrication methods for extracellular matrix (ECM)-like polymer structures include fiber bonding, phase separation, solvent casting, and gas foaming associated with particulate leaching. Fiber bonding is a technique easily creating mesh-like porous structures [23]. For example, polyglycolic acid (PGA) fiber is first immersed in poly-L-lactic acid (PLLA) and solvent solution. After solvent evaporation, the PGA fibers organize into a network in PLLA. The PLLA is then removed by heating and dissolving. Phase separation methods can be classified into two different groups: emulsification/freeze-drying and liquid-liquid phase separation. For the former [24], poly (lactic-co-glycolic acid) (PLGA) is dissolved in methylene chloride, and an emulsion is formed by adding distilled water. The solution is cast into a mold and frozen via liquid nitrogen. The water and organic solvent were removed using freeze-drying at -55 °C. For the later [25], PLLA and PLGA scaffolds have been fabricated using polymer-rich and polymer-poor phases in the polymer solution. The solvent should have a low melting temperature and be easy to evaporate. The polymer is dissolved and cooled below the melting temperature of the solvent, and then the solution is vacuum dried to evaporate the solvent. By doing so, the polymer-poor phase is removed to lead to a porous polymer network. Solvent casting is a technique using a porogen, such as NaCl, and a solvent, such as chloroform, to dissolve polymers [26]. PLLA and PLGA

are dissolved in chloroform, and then the porogen is added. The mixture is cast and the solvent is removed. After that, the porogen is leached from the polymer/ porogen composite by water. Harris *et al.* saturate a composite of PLGA and NaCl with CO_2 [27]. Then, the samples are foamed by the sudden pressure drop and particulate leaching in distilled water. Most of the methods mentioned above utilize a toxic organic solvent and have limitations in biomedical applications.

Solid freeform fabrication (SFF) methods, so called rapid prototyping (RP), have been studied for porous polymer fabrication [28-33]. These techniques uses model data designed in Computer Aided Design (CAD) solid modelling programs to created 3D objects. Generated 3D CAD data are processed by slicing the physical model into layer of equal thickness. Sliced data are utilized by each RP system to fabricate 3D objects layer-by-layer. In this process, Solid powder or liquid layers are accumulated vertically and fused with each other to form the final physical object [34, 35]. SFF methods include selective laser sintering (SLS) [28], matrix-assisted pulsed laser evaporation direct writing (MAPLE DW) [29], biological laser printing (Bio-LP) [30], stereolithography (SLA) using laser and digital micro-mirror-array device (DMD) [31, 33], and two-photon polymerization (2PP) [32]. The SFF methods have their own advantages, such as a high reproducibility, but they have limitations in material selection and removing supporting materials.

Solid-state foaming is a technique to fabricate microcellular thermoplastic polymer foams. Solid state foaming consists of two major steps [36]. The first step is the saturation of blowing agent. The blowing agents commonly used are carbon dioxide and nitrogen. The polymer sample is exposed to pressurized gas. The gas saturation of the polymer is allowed for a fixed duration so that the gas reaches an equilibrium concentration. The second step is nucleation and growth of bubbles in the gas saturated polymer by introducing a thermodynamic instability. Either a sudden increase in temperature or a sudden decrease

in pressure is commonly used to introduce the thermodynamic instability. The glass transition temperature (Tg) of the system is reduced by the dissolved gas and this results in the phenomenon of plasticization. The thermodynamic instability reduces the solubility of gas in the polymer and leads to nucleation of bubbles. The easiest procedure to nucleate bubbles is to increase the temperature of the sample to the reduced Tg. This step can be achieved in many ways: immersing in a hot bath maintained at the required temperature or placing the sample between two plates heated to the desired temperature. The major advantage of this technique is that it provides a way of controlling the pore sizes (300 nm – 300 μm) and porosity (10 – 95 %) of the polymer foams [37, 38]. Wang *et al.* [38-41] developed a new method to fabricate porous scaffolds by combining ultrasound and solid state foaming. Highly interconnected porous structure can be created by controlling the ultrasound power and exposure time. The foam size is determined by the focal zone, which is a few millimeters wide.

2.3 Laser-Based Fabrication Processes for Three-Dimensional Tissue Engineering Scaffolds

Based on the working principles, the existing fabrication techniques can mainly be categorized into three groups: (1) powder fusion based techniques, such as selective laser sintering (SLS); (2) particle or cell deposition based techniques, such as laser-guided direct writing (LG DW), laser-induced forward transfer (LIFT) and matrix-assisted pulsed laser evaporation direct writing (MAPLE DW); (3) photo-polymerization based techniques, such as stereolithography and two-photon polymerization (TPP) [42].

Selective laser sintering (SLS) [28, 35, 43-45] was developed in the mid-1980s [46]. This technique uses a laser beam (usually CO_2 laser) to sinter slices of powdered materials via repeated process of spreading layers and selectively heating and fusing each powdered layer in order to fabricate three-dimensional structures. Thus, the objects are

formed layer-by-layer from sliced CAD data. During the process, the unmelted powders act as the support for the fused object. Figure 2-1 represents the selective laser sintering process.

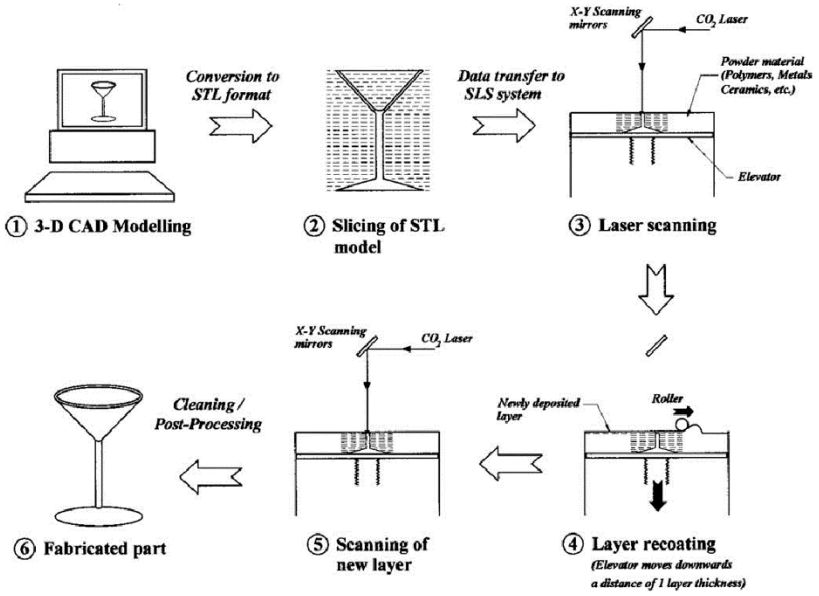

Figure 2-1 Schematic layout of the SLS process [35]

Laser-guided direct writing (LG DW) [47-51] was first performed for micropatterning of embryonic-chick spinal-cord cells [52]. The driving force of the LG DW method arises from the scattering of laser light by the micro-particles or cells. In contrast to the high-numerical-aperture lens used in the optical trapping systems, the LG DW system uses a low-numerical-aperture lens so as to provide an axial propelling force to the particle instead of trapping it in the vicinity of the focal point. Once a particle or cell interacts with the laser, it is drawn to center of the beam where the intensity is maximal and simultaneously pushed along the axial direction of laser beam by the radiation pressure. The guided object is deposited on the target surface, which is placed vertically at a certain point along the optical axis. By moving the target surface relative to the laser beam, three

dimensional patterns of particles can be drawn on the target surface. The basic concept of cell deposition of LG DW method is illustrated in Figure 2-2.

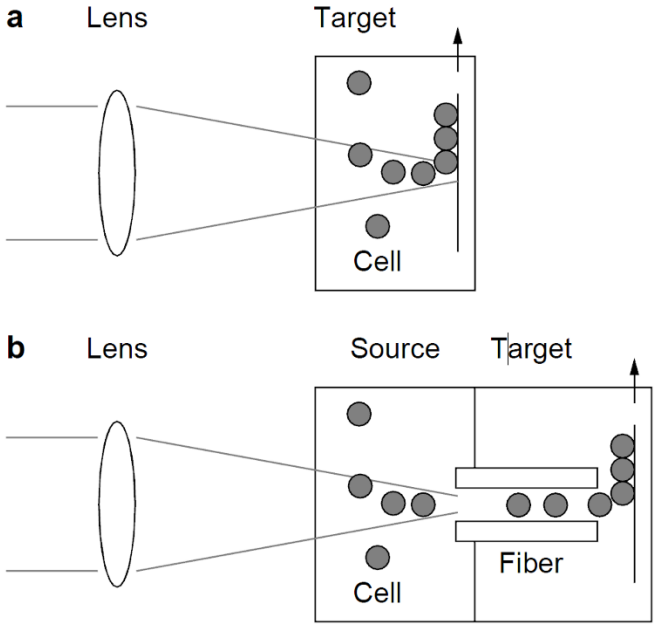

Figure 2-2 Laser-guided direct writing system. (a) Laser light is focused weakly into a suspension of particles. The particles are propelled by the light through the fluid and deposited on a target surface. Moving the target relative to the laser beam results in a line of particles being drawn. (b) Light is coupled into a hollow optical fiber and particles are carried through the fiber to the target surface. The process can be observed in real time by optical microscopy [52].

Laser-induced forward transfer (LIFT) [53-55] mainly employs a high-powered pulse laser and two coplanar glass slides. The experimental setup is described in Figure 2-3. The upper, so called “donor-slide”, is coated with an energy absorption metal layer and a layer of material containing cells. Laser pulses are focused on the metal layer via glass slide, evaporating the laser absorbing layer locally. During the process, the laser pulse generates a high gas pressure that transfers the underneath cell compound toward the lower slide, referred to as “collector-slide”. The biological materials containing cells are

usually a culture medium or hydrogel which provide humid environment preventing from cell dehydration. The hydrogel has an additional function to sustain cell structure.

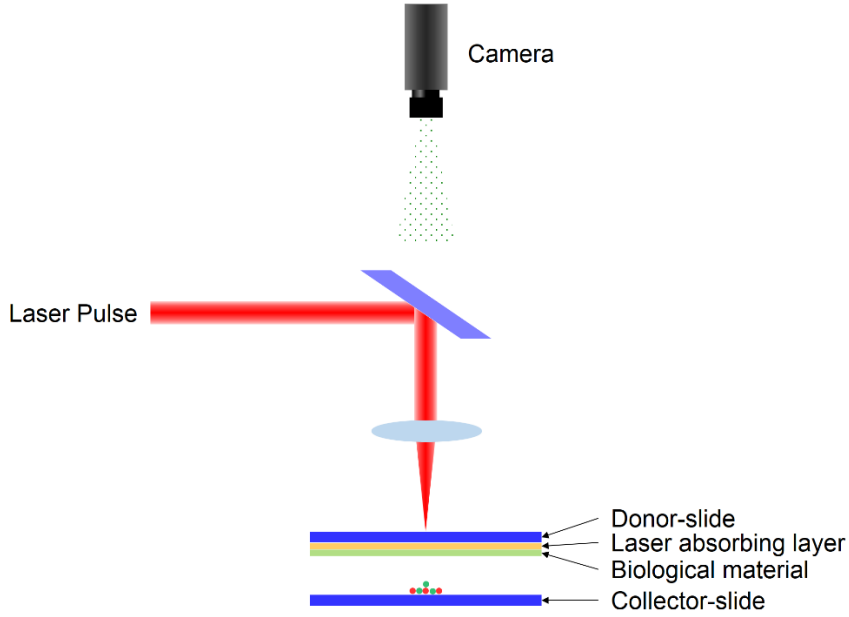

Figure 2-3 Schematic of LIFT

The setup of matrix-assisted pulsed laser evaporation direct writing (MAPLE DW) [29, 56, 57] is similar to the LIFT system shown in Figure 2-3. Instead of using the glass slide for the "donor-slide", MAPLE DW employs an optically transparent quartz support called a "ribbon". The ribbon is coated with biological materials, such as Matrigel® or bio-ceramic. The biomaterials with cells are referred as the "Matrix". The substrate, similar to the "collector-slide', might be covered with hydrogel or not. The laser is focused on the interface of the quartz support and a laser-absorptive layer containing cells. The laser beam causes evaporation of part of the biomaterial layer which generates gas bubbles locally. The gas bubbles result in the release and propulsion of the cell-seeded matrix to the receiving substrate.

Biological laser printing (BioLP) [30, 58-61] was developed by Barron *et al.* It is similar to the previous two processes, LIFT and MAPLE DW, illustrated in Figure 2-3. BioLP utilizes an optically transparent quartz instead of glass slide used in LIFT. Metal or metal oxide is coated on the quartz support as laser absorption layer. The biomaterial layer with cells, such as powder, liquid, or gel, is coated on the laser absorbing layer. The incident laser energy is focused and absorbed at the interface of quartz support and laser absorption layer. The heat generated by laser-laser absorption layer causes vaporization of the water in biomaterials. The biomaterial is then transferred from ribbon surface to the receiving substrate surface. Thus, this technique reduces a potential damage to biological materials.

Stereolithography (STL) process was developed in 1986 and was described in a patent 'Apparatus for Production of Three-Dimensional Objects by Stereolithography' [62]. Stereolithography techniques could be classified into two sub-types based on the optical source, i.e. laser and UV irradiation. Both systems employ bath that has liquid photocurable resin and movable platform.

Two photon polymerization (TPP) [32, 63-66] has been widely used as a laser direct writing technique due to its high fidelity and resolution. TPP systems usually utilizes a femtosecond laser to induce two-photon absorption (TPA). TPA is a process by which one molecule is excited to a higher energy electronic state by the simultaneous absorption of two photons[63]. TPA was described theoretically in 1931 [67] and first demonstrated experimentally in 1961 [68] in a CaF2:Eu2+ crystal and in 1962 in caesium vapor [69]. Figure 2-4 shows the schematic of a typical TPP fabrication system [63]. The laser used in the system is a Ti:Sapphire femtosecond laser (100-femtosecond pulses at a repetition rate of 80 MHz and wavelength of 800 nm). The laser beam is expanded and guided by a group of mirrors into an inverted microscope. It is then focused by an oil-immersion objective

lens onto the sample that is mounted on a motorized stage with high resolution (< 20nm), which moves three-dimensionally to draw a defined 3D nanostructure in the sample. The 3D structure is first designed in AutoCAD and then imported to the software of the motorized stage, which controls the motion of the stage in xyz directions. A CCD camera is used to monitor the fabrication process in real time. The laser power can be continuously adjusted with an attenuator. With this femtosecond laser fabrication system, Zhang *et al.* were able to fabricate defined and complex 3D structures at a resolution of 100 nm [63].

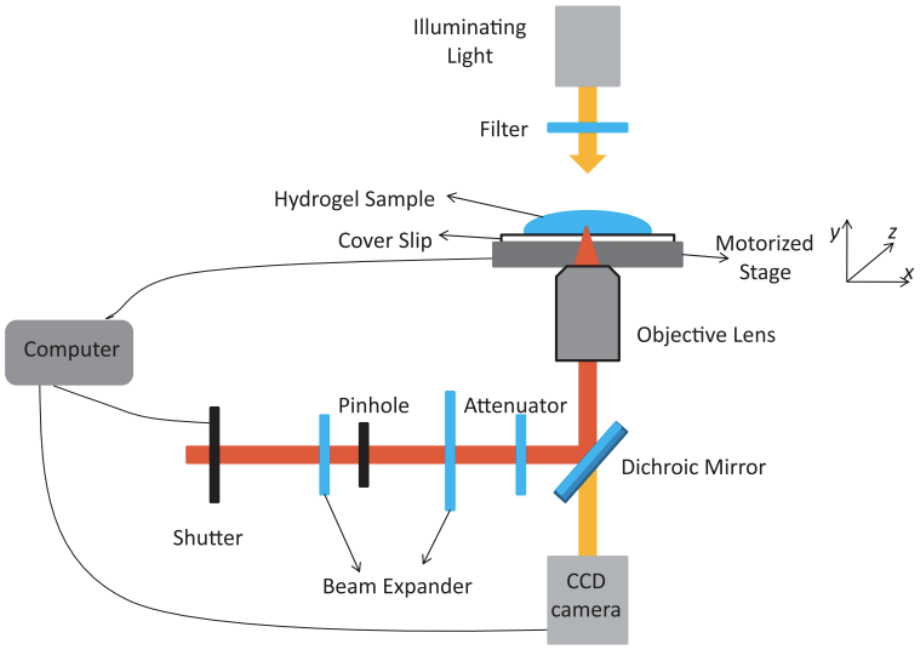

Figure 2-4 Schematic setup of a TPP fabrication system [63]

Stereolithography using UV irradiation [33, 70-74] can utilize a digital micro-mirror-array device (DMD). The DMD is an array of up to several millions of micro-sized mirror that can be controlled independently to on and off state [75]. In this approach, the structure is not created via point-by-point scanning, but in a layer-wise fashion by curing the entire layer simultaneously. After one layer is fabricated, the platform is lowered or

raised to accumulate a new layer. The thickness of each layer is controlled by the distance between the surface of the platform and the liquid resin surface. Based on the above basic concept, Zhang *et al.* developed a dynamic optical projection stereolithography (DOPsL) system for the rapid fabrication of complex 3D extracellular scaffolds [76]. The setup of the DOPsL system is shown in Figure 2-5. Since this DMD-based stereolithography technology simultaneously utilizes a million micro-mirrors rather than one single focused point, the DOPsL system offers superior processing speed compared to other nanofabrication techniques, thus making it more suitable for manufacturing large structures with complex details in a submicron resolution [76]. With these many advantages, including rapid fabrication speed, maskless, flexibility and relatively high resolution, the DOPsL system is an appealing platform for the manufacturing of complex 3D designer scaffolds for *in vitro* tissue engineering as well as functional cellular constructs for *in vivo* implantation [76].

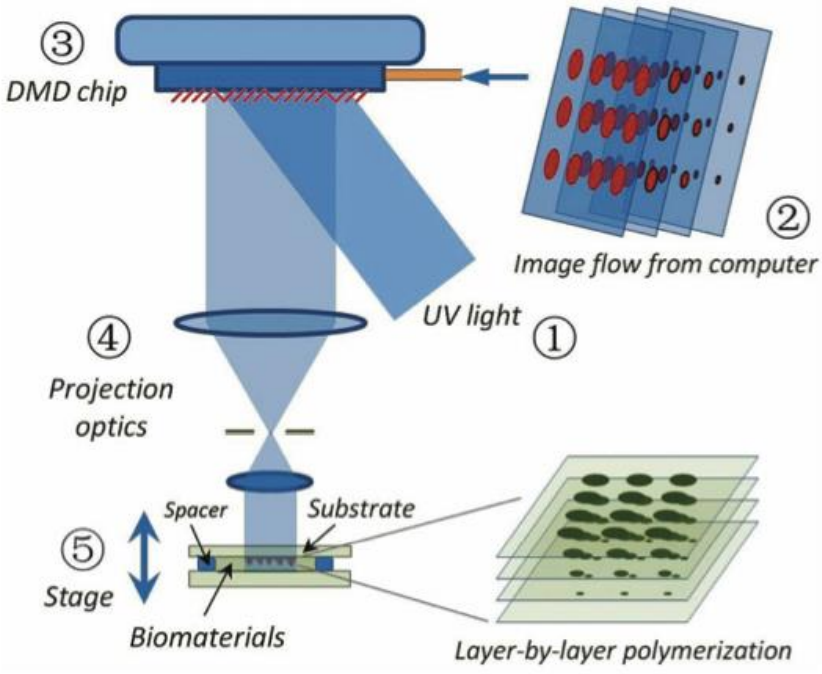

Figure 2-5 Schematic setup of the DOPsL system [76]

There are two configurations of additive manufacturing: top-down and bottom-up configuration shown as Figure 2-6. Most forms of laser-assisted additive manufacturing, such as SLS, LG DW, LIFT, MAPLE DW, BioLP, and SLA, are classified as bottom-up approaches. The accumulation starts from the bottom of platform and prepolymer materials are supplied for each layer. This approach has the advantage of fabricating multiple layers with different materials in each layer [31, 48, 52, 53, 55, 77-79]. SLA employs both the top-down and the bottom-up approaches. The top-down configuration consists of a container and a movable platform that is located in the container. The platform is immersed just below the surface of pre-polymer solution. The laser beam is focused onto the surface (x-y plane) of liquid resin to polymerize the resin. Once a layer is photo-polymerized, the platform is lowered by a specific distance to fabricate a new layer. In the bottom-up approach, the container is a movable platform on which a polymerized resin layer is created. The liquid prepolymer is supplied into container for one layer from the bottom to the top.

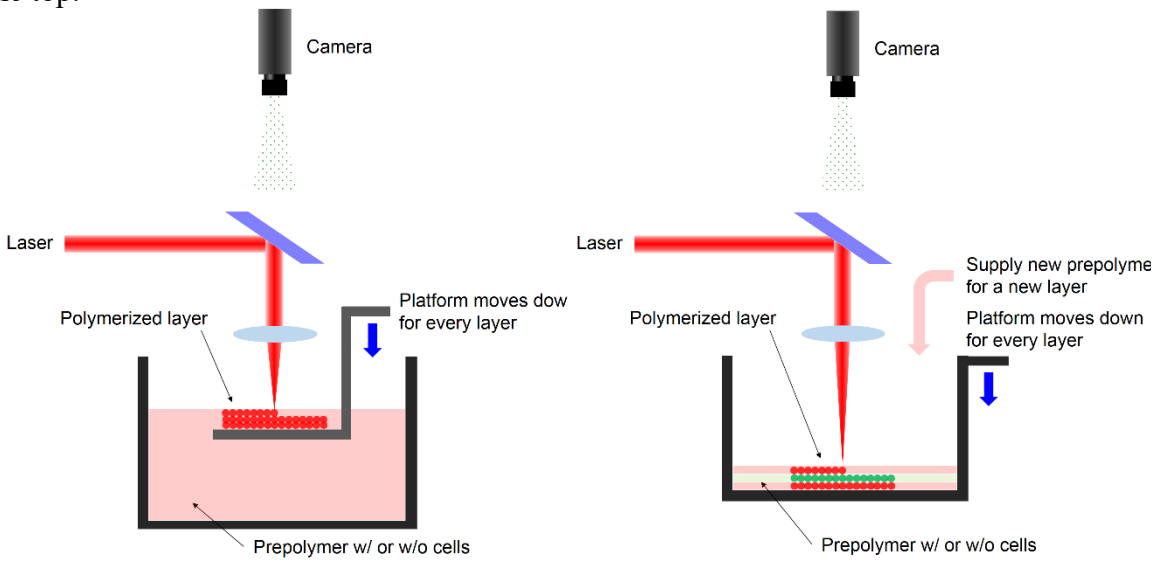

Figure 2-6 A schematic representation of SLA. (a) top-down approach, (b) bottom-up approach.

2.4 Drug Testing using Single Chamber 3D Cell Cultures

Drug discovery is a money- and time-consuming process. It is comprised of several stages. Initially the screening of thousands of compounds by their efficacy and toxicity is done using 2D cell cultures [22]. After that the test of animal models is conducted before clinical trials [80]. As discussed in Chapter 1, 3D cell cultures are motivated by the need to better mimic physiological tissue. Moreover, cellular or tissue model systems have a potential in drug study for efficacy and toxicity [81]. Recent studies have found that 3D tissue models can be effective in drug-screening applications for the benefit of cost and time. For example, Wu *et al.* developed a microfluidic self-assembly device for anticancer drug assays [82]. Polydimethylsiloxane (PDMS) was replicate molded using soft lithography. MCF-7 breast cancer cells were captured and formed tumor spheroid in a U-shaped trap. Three dimensional micro-patterned arrays were fabricated using deep UV irradiation [83]. Micro-well arrays were fabricated and coated with an ECM protein, such as fibronectin. HeLa cells were seeded and cultured in the micro-wells. The cellular micro-array was evaluated using comet assay to prove the suitability of the system for high-throughput drug screening applications. Tung *et al.* developed the hanging drop array fabricated by injection molding for drug studies [84]. Three different types of cells were suspended and formed spheroids. Two type of drugs, tirapazamine (TPZ) and 5-fluorouracil (5-FU) were tested for anticancer efficacy and the results were evaluated using Alamar Blue assay and Live/Dead cell staining.

2.5 Liver Models

In the human body, a drug goes through a complicated dynamic process of absorption, distribution, metabolism and excretion (ADME) [80]. Liver plays a key role in metabolism in human body. A set of Phase I and Phase II enzymes in the liver metabolize and bio-transform all the drugs. This leads to activation of prodrugs or detoxicating the

effective part of some drugs via a series of biochemical interaction in the liver cells. A variety of *in vitro* liver models have been developed to reproduce the function of a natural liver: isolated perfused liver [85, 86], liver tissue slices [87-90], freshly isolated hepatocytes in suspension [91, 92], primary hepatocyte culture [93-95], liver microsomes [96, 97]. However, these models have not been able to faithfully mimic the liver functions. Isolated perfused liver system employs the liver taken directrly*in vivo*, thus has most of the liver functions. However, these functions can be maintained for only a limited time, a few hours, and the usage of the model is too complex. It is hard to use the isolated perfused liver as a high throughput platform for drug screening; therefore, perfused liver tissue slices were developed to substitute the organ. However, the system can sustain liver functions no longer than 10 hours. High throughput screening can be accomplished via freshly isolated hepatocytes in a suspension system, and the system also sustains most of the metabolizing enzymes. However, it is hard for the cells to form a 3D structure and to survive a long time. They can only preserve their functions for about 2-4 hours. Primary hepatocytes culture systems can preserve the primary liver functions for a desired time, but hepatocytes in the systems would lose the functions in a long time culture. Liver microsomes can be easily used. However, it can only maintain Phase I enzymes, not Phase II enzymes.

Bio-chips, so called tissue chips, containing engineered tissues have been developed as a surrogate for drug testing. Human or animal cells are built on a polymer support in order to retain the functions related to the intact organ. Griffith *et al.* developed a physiological liver model. In the bioreactor, liver cells in 3D scaffolds formed tissue-like structures via perfusion with culture medium. Primary rat hepatocytes in the bioreactor expressed viability for up to two weeks [16]. A perfused multiwall plate was developed to engineer 3D liver tissue in micro-sized wells [17]. Constant perfusion in the bioreactor maintained 3D tissue culture, and a high throughput rate in the multi-well format was

achieved via integrating multiple bioreactors into one biochip. Spheroids of rat liver cells were formed and the result of immunostaining demonstrated the tissue was functionally viable after seven days of culture.

2.6 Drug Testing using Multi-chamber Tissue Model Systems

The liver metabolism should be applied to a 3D model for testing liver toxicity and its influence on drug efficiency. In this manner, one-chamber systems including high-throughput microarrays have certain limitations. Perfusion-based multi-chamber systems containing liver and disease models can better mimic the *in vivo* environment by reproducing major functions of liver. Viravaidya *et al.* developed a microscale cell culture analog (μCCA) which is a physiologically-based pharmacokinetic (PBPK) model for prediction of concentration profiles of a drug and its metabolites [18]. The analog was comprised of three chambers containing cell lines representing lung cells (L2 cells), fat cells (3T3-L1 adipocytes) and liver cells (HepG2/C3A cells). The toxicity of the liver-derived metabolite of naphthalene on lung tissue was demonstrated. A hydrogel-cell solution was inserted into the μCCA device modified to accommodate a 3-D gel-cell structure, and Tegafur–uracil combination had been utilized to observe the metabolism-dependent toxicity [19]. In this model, three different types of cells were used including liver (HepG2/C3A), colon cancer (HCT-116), and bone marrow (Kasumi-1). Cells were captured and cultured in hydrogels such as alginate and Matrigel^{TM}. Tegafur is a prodrug which needs to be activated in the liver in order to become an active (toxic) metabolite 5-fluorouracil (5-FU). Tegafur demonstrated a cytotoxic effect in a μCCA due to the liver metabolism in comparison to a negligible effect in a 96-well plate assay without liver cells. Uracil acts as an inhibitor of the liver enzyme dihydropyrimidine dehydrogenase (DPD), which results in the catabolism of 5-FU. Uracil is often used with Tegafur as a modulator,

because inhibition of 5-FU metabolism is responsible for increased efficacy of the drug [98]. In a μCCA, addition of uracil also improved the cytotoxic effect of Tegafur on tumor cells.

Gel-based 3D cell cultures suffer from diffusion limitations, which could hinder nutrient and metabolite exchanges. Ma *et al.* [13] developed a 3D perfusion-based two chamber tissue model system based on porous polymeric scaffolds. Brain tumor cells and HepG2 liver cells were seeded in 3D PLA scaffolds and then the cell-containing scaffolds were inserted in a perfusion-based 3D tissue model device. The major advantage of this system is that liver metabolism similar to *in vivo* environment can be simulated in the system for drug study. However, the system has multiple components that need to be assembled. In addition, the size of the system needs to be dramatically reduced to integrate multiple systems on the same platform for high throughput applications.

2.7 SURFACE TREATMENT WITH POLYDOPAMINE

Polydopamine (PDA) coating has been studied in recent years after Lee *et al.* discovered the facile surface coating [99]. It has drawn much attention due to its universal adhesive nature [99-106]. The PDA coating can functionalize a wide range of material surface including super-hydrophobic surfaces [107]. PDA is synthesized by pH-induced, oxidative polymerization of dopamine-Hydrochloride in alkaline solution (pH > 7.5, typically 10 mM TRIS buffer) [107]. Substrates can be coated with a thin PDA film by immersing the samples in a dilute aqueous solution of dopamine [99].

Polydopamine (PDA) shows excellent biocompatibility due to naturally occurring melanin. The adhesion of bone marrow cells was studied by Lee *et al.* [99]. The PDA coating enhanced the adhesion of fibroblast cells, while the adhesion of megakaryocytic was limited on PDA coatings. This could conclude that the cytocompatibility of the PDA

coating depends on cell types. The *in vitro* biocompatibility of PDA was accessed by Park's group [100] using human umbilical vein endothelial cells. It was observed that characteristics of cytocompatibility were highly enhanced including cell adhesion and viability. It has been reported that the PDA coating could convert various bioinert substrates into bioactive ones such as non-wetting surfaces [103]. The increased adhesion of rabbit chondrocytes was exhibited on the PDA coated biodegradable polymers including polycaprolactone, polyurethane, poly(L-lactide), and poly(lactic-co-glycolic acid) [102]. Tsai *el al.* suggested that the enhanced adhesion might result from increased immobilization and/or adsorption of adhesive proteins including fibronectin.

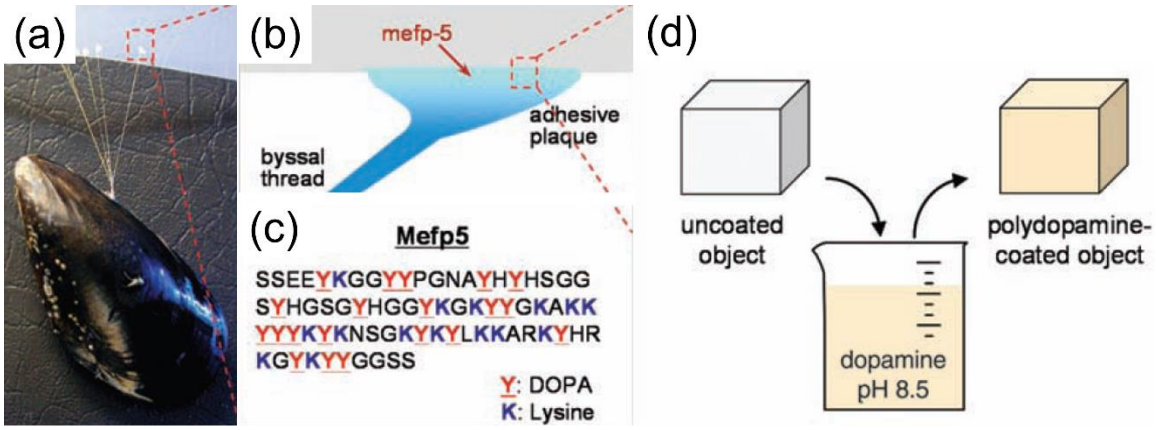

Figure 2-7 (a) Photograph of a mussel attached to commercial PTFE. (b) Schematic illustrations of the interfacial location of Mefp-5. (c) The amino acid sequence of Mefp-5 ([108]). (d) A schematic illustration of thin film deposition of polydopamine by dip-coating an object in an alkaline dopamine solution [99].

2.8 Centrifugal Force Driven Microfluidics for Bio-Application

The high throughput 3D tissue model device in chapter 5 is rotated to enhance the diffusion in each system on the device. The idea of using centrifugal force to drive diffusion has been proven by many researchers [109-111]. The nutrient and drug diffusion can be

accelerated by the centrifugal force driven by rotation [112-114]. For better understanding, the basic physical background for the centrifugal force is reviewed as follow [115]. The centrifugal force can be expressed as below:

$$f_c = m\omega^2 r \tag{2.1}$$

where m, ω, and r are the mass of the sample in channel, the angular rotational frequency, and the position of the disc, respectively. The pressure at the far end of a radial column of incompressible fluid extending from radius r_1 to r_2 can be described using following equation:

$$p_c = \int_{r_1}^{r_2} \rho\omega^2 r \, dr = \frac{1}{2}\rho\omega^2 \left(r_2^{\,2} - r_1^{\,2} \right) \tag{2.2}$$

where ρ is the density. In the centrifugal microfluidics, additional forces should be considered: the Coriolis force (f_{co}) and Euler force (f_e). Those forces are given by:

$$f_{co} = -2m\omega \times \mathbf{v} \tag{2.3}$$

$$f_e = -m\frac{d\omega}{dt} \times r \tag{2.4}$$

Effects of the centrifugal force on the cell were evaluated by Hino *et al.* [116]. The test was conducted using a centrifugation of mouse myoblast cells in a tube. The shapes and orientation of the cells were observed using a maker and a phase contrast microscope. Cells could be damaged under strong force, but the myoblast cells showed extended pseudo, proliferation in confluent manner, and differentiation to the myotube.

Thomas *et al.* developed 2D cell based assays on a compact disk (CD) [117]. The assay was fabricated using electroplating etched silicon masters, micro-molding, and micro-machining. A number of cell lines were cultured in the system including HeLa, L929, MRC-5, and CHO-M1. Cell viability was evaluated using Live/Dead cell staining. Flow in micro channels was induced by centrifuge force of spinning at a speed up to 6000

rpm. Enzyme-linked immunosorbent assay (ELISA) was built on a disc-type device in order to evaluate mental stress using biomarkers [118]. Immunoassays are tools in proteomics used to measure drug targets (identification of biomarkers) in a high through-put manner, and to support clinical diagnostics [112]. Nagai *et al.* fabricated ELISA system using PDMS. In that system, micro channels connected a loading chamber to a purification chamber and a detection chamber. The loading chamber and injection reservoir contained the solution having targeted antigen to be mixed with enzyme-labeled antibodies. The solution then reached the purification chamber having a single glass bead functionalized with the antigen after the 1st rotation. The purified solution flowed into the detection chamber with a substrate of the enzyme by the 2nd rotation. Fluorescence imaging scanner was utilized to analyze the result of reaction.

An automated immunoassay system on a centrifugal platform was developed using the sequential control of the multiple pinch-valves [119]. The system was composed of a servo-motor, a flyball-governor, an actuation disc, and a microfluidic disc. The pinch-valves were actuated by mechanical compression of the covering membrane. Mouse immunoglobulin G (IgG) was utilized as a model analyte to evaluate the feasibility of the device. It was observed that the device achieved targeted antigen detection without any cross-contamination.

Chapter 3. The Selective Laser Foaming Process for Small Scale Tissue Engineering Scaffolds

3.1 INTRODUCTION

The last decade has seen rapid development of the microarray technology and its successful application in genomic and enzymatic analyses [120-122]. A microarray is a two-dimensional (2D) grid of a large number of unique materials deposited at known or defined locations on a flat substrate. The advantage of the microarray technology is that experiments can be carried out under essentially identical reaction conditions, while only using minute amounts of material for parallel interrogation. Conventional microarrays do not involve cells [123-125]. Cell-based microarrays have just begun to make inroads in the high throughput screening field in the last few years [125], with potential applications such as global gene function analysis, selection of biomaterials, and drug cytotoxicity studies.

Most of the existing cell-based microarrays share the same general procedure, *i.e.*, to print microdots or discs of testing compounds, polymers, or biomolecules on a flat substrate, incubate the printed substrate in a cell suspension, and analyze the binding characteristics of the cells to the microdots or discs. For example, How *et al.* developed a cell-based microarray using small molecules embedded in a gelatin matrix to screen human embryonic kidney (HEK) cells with fluorescence detection [126]. Bailey *et al.* embedded small molecules into biodegradable polymer and conducted cell-based screenings for their antitumor activities [127]. In both the studies, cells were seeded on top of the printed substrate, which is a 2D surface of a biodegradable polymer chip, while the compounds slowly diffused out, affecting the proximal cells. Cell-based microarray technology is also helping the discovery of new materials in tissue engineering. Anderson *et al.* developed a microarray platform that allowed micro-scale synthesis and screening of a library of poly(acrylates) for testing embryonic stem cell (ESC) differentiation [128]. Following the

generation of the polymer library, the ESCs were seeded onto the polymer spots of the microarray and incubated to form a monolayer of ESCs on the polymer spot surface.

The challenge of cell-based microarrays has been to provide a suitable microenvironment for cells to grow and differentiate in a way closely resembling the situation *in vivo*. The limitation of existing cell-based microarray technology is that the cells are cultured on a 2D substrate, which is known for forcing the cells to form a monolayer that could cause a loss in *in vivo* functionality. There has been research to create three-dimensional (3D) microenvironments for cell culture by embedding cells in gels or by creating simple micro-well structures to retain the cells [129-133]. One could use conventional cell culture plates, loaded with tissue engineering scaffolds to form a 3D tissue model array. Cheng *et al.* fabricated such a device using a solvent casting approach [134]. In their method, a thin layer of 3D tissue engineering scaffold was fabricated at the bottom of a standard cell culture plate by incorporating ammonia bicarbonate particles in a polystyrene or poly-L-lactic acid (PLLA) solution with chloroform as the solvent. This device was used to examine neural stem (NS) cell growth, morphology, cell-matrix interaction, gene expression, and voltage gated calcium channel (VGCC) functionality. The results showed that unlike the NS cells cultured on traditional 2D planar surfaces, cells in 3D scaffolds were more physiologically relevant with respect to their *in vivo* characteristics.

Much of the 3D cell culture research comes from tissue engineering, where a patient's own cells are used to regenerate damaged tissues or organs, leaving only natural substances to restore the organ function [135]. For cells to maintain their tissue-specific functions, a porous scaffold must be inserted to retain the organ's shape and structure, allow diffusion of nutrients, promote vascular ingrowth, and permit cellular proliferation and function [136]. Tissue engineering scaffolds have been fabricated using a variety of

techniques such as fiber bonding [137], solvent casting [138-140], phase separation [141-143], gas foaming combined with particulate leaching [144-148], and solid freeform fabrication (SFF) methods include 3D-printing, fused deposition modeling (FDM), and selective laser sintering (SLS) [149]. However, most of these methods involve the use of organic solvents, which may leave residuals that are detrimental to cells. Others may have difficulty in fabricating biomimetic architectures as the tissue microstructures are often smaller than the spatial resolution currently achievable. The compatibility of the existing scaffold fabrication methods with tissue model microarrays is another issue.

Fabrication of 3D tissue model microarrays will benefit many applications, one of which is screening the interaction effects of chemotherapy drugs after cancer resection. The most often used protocol for cancer treatment involves tumor removal followed by chemotherapy treatment [150]. Drug administration is crucially important in cancer treatment after tumor removal. The type of drug, dosage, and treatment schedule needs to be determined early to effectively control tumor recurrence. Standard chemotherapy regimens call for a certain dose of chemotherapy given at certain time intervals. However, the types of chemotherapy drugs and dosage to be used are currently experience-based. There has not been a simple and rapid method for multi-drug efficacy test that will assist the doctors to determine a suitable drug or a combination of drugs to use. Tumors are three dimensional. The drug effect could be significantly different depending on whether it is tested with 3D or 2D cell cultures [13]. Individual patients could react differently to the type and dosage of chemotherapy drugs. In addition, multiple drugs are often administered at the same time without a clear understanding of the drug interaction effect. A 3D tissue model microarray could provide a much needed tool to determine a personalized cancer treatment plan.

In this chapter, we present a fabrication method for tissue engineering scaffolds using laser foaming of gas-impregnated biodegradable polymer. The fabrication method employs a laser beam to foam CO_2-saturated polymers, creating micro-scale foamed spots without any organic solvent or other harmful substances. In addition, the foamed spot size and depth of the inverse-cone shape could be adjusted with the laser power and lasing time, providing flexibility for process control. The goal is to create 3D tissue model microarrays to enable tissue-based parallel study of cancer drugs. Polylactic acid (PLA) samples were injection-molded and saturated under high pressure CO_2. Micro-scaled tissue engineering scaffolds were foamed using a continuous CO_2 laser on a computer controlled positioning stage. The effects of key process parameters of laser foaming were studied, including gas concentration, laser power, and exposure time. Both foamed and unfoamed samples were evaluated using a cell culture study with human glioblastoma cells.

3.2 EXPERIMENTAL

3.2.1 Materials, cells, and chemicals

The PLA used in this study was ECORENE^{TM} NW40, a mixture of D/L product, acquired in powder form from ICO Polymers. The average powder size was 20 μm in diameter. The material had a density of 1.25 g/cm^3, tensile modulus of 1.5-2.7 GPa, and melt flow rate of 15 g/10 min. The melt and glass transition temperatures of PLA were 150-180 ºC and 60-65 ºC, respectively. A previous degradation study reported that a similar foamed PLA sample lost 60% of the initial weight after 20 days in 0.01 N NaOH solution [151]. The PLA molecular structure is shown in Figure 3-1. It decomposes into non-toxic components via simple hydrolysis of the ester (CO-O) bond, and no catalyst is required for hydrolysis [152]. The degradation time is 12-18 months in environment [153]. Medical

grade CO_2 was used as the physical blowing agent in the laser foaming process. CO_2 (99.95% purity) was obtained from Airgas Nor Pac, Inc.

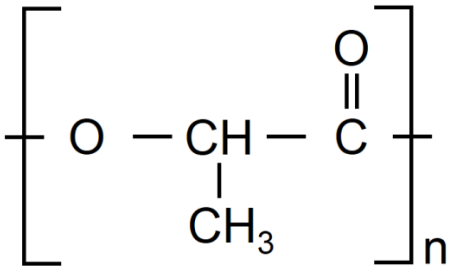

Figure 3-1. Polymer structure of PLA [153]

Human brain glioblastoma multiforme cells (cell line T98G, purchased from ATCC) were used in the cell culture study. Dulbecco's modified eagle medium (DMEM) with 1000 mg/L glucose, L-glutamine, pyridoxine, and sodium bicarbonate was purchased from Sigma-Aldrich (St. Louis, Missouri). Fetal bovine serum (FBS) with endotoxin and Hemoglobin levels below 5EU/ml and 10mg/dl, respectively, was obtained from Invitrogen (Carlsbad, CA). Dulbecco's Phosphate Buffered Saline (DPBS) was acquired from Thermo Fisher Scientific (South Logan, Utah).

Cell viability was evaluated using the live/dead stain assay and the Alamar blue assay. The live/dead staining solution was purchased from Invitrogen Inc. (Carlsbad, CA). The Alamar blue assay kit was obtained from Fisher Scientific, Inc. (Pittsburgh, PA). Karnovsky's fixative was acquired from Electron Microscopic Sciences (Hatfield, PA) for scanning electron microscope (SEM) examination.

3.2.2 3D scaffold array fabrication

PLA powder was dried overnight in a vacuum oven at 60 ºC to prevent moisture. The powder was injection molded using a lab-scale injection molder (Haake MiniJet, Germany) at 200 ºC barrel temperature and 30 ºC mold temperature under 800 bar injection

pressure. The holding time was 10 seconds. Disc-shaped samples were obtained through injection molding, with a diameter of 35 mm and thickness of 1.5 mm.

The laser foaming process consisted of two stages: CO_2 gas saturation and foaming. In the gas saturation stage, injection-molded PLA samples were impregnated with CO_2 in the pressure vessel under saturation pressures of 1 and 2 MPa for 80 and 220 hours, respectively. The saturation conditions were chosen based on previous research, which showed that the most desirable porous structure was obtained with 2 MPa and the pore size tended to be larger as gas saturation pressure increased [151]. Before they were processed with laser, the gas-saturated samples were retrieved and their weights measured to determine the CO_2 concentration. The second stage of the process is laser foaming, as shown in Figure 3-2. The CO_2-impregnated PLA samples were mounted on a computer controlled XYZ positioner (MAXNC 10 from MAXNC, Inc.) for laser treatment. The foaming conditions in this study are summarized in Table 3-1. Each disc has six foamed spots. The laser used was a CO_2 laser (Synrad Firestar v30 from Synrad, Inc., WA) with 10.6 μm wavelength, 2.5±0.5 mm beam diameter, 45 W maximum power, and 917 W/cm^2 maximum laser power density. The average laser power was varied from 2.0 W to 10.5 W, corresponding to a power density between 41 W/cm^2 to 203 W/cm^2, and the lasing times used were 0.25 s, 0.50 s, and 1.00 s. The laser was controlled by a Synrad UC-2000 control unit through a LabVIEW program developed in house.

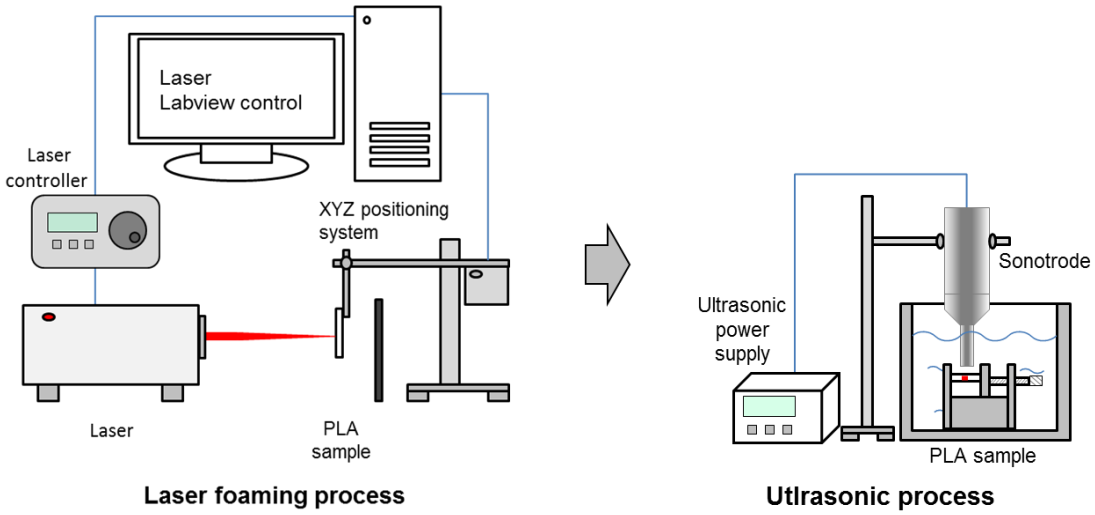

Figure 3-2. Schematic of the PLA sample fabrication processes

Table 3-1. Parameters for laser foaming experiment

Parameters	Values
Saturation pressure (MPa)	1, 2
Saturation temperature	room temperature
Saturation time (hour)	80, 220
Laser power (W)	2.0-10.5
Lasing time (s)	0.25, 0.5, 1

Foamed samples were exposed under the atmospheric condition to desorb the remaining CO_2 for four days. This desorption time was suggested in [151], where it showed that after four days, the residual CO_2 concentration was as low as 2% even for a solid, unfoamed PLA sample. Since foaming causes degas of CO_2, it is expected that the CO_2 concentration at foamed regions will be even lower. Fully open-celled structure was required to culture the cells in the PLA scaffold. The foamed samples were therefore

processed with ultrasound (Model VC750 from Sonics Concept, Inc.), a schematic also shown in Figure 3-2, to remove any possible solid skin layer of the porous structure. A solid skin layer could prevent cells and cell culture media to access the internal porous structure. The ultrasonic processor had a frequency of 20 kHz and a maximum power of 750 W. The samples were held in a vice in distilled water. The distance between the sonotrode and foamed specimen was 2 mm. Pulsed ultrasound was applied for one minute with a 3:3 on and off ratio. The amplitude setting of the ultrasound was 90%.

For comparison, unsaturated samples were also processed with laser to obtain similar geometric features, except for the porous scaffold structure. Cell cultures were conducted with both foamed and unfoamed samples to compare the cell growth behavior.

3.2.3 Scaffold characterization

Microstructures of both foamed and unfoamed samples and the morphologies of cells were characterized using a JEOL NeoScope JCM-5000 (Nikon®, UK) SEM under an accelerating voltage of 5-10 kV and a beam current of 0.1 nA. The samples were freeze-fractured in liquid nitrogen. A gold and palladium alloy layer was sputter-coated onto each sample using an EMS 500x sputter coater (Electron Microscopy Sciences, Hatfield, PA). Geometrical features of the laser processed spots were analyzed from the SEM images using the image analysis software Image J [154]. Pores were numbered and their areas measured to calculate an averaged diameter D using the following formula [155]:

$$D = \frac{\sum_{i=1}^{N} \sqrt{4 \times A_i / \pi}}{N} \tag{3.1}$$

where A_i is the area of i^{th} pore and N is total number of pores.

3.2.4 Sterilization and cell culture

For easy handling in this study, the samples were sectioned into individual pieces, each with a laser processed spot. The samples were rinsed using running distilled water for 20 seconds, sterilized with 1% bleach solution and 70% ethanol for 30 min each, and then exposed to ultraviolet light for 30 min. Sterilized samples were soaked in complete cell culture medium at 37 ºC and 5% CO_2 for more than 3 days before cell seeding. DMEM was blended with 10% of FBS and 1% penicillin/streptomycin (PS, from MP biomedical, Solon Ohio) using Stericup®/Steritop® and vacuum pump to make the complete cell culture medium. The samples were taken out and washed repeatedly in DPBS, then placed into a 24 well plate for cell seeding. Human brain glioblastoma multiforme cells (T98G) were seeded in the laser process spots in both foamed and unfoamed samples. Approximately 6,400 T98G cells were seeded on the foamed and unfoamed samples. Seeded samples were cultured with DMEM medium with 10% FBS at 37 ºC and 5% CO_2. The cell culture medium was changed every 2-3 days. Cell concentration was counted under a microscope using a cell counting chamber.

3.2.5 Cell viability assessment

A microplate reader (Synergy HT, BioTek Instruments) was used to assess the cell viability over time. Before the measurement, it is required to calibrate a microplate reader. The glioblastoma multiforme cells were detached from the cell culture flask using 0.25% trypsin and centrifuged at 1000 rpm for 5 min. Separated cells were mixed with 2 ml complete cell culture medium and directly seeded in 24 well plates. Cell solution was added from 10 µL to 230 µL with a 10 µL increment in each well. There were about 2,200 T98G cells per 10 µL cell solution. Complete culture medium was filled in each well to a final amount of 450 µL. Approximately 50 µL Alamar blue dye was added. After incubating for 2 hours at 37 ºC and 5% CO_2, the plate was scanned to measure the fluorescence intensity

and correlated to the cell numbers. The fluorescence signal was detected at 530±25 nm emission wavelength with the 590±35 nm excitation band. A linear relationship was obtained between the number of cells and fluorescence intensity, as shown in Figure 3-3.

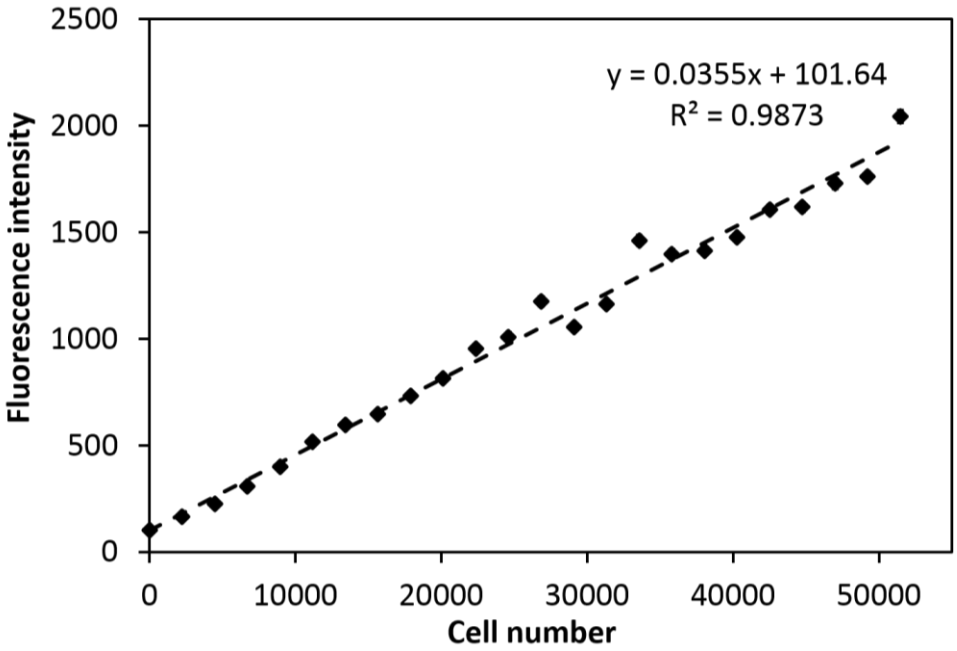

Figure 3-3. Calibration data of a microplate reader

Once the microplate reader was calibrated, the PLA samples were transferred to a 24 well plate, and approximately 6,400 T98G cells were seeded on the foamed and unfoamed samples. After 4 hours of incubation at 37 ºC and 5% CO_2, DMEM culture medium was added to a final amount of 450 µl into each well. Two batches of cell culture samples were prepared. One batch was incubated under the cell culturing condition and scanned every 4 hours to check the viability using the Alamar blue dye. The other batch was cultured for 72 hours and stained with a live/dead viability/cytotoxicity kit for 20 minutes, after which the samples were moved from the 24 well plate to a Petri dish and observed under an upright stereo zoom fluorescent microscope (LEICA M250 FA) to

obtain the fluorescence images of live/dead cells. The images were used for a qualitative analysis as shown in Figure 3-10 and 3-11. For SEM examination, the T89G cells were fixed using 1 ml Karnovsky's fixative consisting of 5% Glutaraldehyde and 4% Formaldehyde in a 0.08 M buffer [156]. The samples were submerged in the fixative overnight at room temperature and dehydrated using an ethanol gradient (75%, 90%, 95% and 3 × 100% for 15 min each step) [157]. After the drying process, the cell morphology was characterized with SEM.

All data were analyzed and described as mean ± standard deviation. Student's *t*-tests were used for comparisons. The probability was calculated and a level of $P < 0.05$ was used to determine the statistical significance.

3.3. Results and Discussion

3.3.1 Effects of laser foaming parameters

Figure 3-4 shows a set of PLA samples at each stage of the fabrication process. The first column (a) shows the discs after CO_2 absorption. There is no difference in the sample appearance from unsaturated samples; however, it required caution to handle the saturated sample. The PLA discs were fully saturated and could easily be foamed at the body temperature with simple hand touch. Therefore, care must be taken to avoid accidental foaming. The second column (b) shows the samples after laser foaming. The third column (c) shows individual foamed samples sectioned for characterization. The arrows in the figure indicate increasing laser power and exposure time. Each column of the spots shares the same laser exposure times, 0.25 s, 0.5 s, and 1.0 s, from left to right. Each row has same laser power, 2.0 W, 4.8 W, 8.0 W, and 10.5 W, from top to bottom. In general, the size of the foamed spot becomes larger as the lasing power and time increases.

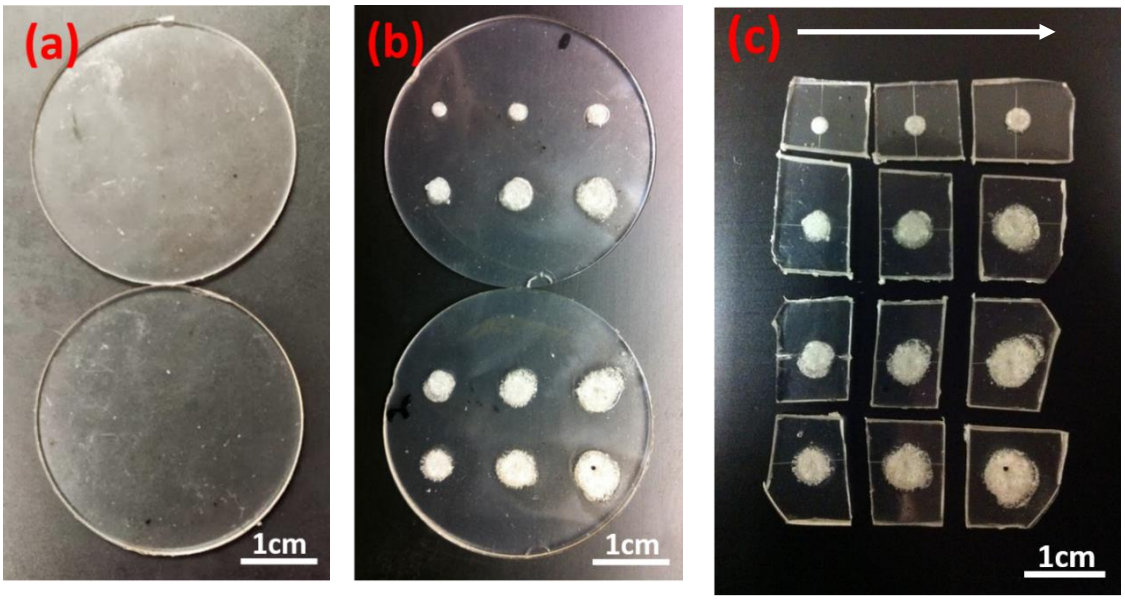

Figure 3-4. PLA samples after each step: (a) CO_2 absorption, (b) laser foaming, (c) gas desorption and cutting, the arrows indicate the direction of power and time increase.

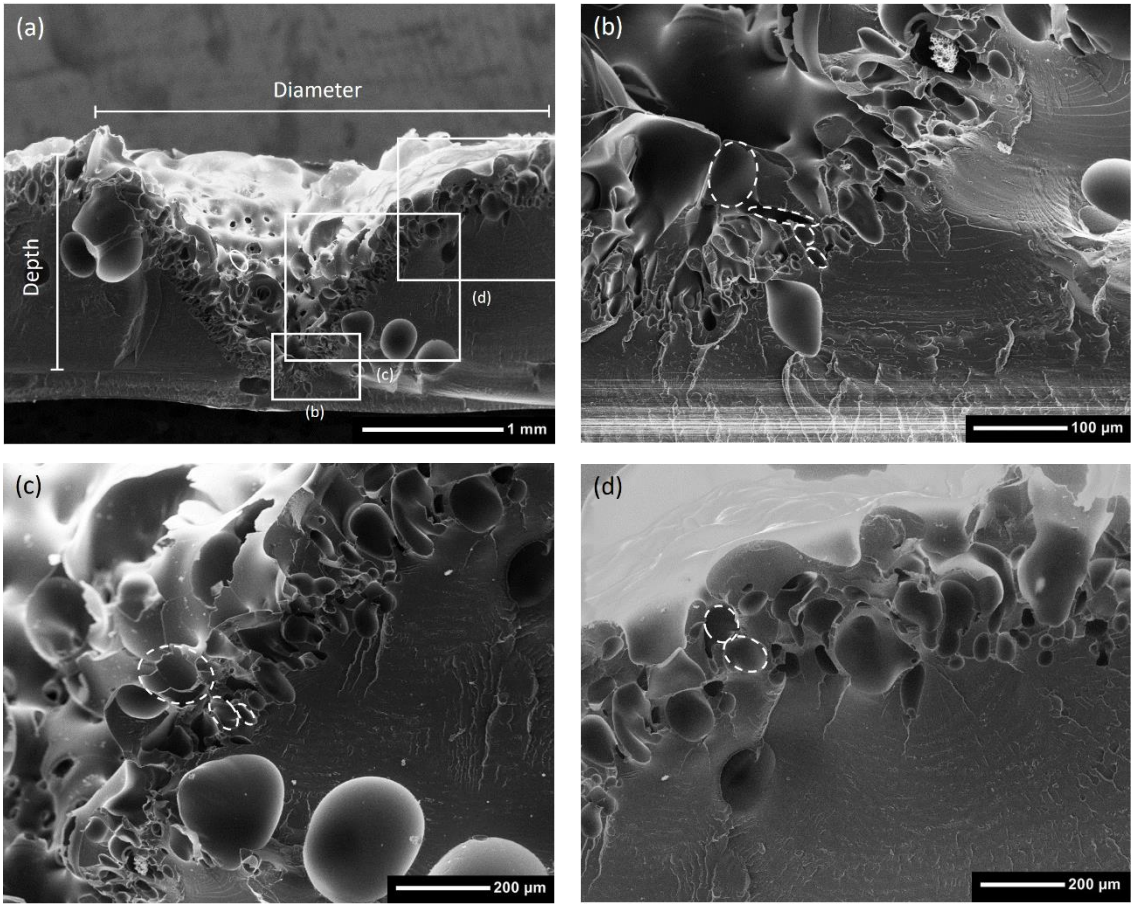

Figure 3-5. SEM images of the cross-section of a PLA scaffold, scale bars indicate (a) 1 mm, (b) 100 µm, (c) 200 µm, and (d) 200 µm. Dashed lines indicate outlines of selected pores.

Figure 3-5 shows SEM images of the cross section of a foamed sample. It is seen that laser foaming created an inverse cone-shaped well, with porous structure on the wall of the well. This unique structure is a result of both laser ablation and heating. The laser ablation effect helped remove the material in the center of the well, while the laser heating effect induced the gas foaming process. The porous structure obtained in this study is different from bulk porous structures that are usually used in tissue engineering, e.g., in [13, 41, 158]. However, the laser foamed structure does show a few layers of pores that are

mostly interconnected. This can be seen in Figure 3-5(a), where the surface of the foamed region has openings that lead to the internal porous structure. The 3D open-celled porous structure is also evident in Figure 3-11(c) where a fluorescence image shows cells growing inside the porous structure. It is also observed that the pore size varied slightly from the bottom of the well to the top. This could be explained by the fact that the center of the sample had a slightly higher gas concentration due to the surface desorption effect of gas saturated polymer samples [159, 160]. It could also be due to the fact that the center had a higher temperature in the laser heating process [160].

Quantitative results of laser foaming are shown in Figure 3-6. Broadly speaking, it can be observed that as the laser power and lasing time increase, the maximum diameter and depth of the foamed region (shown in Figure 3-5(a)) becomes lager. The effect of laser parameters on the diameter of the inverse cone-shaped well is shown in Figure 3-6(a). The gradient of the diameter is higher at lower laser powers than at higher ones. The laser intensity of a continuous laser follows the Gaussian distribution. Therefore, the more power is used, the larger foamed region will be obtained. Figure 3-6(b) shows the depth change with laser power and exposure time. The laser generated wells become deeper as exposure time and laser power increase. The depth difference caused by lasing times becomes larger at higher laser powers. In the case of 1.0 s, the depth increase appears to level off after 8W laser power. This is because that the maximum depth has been reached, which is 1.45 mm, the thickness of the polymer sample. The volume of the inverse cone shaped wells increases with the laser power and exposure time, as seen in Figure 3-6(c). The volume is more sensitive to laser power when the lasing time is longer. Figure 3-6(d) shows the average pore size in diameter as a function of laser power and exposure time. It is interesting to see that a longer laser exposure time produced a larger pore size, whereas laser power had little effect. This phenomenon could be a result of gas diffusion process in the bubble growth

process. It takes time for dissolved gas to diffuse into the bubbles; therefore, a longer foaming time (exposure time) corresponded to a larger pore size.

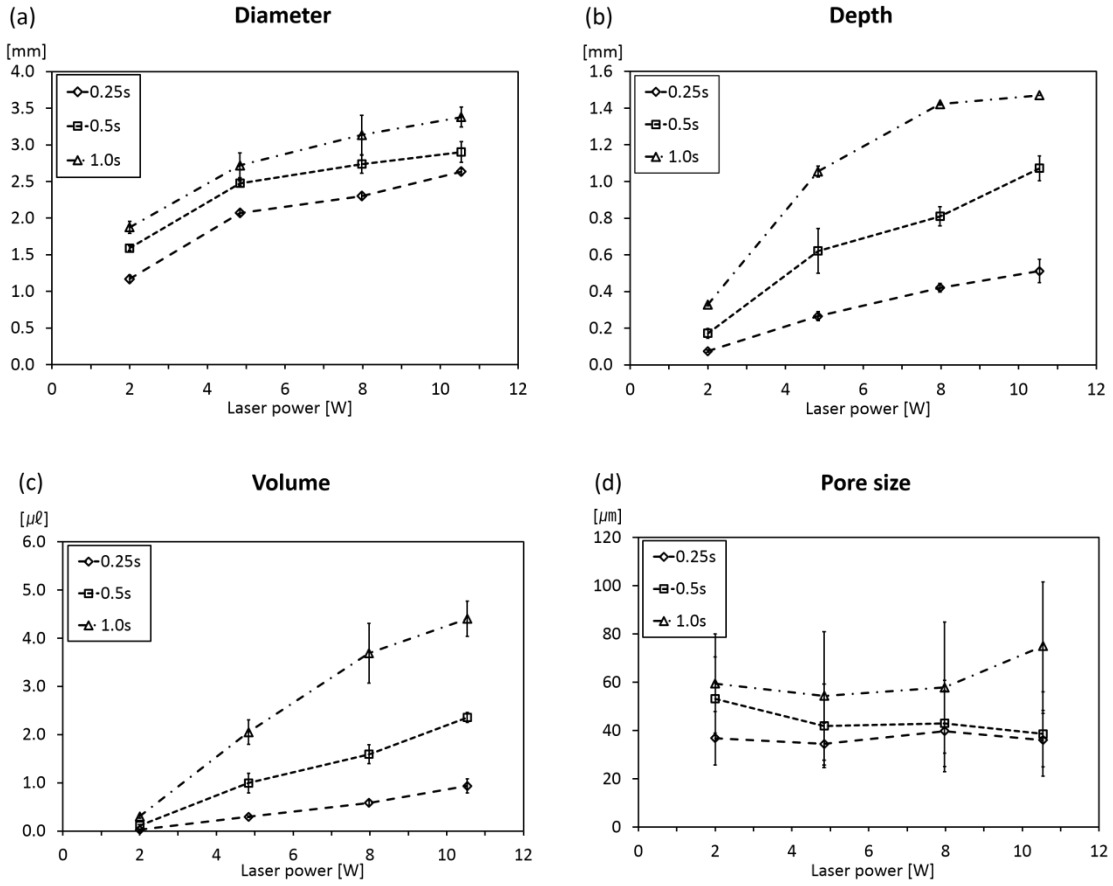

Figure 3-6. Effect of laser foaming conditions including lasing time and laser power

Statistical analysis results for each of the response variables are shown in Table 2. Laser parameters including Laser Power, Lasing Time, and the interaction effect between them, Power×Time, were examined using a least-squares regression method. The R^2 values in the parentheses indicate the goodness-of-fit of the models. For each response variable, *t*-ratio and Prob > |*t*| represents the statistical significance of the corresponding parameter. For example, both Laser Power and Lasing Time are statistically significant for Diameter;

however, the interaction effect between them is not. For Volume, on the other hand, neither Laser Power nor Lasing Time is significant; however, the product of them is strongly significant (P<0.0001). While at least one of the three effects (Power, Time, and Power×Time) is significant for Diameter, Depth, and Volume, it is interesting to see that none of them is significant for Pore Size. All the samples used for this analysis were saturated at 2 MPa.

Table 3-2. Statistical Analysis Results

	Diameter	(R^2=0.88)
Effects	*t*-ratio	Prob>|*t*|
Laser Power	5.73	<0.0001
Lasing Time	3.05	0.0045
Power×Time	0.43	0.6682
	Depth	(R^2=0.93)
Effects	*t*-ratio	Prob>|*t*|
Laser Power	5.59	0.0242
Lasing Time	3.9	0.0570
Power×Time	22.98	<0.0001
	Volume	(R^2=0.96)
Effects	*t*-ratio	Prob>|*t*|
Laser Power	-0.35	0.7285
Lasing Time	-0.86	0.3978
Power×Time	9.7	<0.0001
	Pore Size	(R^2=0.61)
Effects	*t*-ratio	Prob>|*t*|
Laser Power	-1.03	0.3110
Lasing Time	1.99	0.0555
Power×Time	1.31	0.2000

Since the product of Power and Time is energy, it would be interesting to examine the relationship between Volume and laser energy. The effect of laser energy on the resulting volume of the inverse cone shaped wells is shown in Figure 3-7. There is linear relationship between the laser energy and the volume of the wells. The fitted linear model has an R^2 of 0.96. This suggests that the foam volume is basically a function of laser power. However, it should be noted that there are cases where laser power and exposure time need to be controlled separately in order to control the diameter and depth of the well individually. For example, it would be beneficial to have a small lateral size (diameter of the cone) such that a high density tissue model array can be achieved and more foamed spots could be packed in a given polymer chip. In the meantime, it would be necessary to maintain a certain volume for each of the scaffolds, such that the volume of cultured tissue would be large enough to have statistical significance in drug testing. The results in Figure 3-6 and Table 3-2 show that a separate control of the lateral size and depth could be achieved by adjusting Laser Power and Lasing Time.

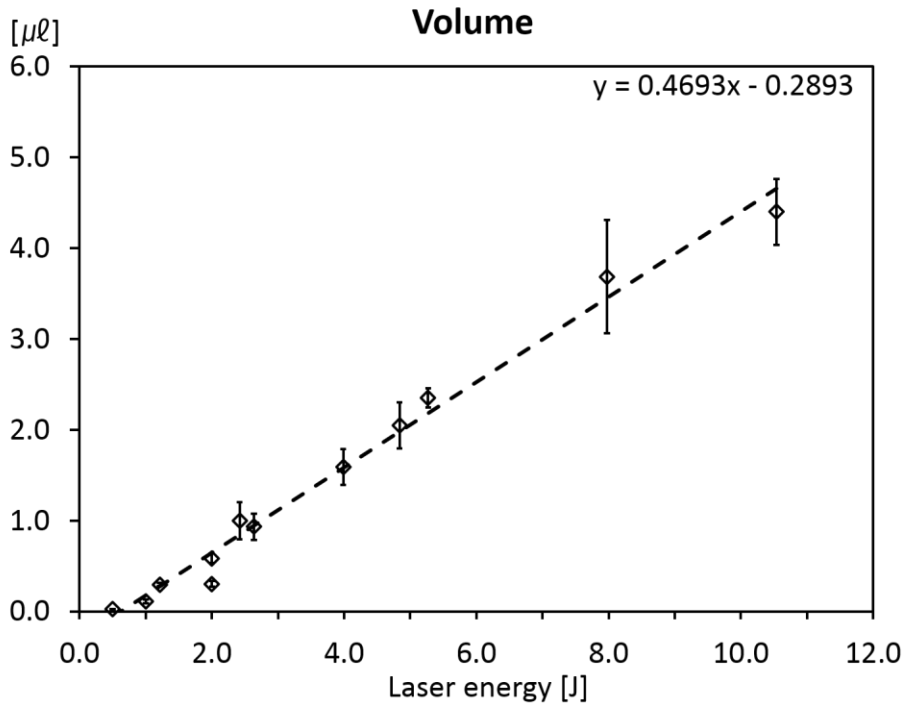

Figure 3-7. Relationship between laser energy and the volume of the laser generated well

3.3.2 Effects of gas saturation pressure

Different types of cells may require different pore size for optimal cell seeding and growth [13, 158, 160-163]. It is therefore important to control the pore size in the scaffold fabrication. Figure 3-8 shows the effect of gas saturation pressure on pore size under various laser power conditions. In the case of 2 MPa, the pore size had a range between 30 μm and 70 μm. At 1 MPa, the pore size ranged from 60 μm to 140 μm. Statistical analysis indicated that saturation pressure was significant with $P<0.0001$. It is also seen that the saturation pressure has a stronger effect on pore size than laser power and lasing time. Pore size is highly dependent on CO_2 gas concentration in polymers, and increases as gas concentration decreases [159, 164]. This is because a higher saturation pressure allows more CO_2 molecules to diffuse into the polymer, inducing a higher nucleation density and hence smaller pores in the foaming process [159]. The gas concentrations of 1 MPa and 2

MPa samples were 3.3 ± 0.3 wt% and 7.0 ± 0.07 wt% of CO_2, respectively [159, 160]. Therefore, the lower saturation pressure, 1 MPa, resulted in lager pores in this chapter.

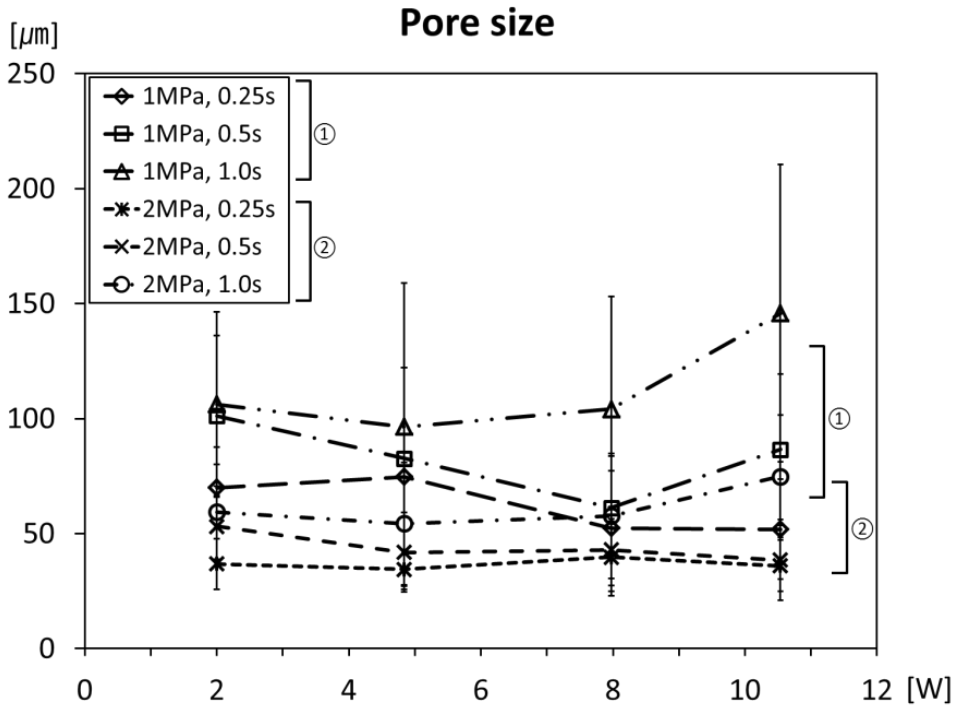

Figure 3-8 Comparison of pore sizes with saturation pressures of 1 MPa and 2 MPa

3.3.3 Cell culture results

The T98G cells were cultured on both foamed and unfoamed samples. The unfoamed samples were fabricated with unsaturated PLA using a laser power of 4.8 W for 1 s, whereas the foamed ones were fabricated using a laser power of 5.9 W for 1 s. The foamed samples were saturated with 1 MPa CO_2. These conditions were used to obtain inverse cone-shaped wells with similar diameters and depths, thus similar volumes. As a result, the unfoamed samples could be a good reference which only shows the effect of inverse cone-shaped well on cell culturing. Figure 3-9 shows a SEM comparison of the foamed and unfoamed samples for cell culture. Fluorescence images after 72 hours of

culturing are shown in Figure 3-10. The left column shows the cells growing in the unfoamed sample, representing a 2D cell culture case due to the lack of porous structure. The right column shows the cells inside the foamed sample with the 3D porous structure. The 1st, 2nd, and 3rd rows show the characteristics of cell morphology at top, middle, and bottom part of laser generated wells. Comparing to the unfoamed sample, the cell adhesion and proliferation were more efficient in the foamed sample, because of the increased surface roughness and the 3D porous structure. The 3D cell culture also showed a stronger fluorescence signal comparing to the 2D cell culture.

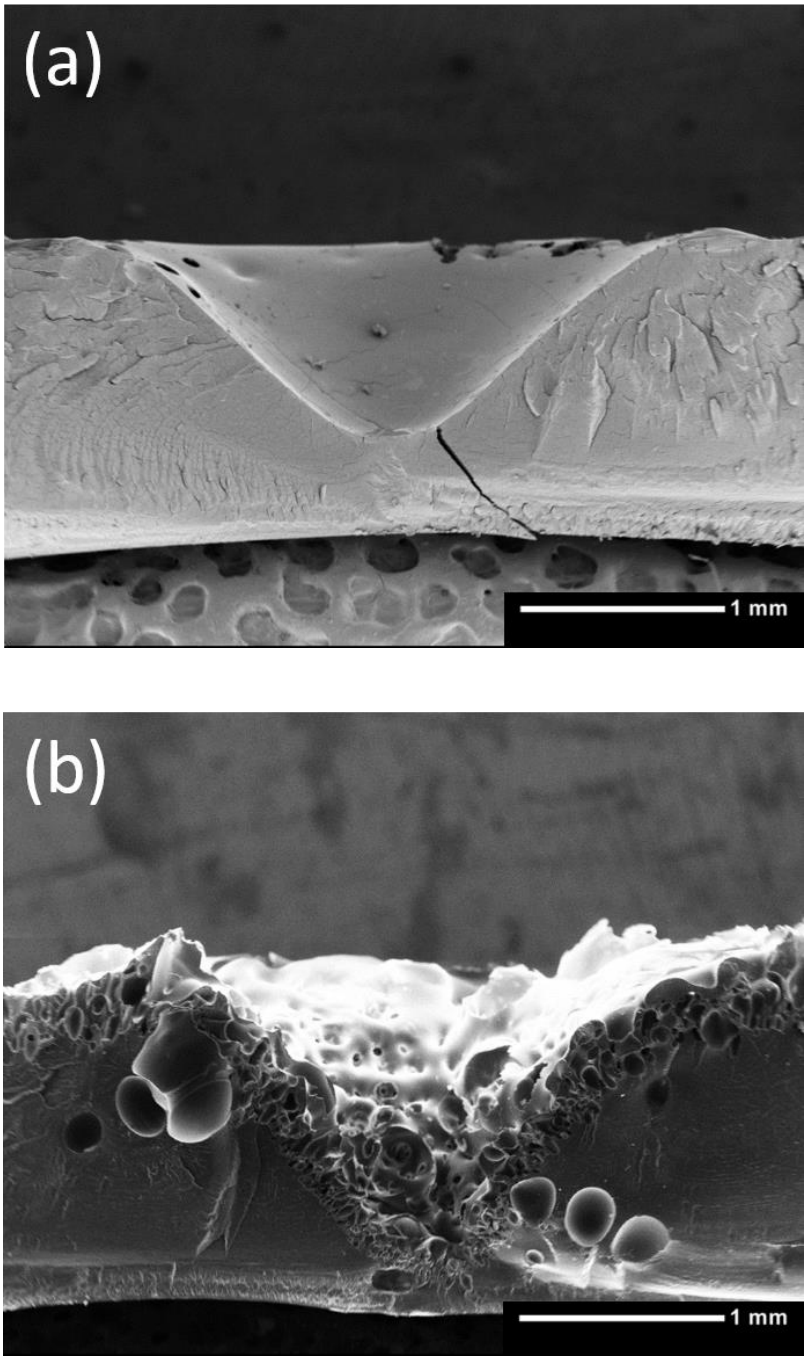

Figure 3-9 Comparison between 2D PLA sample (a) and 3D PLA scaffold (b)

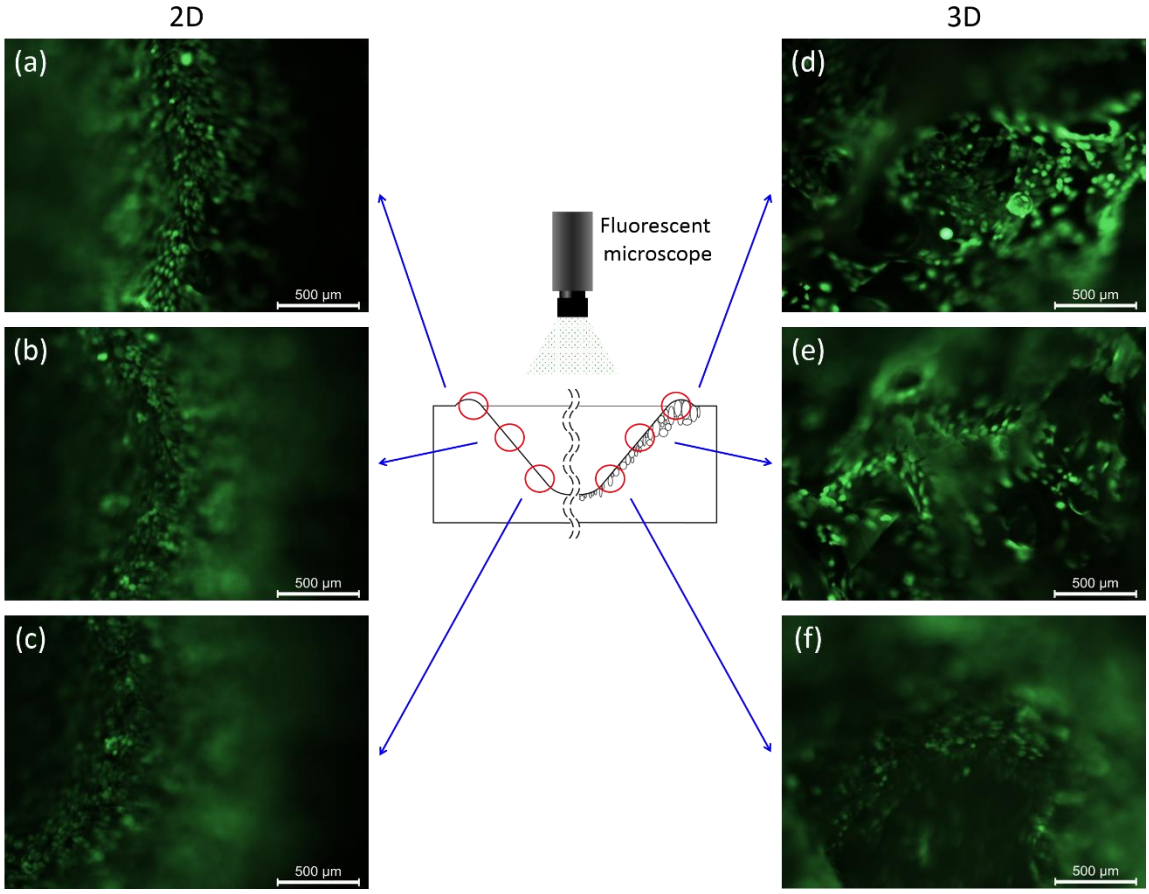

Figure 3-10 Fluorescence images of T98G cells after 72hr of cell culturing. (a-c) T98G on two dimensional inverse cone shape surface, (d-f) T98G on three dimensional surface of laser-foamed scaffolds.

The key difference between the 2D and 3D cell cultures can be seen in Figure 3-11. The left two images in the figure shows the results from the 2D cell culture, whereas the right two are from the 3D cell culture. Cells in the 3D cell culture have more cell-cell contact because they are organized in small pores. The cells in the 2D cell culture have tendency to spread out, as can be seen in Figure 3-13 later. Even though the cells were cultured in an inverse cone-shaped well in the unfoamed sample, the well is large enough such that the cells treat it as a flat 2D surface. 2D systems are not able to reproduce the dynamic 3D microenvironment of the extra cellular matrix (ECM) *in vivo* [13]. Cancer

cells in 3D scaffolds could better represent *in vivo* tumors by forming hollow cores resembling the necrotic area of *in vivo* ones [3, 165]. The 3D scaffolds in the foamed sample provided the T98G cells with a good micro environment for aggregation inside the interconnected porous structure.

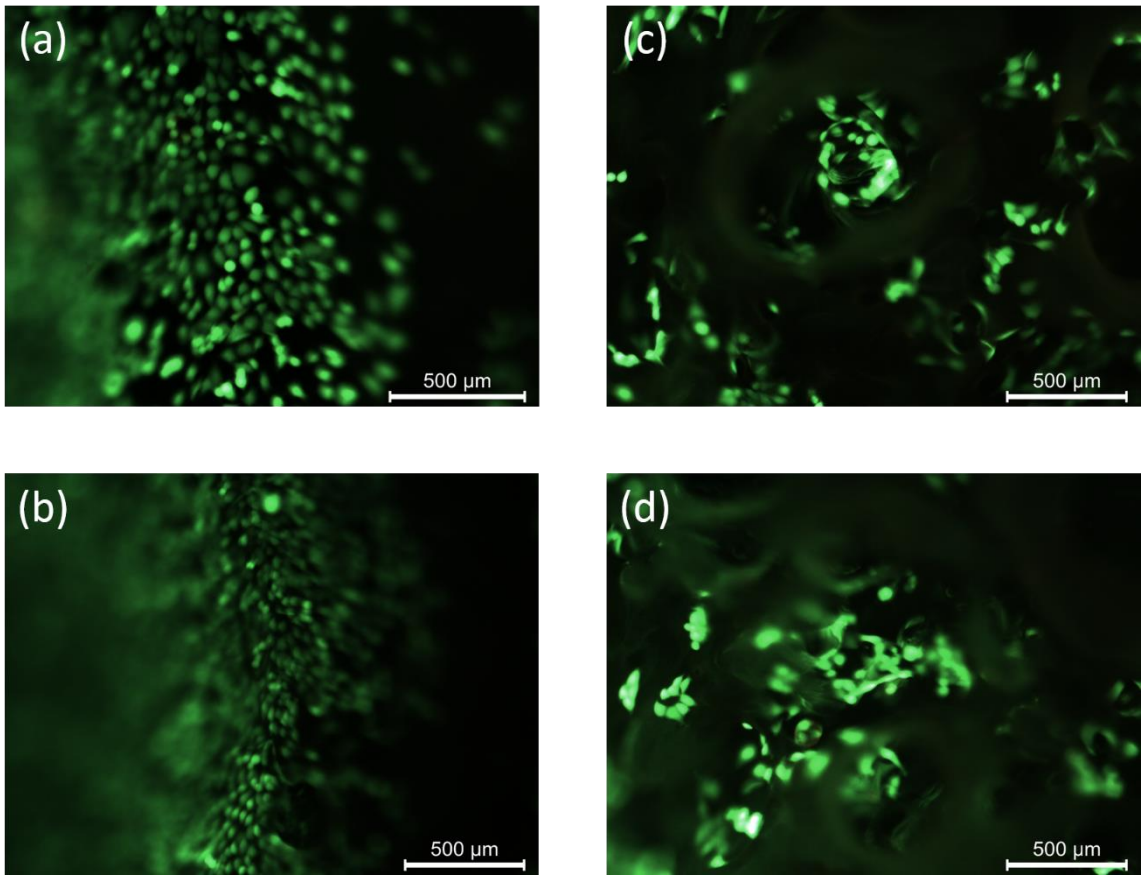

Figure 3-11 Comparison between 2D (a and b) and 3D (c and d) cell culture in unfoamed and foamed samples: fluorescence images of T98G cells after 72 hours of cell culturing.

Cross-sections of 3D and 2D cultures after 150 hours of culturing are examined under an SEM, and the images shown in Figs. 3-12 and 3-13, respectively. The samples were freeze-fractured with liquid nitrogen, and some cells could detach. However, the cells

left in the samples revealed different characteristics of these two types of cell cultures. Confirming the observations from the fluorescence images, cells in 3D scaffolds aggregated and showed clusters of multiple cells. Several cell-cell connections were found in the pores. Microvilli and fibers are well shown in both Figs. 3-12 and 3-13. The 3D spatial environment enhanced the dynamic viability of the cells, as has been observed in [166]. On the other hand, cells on the 2D surface only spread out and attached to the surface, similar to those observed in [167].

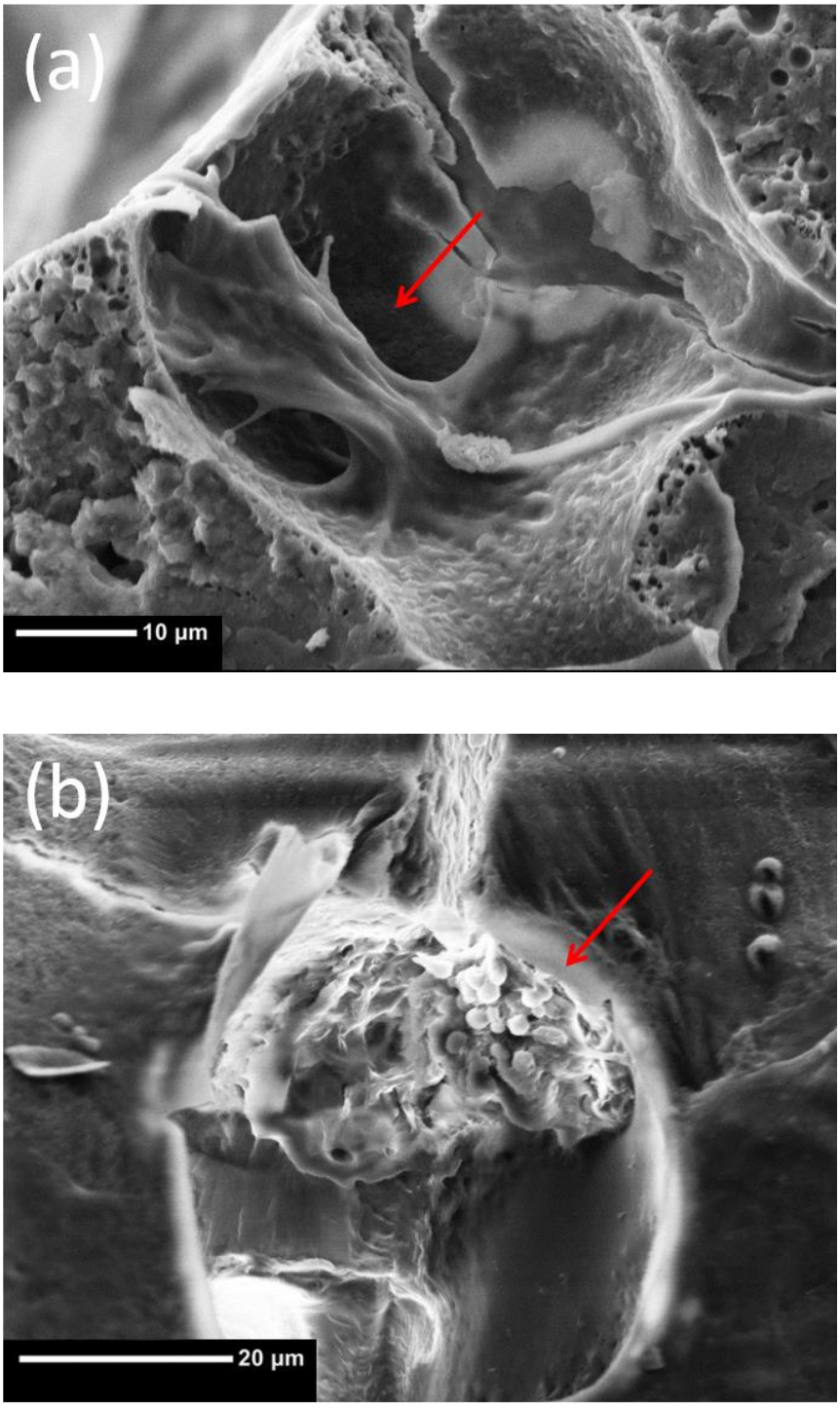

Figure 3-12. Morphology of cultured human T98G cells in a foamed sample after 150 hours of culturing

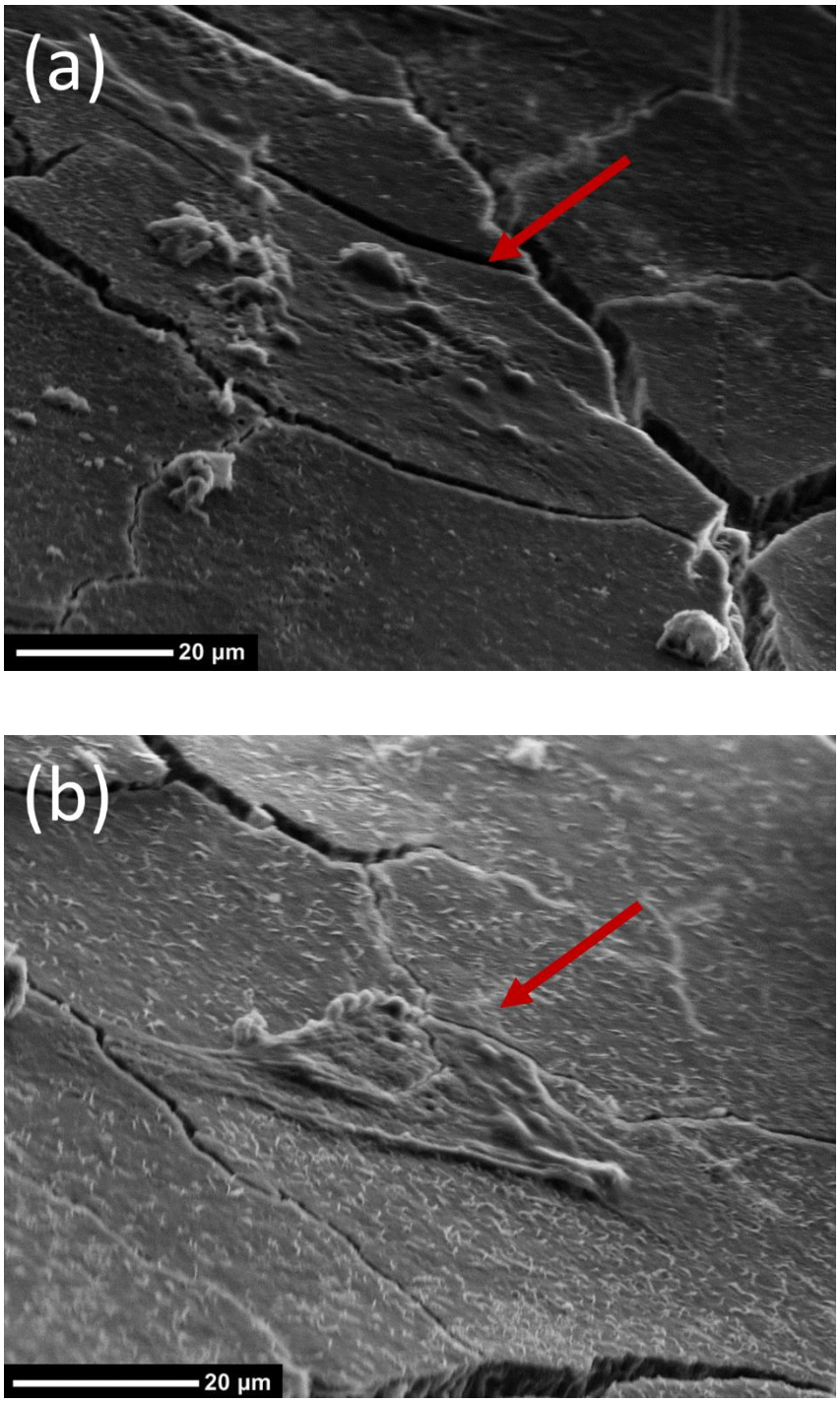

Figure 3-13. Morphology of two-dimensionally cultured human T98G cells in an unfoamed sample after 150 hours culturing

For quantitative comparison between the foamed and unfoamed samples, approximately 6,400 glioblastoma cells were seeded in each specimen. There were seven groups of samples, each with six foamed and six unfoamed specimens. T98G cells were seeded in both the foamed and unfoamed specimens with the same cell density. All samples were incubated in the same cell culture environment at 37 ºC and 5% CO_2. Samples were first incubated for 10 hours for cell adhesion. After that the fluorescence intensity was measured every four hours. Figure 3-14 shows the cell viability along the culturing time. The data were expressed as average ± standard deviation. Overall, the number of cells increased with time in both cases. At each time step, *t*-Tests were performed for foamed and unfoamed samples. At almost all the time steps, the difference between the foamed and unfoamed samples showed weak statistical significance. However, the linear trend of the foamed samples is consistently higher than that of unfoamed samples, which indicates that the 3D scaffolds may significantly enhance the cell viability compared to the 2D case. The weak statistical significance could be caused by large within-group variation due to the error involved in the fluorescence cell number measurement process.

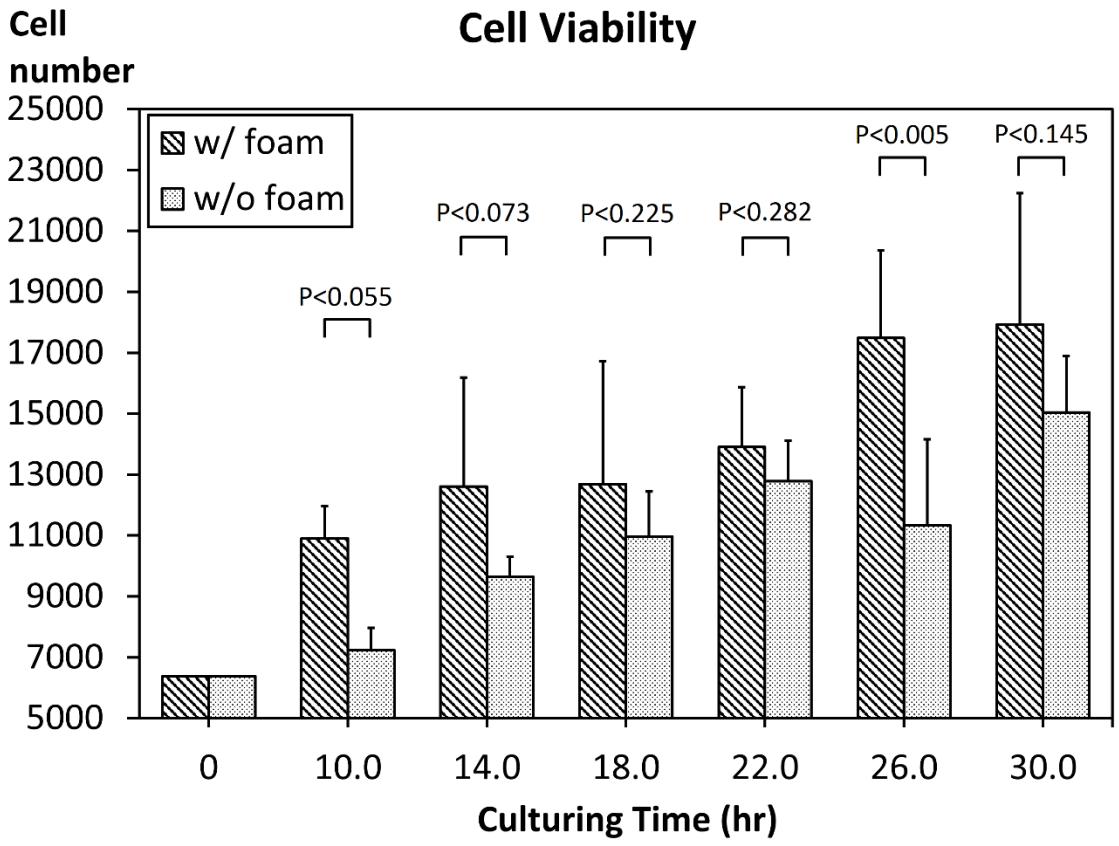

Figure 3-14 Experimental results of cell viability in foamed and unfoamed samples. The samples were seeded with 6,400 T98G cells. Statistical significance is determined by *t*-Tests.

3.4. CONCLUSIONS

A novel laser foaming technique has been developed to create arrays of 3D tissue models for parallel drug screening. The effects of major process parameters and the morphology of resulting porous structure were investigated, including laser power, exposure time, CO_2 concentration, size of the foamed volume, and pore size. For comparison unsaturated samples were also fabricated with the laser to produce similar sized wells without the porous structure. Cell culture studies were conducted with both foamed and unfoamed samples using T98G cells. The results show that laser foaming of

gas impregnated PLA is able to generate an array of inverse cone shaped wells with porous walls. The diameter and depth of the foamed region can be controlled with laser power and exposure time, while the pore size can be manipulated with the saturation pressure. The 3D porous scaffolds can be fabricated with a volume on the level of a few microliters, allowing high density packing of such scaffolds on a small polymer chip. Glioblastoma cells grow well in foamed PLA scaffolds, forming clusters that cannot be obtained in unfoamed samples which represent a 2D cell culture case. Cells are more viable in the 3D scaffolds than in the 2D cell culture. The 3D porous microarray could be used for parallel studies of drug toxicity, guided stem cell differentiation, and DNA binding profiles.

Chapter 4. Modeling and Simulation of a Selective Laser Foaming Process for Fabrication of Microliter Tissue Engineering Scaffolds

4.1. INTRODUCTION

Selective laser foaming is a novel material processing technique developed to fabricate an array of microliter tissue engineering scaffolds for high-throughput drug screening tests [168-170]. Two-dimensional (2D) cell cultures are widely used in the drug discovery and development process. However, cells growing on 2D substrates are forced to form an artificial monolayer, losing their *in vivo* three-dimensional (3D) morphology and the ability to produce realistic drug testing results [1, 2]. It is well known that for cells to recapitulate tissue specific functions a tissue engineering scaffold is needed to support the reformulation of 3D tissue structure [3, 4]. Given the fact that experimental drugs are often available in minute amounts, these tissue engineering scaffolds need to be small and fabricated in a large array such that high-throughput tests could be performed in parallel to reduce the time and cost, as well as the statistical variability, of the drug development process.

Figure 4-1 shows a schematic of the developed selective laser foaming process [168]. It combines the characteristics of laser ablation and solid state foaming, where a polymer sample is first saturated in a high pressure vessel containing an inert gas such as nitrogen (N_2) and carbon dioxide (CO_2). After meeting a certain saturation condition, the sample is retrieved from the pressure vessel and treated with laser irradiation. The heat induced by laser softens the polymer matrix and lowers the solubility of the inert gas, causing gas bubbles to nucleate and grow and the formation of porous structure. As the heat is continuously generated, the center of foamed region undergoes photo-thermal ablation, creating an inverse cone-shaped porous well that is conducive for cell culturing. The selective laser foaming process has been demonstrated with both Poly(methyl

methacrylate) (PMMA) and Poly(lactic acid) (PLA) [168, 169]. The volume of scaffolds fabricated was on the level of a few microliters. Human glioblastoma cells (T98) were successfully cultured in these scaffolds, forming organotypic clusters that could not be obtained in 2D cell culture.

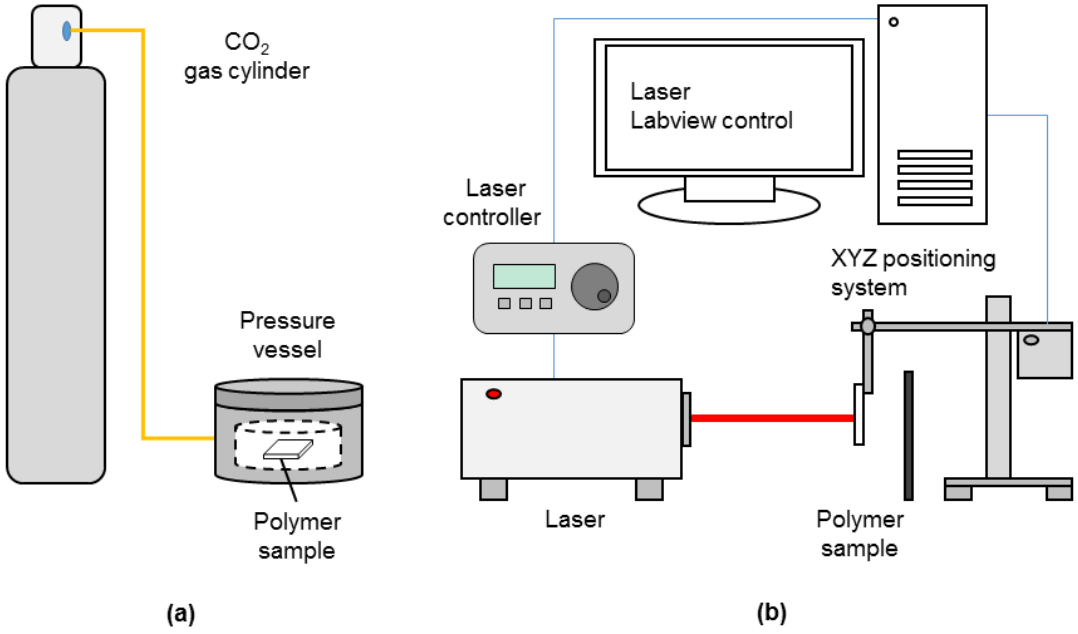

Figure 4-1. Schematic of the selective laser foaming process: (a) Gas saturation and (b) laser irradiation [168].

In this chapter, a finite element analysis (FEA) model is developed to evaluate parameter effects of the selective laser foaming process. The ultimate goal is to control the size and consistency of fabricated tissue engineering scaffolds, such that the process could be used with a range of materials and various cell types that may require different geometric features of the scaffolds. With the FEA model the effects of laser power and lasing time on the size and shape of the fabricated scaffolds were investigated.

4.2. Finite Element Modeling

Finite element modeling is frequently performed to study complex phenomena in laser-based manufacturing processes [171-173]. However, little has been done on modeling of an integrated laser foaming and ablation process. Figure 4-2 shows the model geometry and boundary conditions of the FEA model developed in this study. The polymer sample and laser beam are axisymmetric along the center of the beam. Therefore, the model is simplified into a 2D model and only half of the domain is considered.

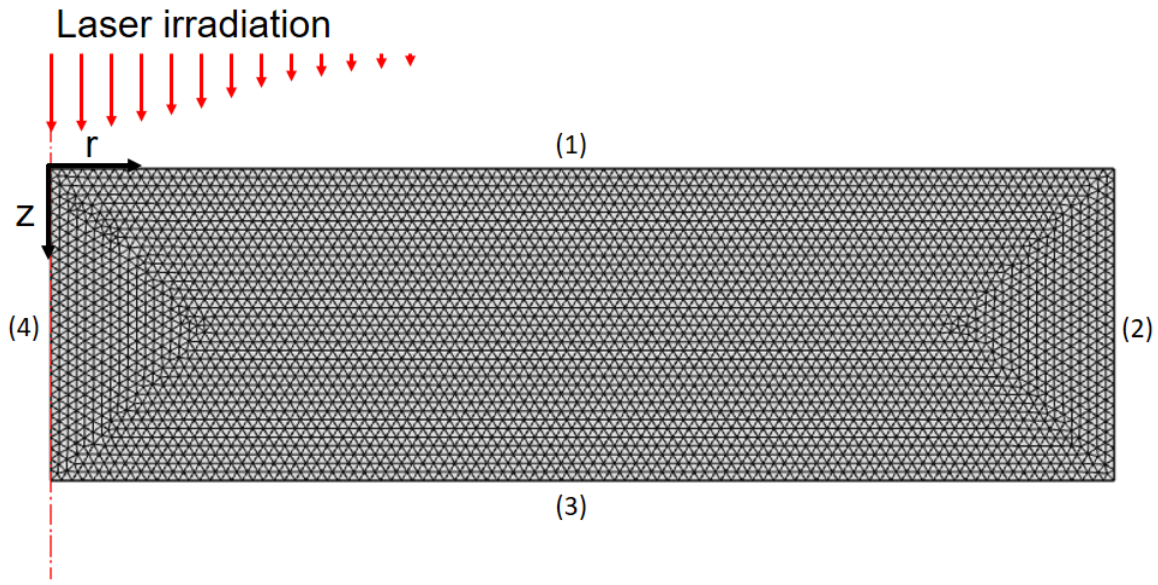

Figure 4-2. Geometry and meshing of the FEA model. (1)-(4) denote the model boundaries.

The model is developed based on a heat transfer process in solid and the laser irradiation is applied as a volumetric heat source in the domain. A non-linear time dependent analysis is used, where material properties are updated according to the local temperature. The radiative heat loss from the sample to the ambient is assumed to be

negligible. A convective heat loss is considered on boundaries 1 to 3 and expressed as follows.

$$\vec{n}\cdot\left(k\nabla T\right)=h\left(T_{surf}-T_{0}\right) \tag{4-1}$$

where h is a convective heat transfer coefficient, T_{surf} is the temperature at the sample surface, T_0 is the ambient temperature, and $\vec{n}$ is the normal vector of the corresponding boundary. The adiabatic condition is imposed on boundary 4. Due to the effect of laser cooling fan, a typical forced convective heat transfer coefficient for moderate speed air flow, 100 W/(m^{2}K) [174], was used in the simulation.

The selective laser foaming process involves the following mechanisms: Heat conduction through the polymer sample, foaming, ablation, and convective cooling. The two dimensional conduction heat transfer process can be modeled as [175]

$$\rho(T)\cdot C_{p}(T)\frac{\partial T\left(r,z,t\right)}{\partial t}-\nabla\cdot\left(k(T)\nabla T\left(r,z,t\right)\right)=Q\left(r,z\right) \tag{4-2}$$

where r and z are the spatial coordinates and ρ, C_p, k are density, specific heat, and thermal conductivity of the material, respectively. The heat source $Q(r, z)$ is the energy input induced by the laser. It is assumed that the laser intensity in the radial direction follows a Gaussian distribution and the absorption of laser energy by the polymer can be defined by the Beer-Lambert law [176]:

$$Q(r,z)=\alpha I_{0}\times\beta\times\exp\left(-\beta z\right)\times\exp\left(-2\frac{r^{2}}{\left(w/2\right)^{2}}\right) \tag{4-3}$$

where α and β are the absorption coefficient and the attenuation coefficient of the polymer, and w is the laser beam width.

The beam diameter on the polymer substrate is calculated using the near-field divergence of the TEM_{00} beam, since the target substrate is placed within the Raleigh range. The divergence is modeled using the following equation [177]

$$w(x) = w_0 \left[1 + \left(\frac{\lambda x}{\pi \left(w_0 / 2 \right)^2} \right)^2 \right]^{1/2} \tag{4-4}$$

where x is the distance between a laser outlet and the sample, $w(x)$ is the beam diameter at the distance of x, w_0 is the beam diameter at the laser outlet, and λ is the laser wavelength.

As the polymer is heated by laser irradiation, there are phase changes occurring during the foaming and laser ablation processes. After foaming starts, air bubbles are generated. As a result, the density (ρ) of the polymer is reduced. At the same time, the absorption coefficient (α) and attenuation coefficient (β) are increased, because the bubbles scatter the laser and more laser energy is absorbed by the polymer. The material properties after the phase changes including the density (ρ), absorption coefficient (α), and attenuation coefficient (β) are defined as follows.

$$\chi = \begin{cases} \chi_s & ;T \le T_f + \Delta T_1 \\ \chi_f & ;T_f + \Delta T_1 < T \le T_A + \Delta T_2 \\ \chi_A & ;T \ge T_A + \Delta T_2 \end{cases} \tag{4-5}$$

where χ denotes any of the above three material properties, χ_s is the material property of unfoamed polymer, χ_f is that of foamed polymer, χ_A is that after ablation, T_f and T_A are the starting temperatures of foaming and ablation [38, 178], respectively, and ΔT_1 and ΔT_2 are the temperature ranges of foaming and ablation. Smoothed Heaviside step functions between phases are used to avoid extreme discontinuity and reduce convergence error in simulation.

The latent heats in the phase change processes are accounted with a discontinuity in the specific heat of material. The following equation described the relationship between the latent heat of phase change and the specific heat.

$$H = \int_{T_{start}}^{T_{end}} C_p dT \tag{4-6}$$

where H is the latent heat of phase change, T_{start} and T_{end} are the starting and ending temperatures of the phase change, respectively. Radice, *et al.* and Groulx, *et al.* [179, 180] suggested to define one parameter that can be used to track the progress of material over phase change. The specific heat of the polymer is thus defined over different temperature ranges as

$$C_p = \begin{cases} C_{ps} & ;T \le T_f \\ C_{p1} + \dfrac{d}{dT} H_f & ;T_f < T \le T_f + \Delta T_1 \\ C_{pf} & ;T_f + \Delta T_1 < T \le T_A \\ C_{p2} + \dfrac{d}{dT} H_A & ;T_A < T \le T_A + \Delta T_2 \\ C_{pA} & ;T \ge T_A + \Delta T_2 \end{cases} \tag{4-7}$$

where C_{ps} is the specific heat of unfoamed polymer, C_{pf} is the specific heat of foamed polymer, C_{pA} is the specific heat of ablated polymer, which has a similar value to air, C_{p1} is the changing specific heat during foaming, which follows a smoothed Heaviside step function from C_{ps} to C_{pf}, C_{p2} is the changing specific heat during ablation that can be expressed again as a smoothed Heaviside step function from C_{pf} to C_{pA}, and d/dT represents a Dirac delta function which is a derivative of the smoothed Heaviside step function.

In this chapter, CO_2 was used as the blowing agent and biodegradable PLA as the polymer matrix material. The latent heat of foaming was calculated using the latent heat of CO_2 sublimation and gas concentration of the saturated polymer sample. The latent heat of

CO_2 sublimation was chosen to be 25.2 kJ/mol [181]. The gas concentration was determined based on previous studies of solid state foaming of PLA [41, 182, 183]. To account for bubble growth in the PLA matrix, it was assumed that a certain amount of sublimation energy was consumed by CO_2 to expand the polymer matrix. This amount was determined to be 10% by matching the modeling and experimental results. The latent heat of ablation was obtained from a published thermal degradation study of PLA [184]. Parameters used in the model are summarized in Table 4-1.

Table 4-1. Parameters used in the model

Material property	Value
Ablation ending temperature	553.15 K
Ablation starting temperature	423.15 K
Absorption coefficient of foamed PLA	0.8
Absorption coefficient of PLA	0.4
Attenuation coefficient of foamed PLA	1075 1/mm
Attenuation coefficient of PLA	200 1/mm
Foamed PLA density (ρ_f)	376.4 kg/m^3
Foaming ending temperature	343.15 K
Foaming starting temperature	323.15 K
Laser beam diameter at laser outlet	2.5 ± 0.5 mm (1/e^2)
Laser peak power density	2.503 x 106 W/m^2
Latent heat of ablation	520 kJ/kg
Latent heat of foaming	55.250 kJ/kg
PLA density (ρ_s)	1250 kg/m^3
Specific heat of foamed PLA	1.195 kJ/(kg·K)
Specific heat of PLA	1.8 kJ/(kg·K)
Thermal conductivity of foamed PLA	0.013 W/(m·K)
Thermal conductivity of PLA	0.13 W/(m·K)

The FEA model was implemented using commercial software COMSOL Multiphysics® (COMSOL, Burlington, MA) with a backward differentiation and automatic time stepping procedure for computation. An extremely fine mesh was used and the minimum element size was 50 μm. The heat source was applied using a user-defined function of location and temperature. Once the entire computation process was completed, the temperature distribution was stored and utilized to estimate the foamed and laser-ablated regions within the simulation domain. The temperature of each element was compared to the foaming and ablation temperatures of PLA to determine the foaming and ablation regions. Figure 4-3 shows a block diagram of the solution procedure.

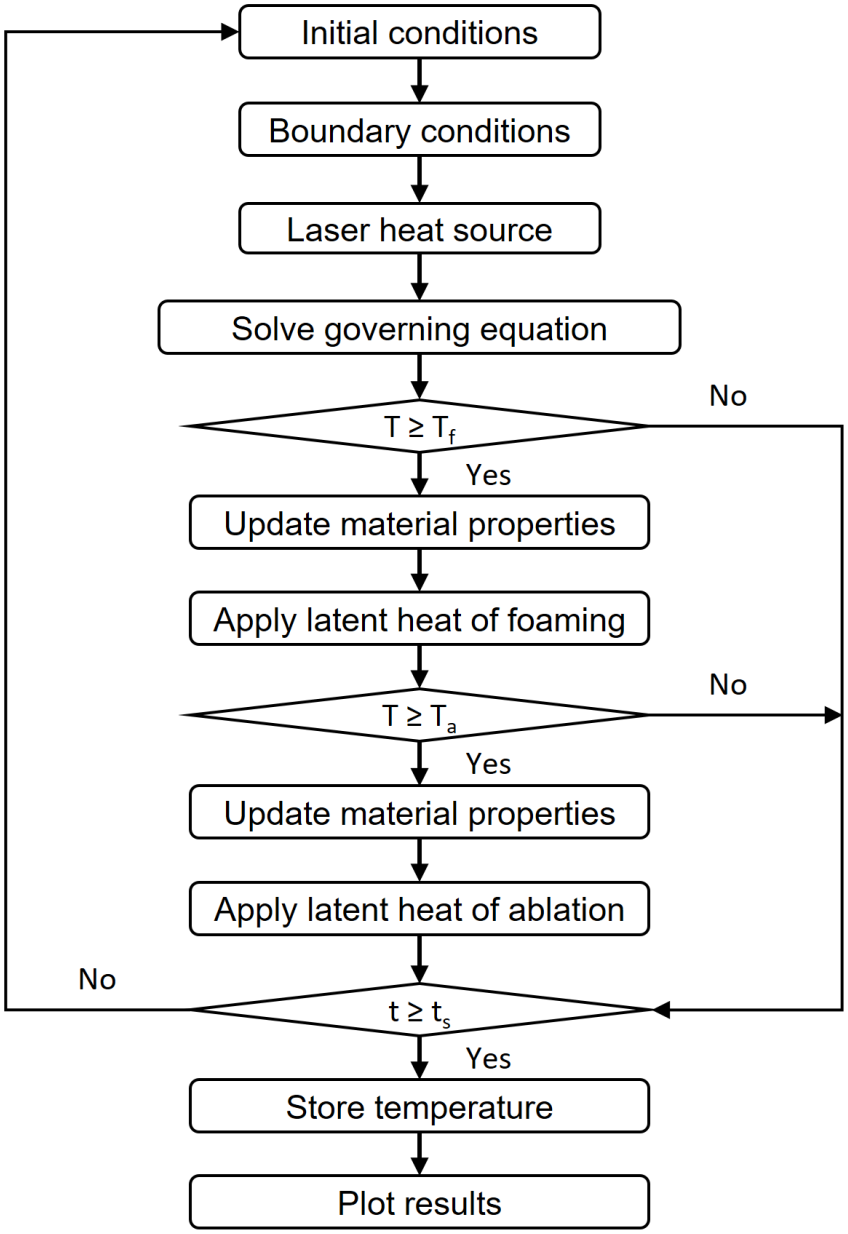

Figure 4-3. Solution procedure of the finite element model

4.3. EXPERIMENTS

The model developed in this study was validated with experimental data. Substrates used in the experiment were disc samples having a diameter of 30 mm and average thickness of 1.5 mm. The samples were injection-molded with PLA powder (ECORENE™ NW40) which is a mixture of D/L product from ICO Polymers (Allentown, PA). The PLA samples were placed in a high pressure CO_2 chamber until they reach the fully saturation condition. The saturation pressure was 2 MPa and the averaged concentration of CO_2 in the PLA samples was 8.5 wt% after the saturation process. After they were retrieved from the pressure vessel, the gas-impregnated samples were exposed under continuous laser irradiation by a CO_2 laser (Synrad Firestar v30 from Synrad, Inc., WA). For comparison, unsaturated samples were treated with the same laser conditions, with which only ablation was generated. Table 4-2 summarizes the sample conditions and laser parameters used in the experiment. Treated samples were freeze-fractured in liquid nitrogen. A scanning electron microscope (SEM) was used to obtain cross-sectional images of treated samples.

Table 4-2. Substrates and laser conditions used in the experiment

Parameter	Value
Saturation condition	Saturated at 2 MPa, Unsaturated
Laser power (W)	2.0, 4.9, 7.7, 10.3
Lasing time (s)	0.25, 0.5, 1.0

4.4. RESULTS AND DISCUSSION

4.4.1 Model validation

Laser attenuation in PLA is not well defined in literature due to its various crystallinity and L/D composition [185]. Therefore, the attenuation coefficients of both

unfoamed and foamed PLA were estimated with the ablation and foaming results with a laser power of 7.7 W and lasing time of 1 s. The attenuation coefficients were varied in the simulation and the predicted ablation and foaming regions were compared with the cross-sectional SEM images of the samples. The ablation and foaming regions were identified based on the ablation and foaming temperatures of PLA. Until the results were matched, these attenuation coefficients were determined to be 200 1/mm for solid PLA and 1075 1/mm for foamed PLA. Figure 4-4 shows the comparison between experimental and simulation results for both unfoamed and foamed samples under these conditions. The laser-ablation profiles were determined by the thermal degradation temperature of PLA. The color in Figure 4-4(d) represents the temperature distribution of foamed region predicted using the solid state foaming temperature of PLA. In both Figure 4-4(c) and 4-4(d), the elements in the ablated region were removed from the model.

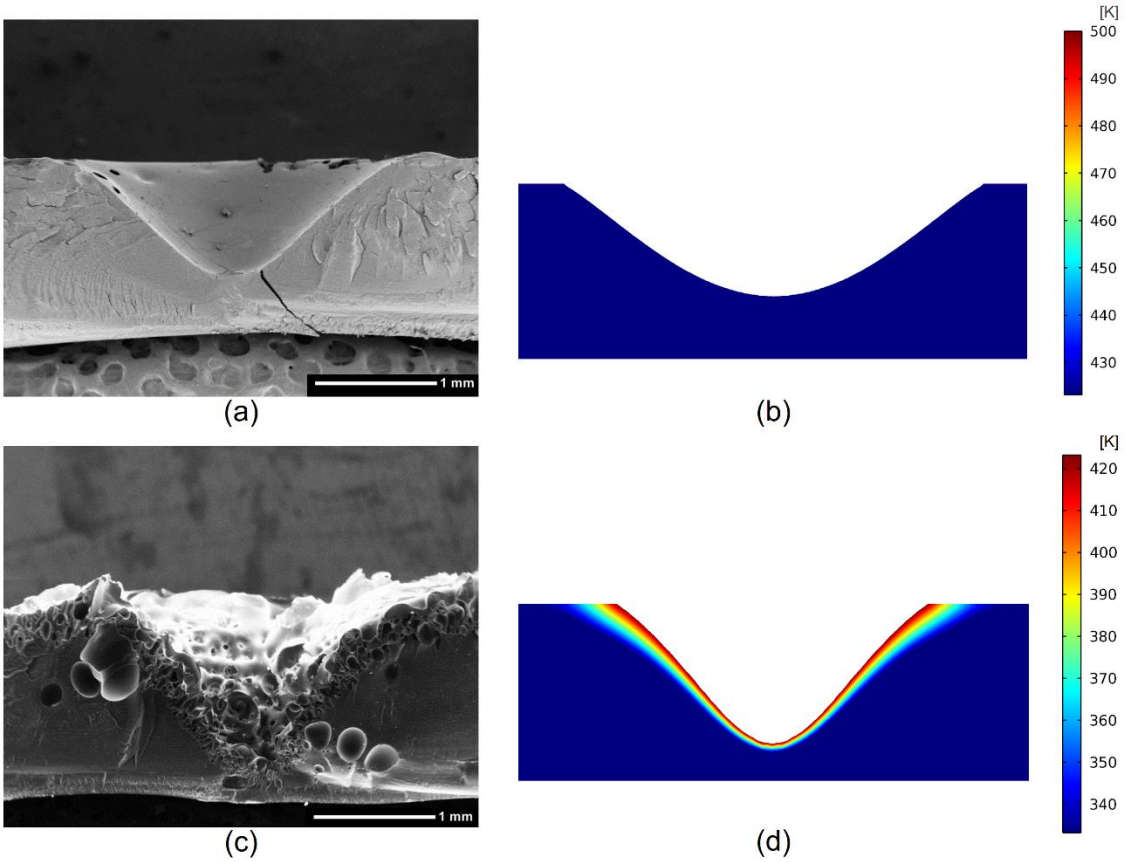

Figure 4-4. Comparison between experimental data and modeling results, (a) cross-sectional SEM image of laser ablated and unfoamed sample, (b) simulation result of the unfoamed sample, (c) cross-sectional SEM image of laser foamed and ablated sample, and (d) predicted temperature distribution of the foamed sample.

Once determined, the attenuation coefficients were used for the rest laser foaming conditions, with the laser power ranging from 2.0 W to 10.3 W and lasing time from 0.25 s to 1.00 s. Figure 4-5 shows the comparison between the modeling and experimental results. The predicted ablation and foaming profiles were overlaid with the corresponding cross-sectional SEM images from experiments. For all the laser foaming conditions, the predicted ablation and foaming profiles showed good agreement with the experimental results.

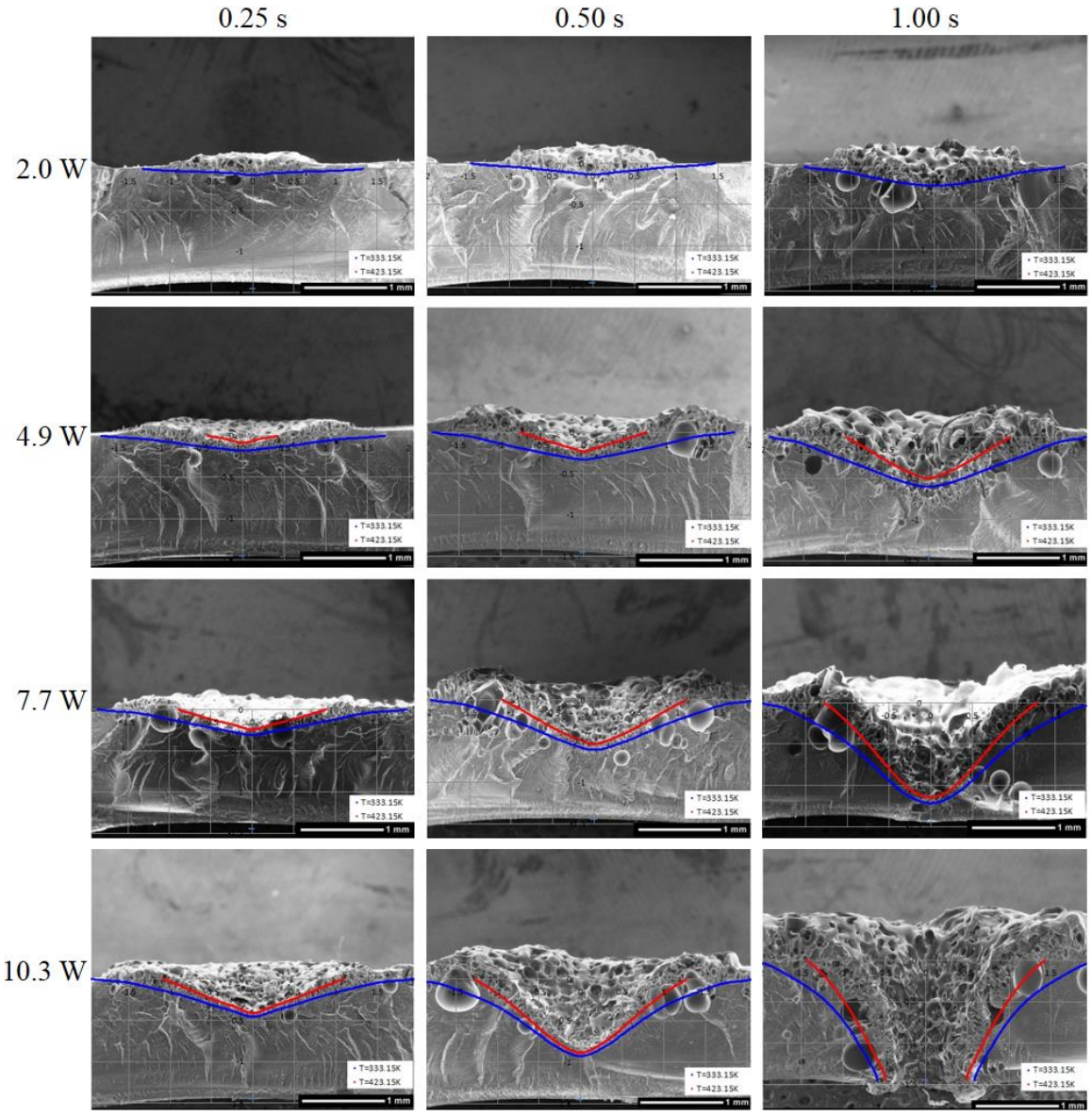

Figure 4-5. Comparison of predicted and experimental results. Ablation and foaming profiles are shown by the upper (red) and lower (blue) curves, respectively. Scale bars are all 1 mm.

In order to examine the combined effects of laser power and lasing time, the relationship between the volume of foamed region and laser energy is plotted in Figure 4-6 for both the simulation and experimental data. The volume of the foamed region was

considered to be cone shaped. The prediction from the FEA model is in good agreement with the experimental data at low laser energy. As the laser energy increases, the volume of foamed region is affected by the sample thickness, and therefore may not be accurately predicted. This however will not affect the applicability of the FEA model, since high laser energy settings will generate a through hole in the sample, a situation should be avoided in normal operations of the process.

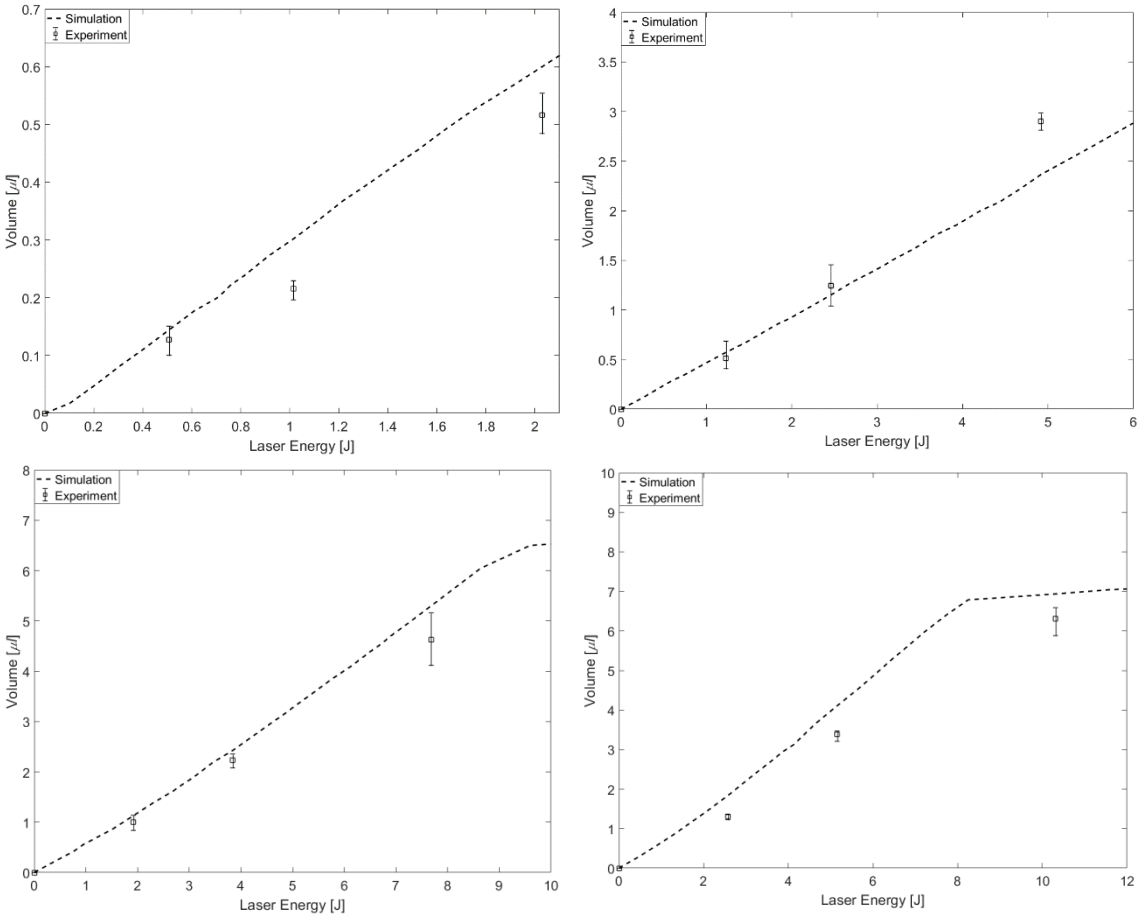

Figure 4-6. Volume of foamed region as a function of laser energy. Each graph has different laser power setup, (a) 2.0 W, (b) 4.6 W, (c) 7.7 W, and (d) 10.3 W.

4.4.2 Predicted temperature distribution

Predicted temperature distribution at the sample surface is shown in Figure 4-7. The laser power used in the simulation was 7.7 W. It is seen that the temperature profile changes significantly with time. Since the laser power density has a Gaussian distribution, the temperature at the center is much higher than that in the outer region. In addition, two phase change regions are observed for foaming and laser ablation, respectively. The first phase change happens at about 340 K when foaming starts. The second happens around 440 K when PLA starts to decompose. During the two phase changes, the temperature at the center of the laser irradiated region continues to rise. After foaming the center temperature increases dramatically due to enhanced laser absorption by the foamed structure.

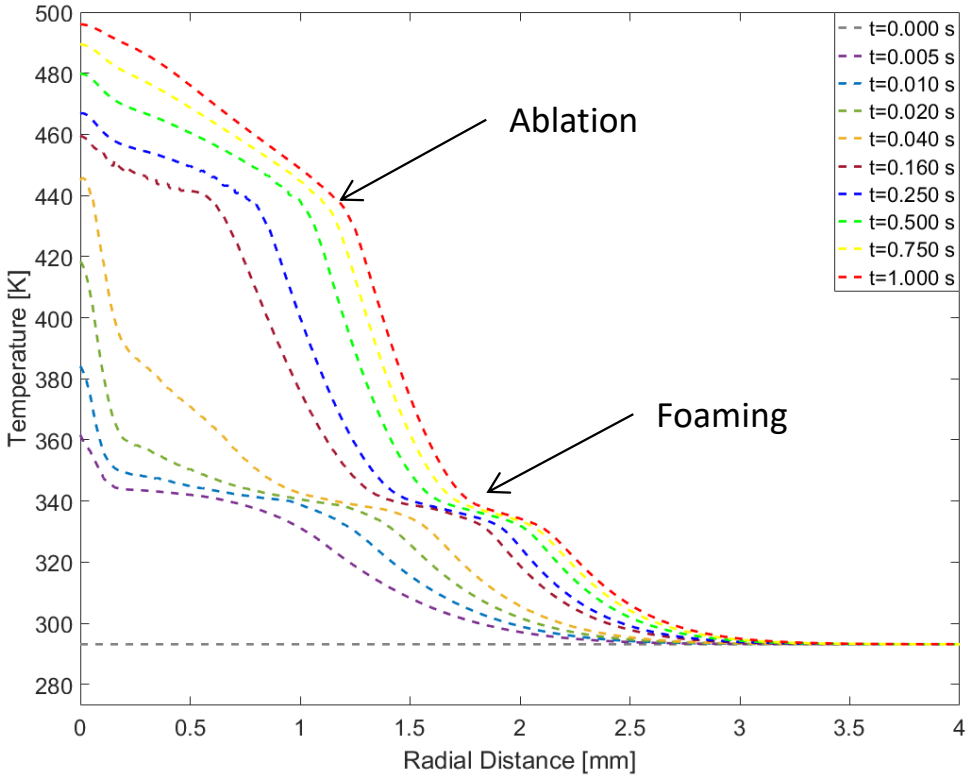

Figure 4-7. Temperature distribution on the top surface of a saturated sample at a laser power of 7.7 W

4.4.3 Effect of laser power and lasing time on the size of ablated region

The simulation model was used to study the effects of laser power and lasing time on the ablated region of foamed samples. The depth of ablated region as a function of lasing time is shown in Figure 4-8. Before it reaches the substrate thickness limit, the ablation depth has a linear relationship with lasing time. The slope of this linear trend is determined by the laser power. If the laser power is higher, the depth of ablated region reaches its limit faster. For example, a through-hole can be created within 0.8 s at a 10.3 W laser power (16% of the max laser power), while a 7.7 W laser power (12% of the max laser power) will not be able to create a through-hole even after 1 s of lasing time. For a lower power, e.g., 4.9 W (8% of max laser power), it is possible that ablation will not start until 0.1 s after the onset irradiation. For a 2.0 W laser power (4% of max laser power), there is no ablation generated. The diameter of ablated region as a function of lasing time is shown in Figure 4-9. Similar trends have been observed. The diameters of ablated regions approach to a certain limit. However, this limit is not caused by the thickness, but different power settings of the laser.

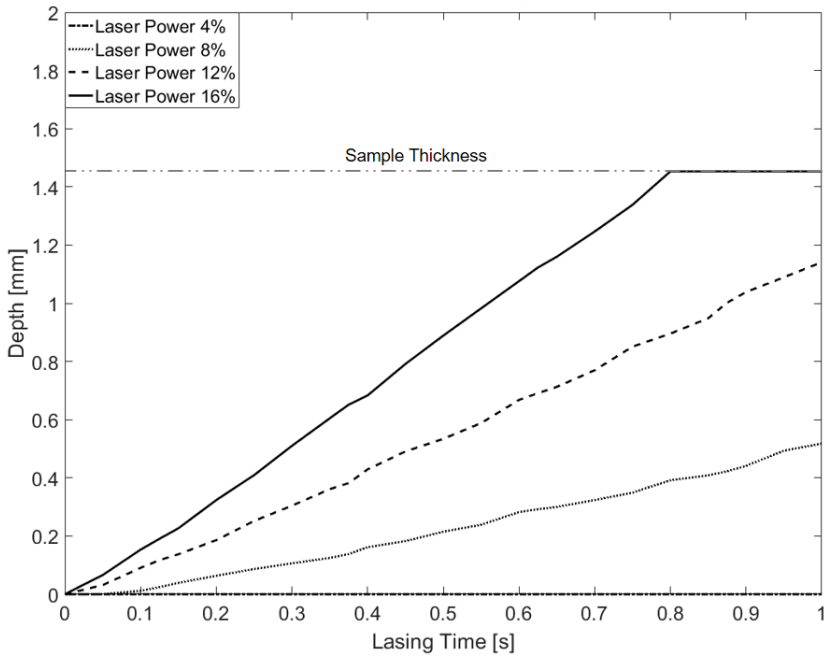

Figure 4-8. Depth of ablated region as a function of lasing time at different laser powers. 100 % indicates the maximum laser power

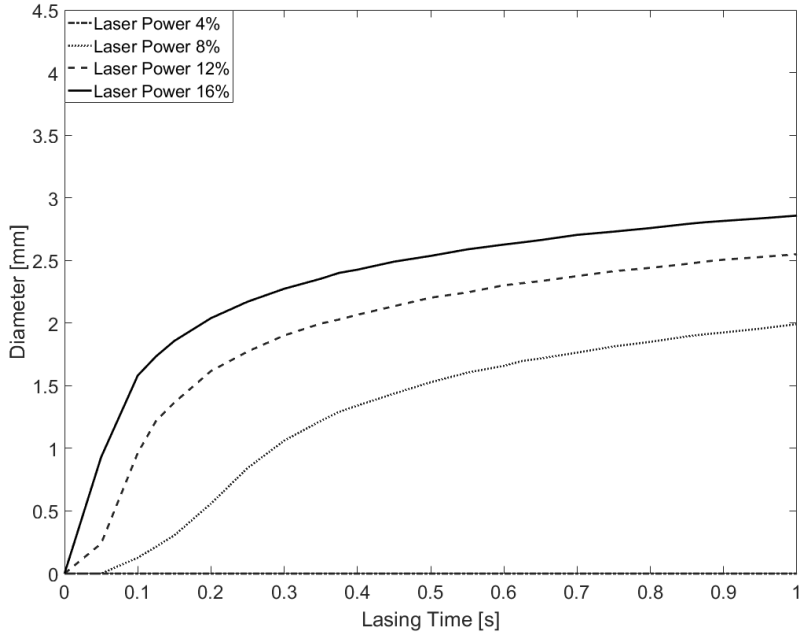

Figure 4-9. Diameter of ablated region as a function of lasing time with different laser powers

4.4.4 Effect of laser power and lasing time on the size of foamed region

The simulation model was also used to study the effect of laser power and lasing time on the size of foamed regions. The depths of foamed region are plotted with lasing time in Figure 4-10, which shows similar characteristics as the ablation depth seen in Figure 4-8. However, there is almost no delay in foaming. Foaming occurs as soon as the laser starts to irradiate on the samples. This is because the temperature threshold for foaming is much lower than that for ablation.

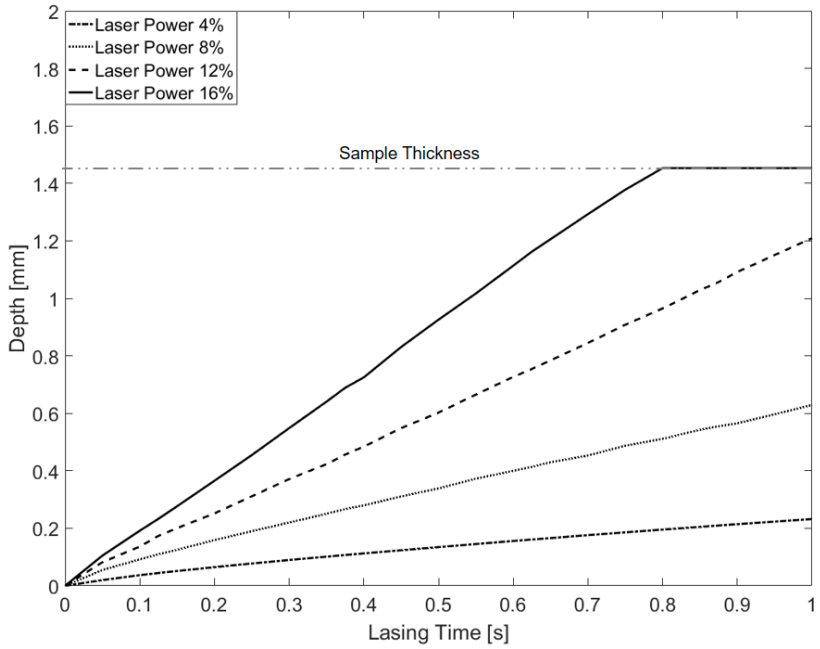

Figure 4-10. Depth of foamed region as a function of lasing time at different laser powers

The diameters of foamed regions under different power settings are shown in Figure 4-11. The foamed diameters are plotted in terms of lasing time and each line represents a different laser power. Similar to the ablated diameter, the relationship between the foamed region diameter and lasing time follows a logistic function. However, the diameter of foamed region is much larger and approaches to its steady state value much faster. For example, the 7.7 W laser power generates a foamed region about 4 mm in diameter,

whereas the ablation region diameter is only 2.5 mm. In addition, the final diameters of foamed regions under different laser powers are also different, similar to the trend seen in Figure 4-9. This is due to the Gaussian distribution of laser power density, which causes a different spot size at any given laser power setting.

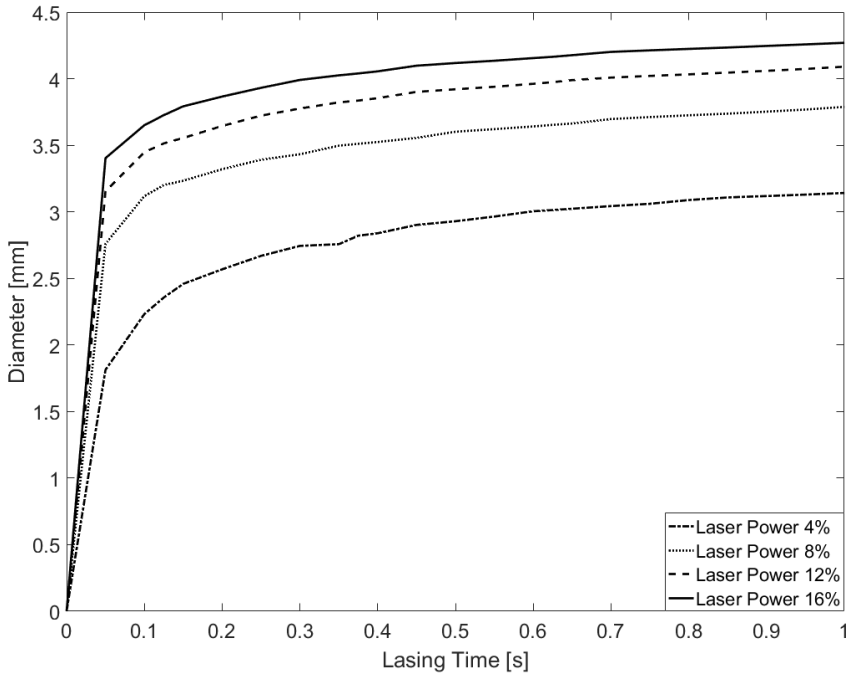

Figure 4-11. Diameter of foamed region as a function of lasing time at different laser powers

As seen in Figs. 4-9 and 4-11, both foaming and ablation occur rapidly in the initial stage of the process and the diameter approaches to a certain equilibrium value at a given laser power. A higher laser power tends to yield a larger foamed and ablated region. This is because that the diameters of the foamed and ablated regions are affected by the distribution of the laser power density. As shown in Figure 4-12, assuming the same power density will lead to the same temperature increase, the foaming and ablation temperature will impose two different thresholds on the Gaussian distribution of the lase power density.

Different power settings will lead to different diameters of the foamed and ablated regions. Therefore, laser power instead of lasing time should be used to obtain scaffolds with different diameters.

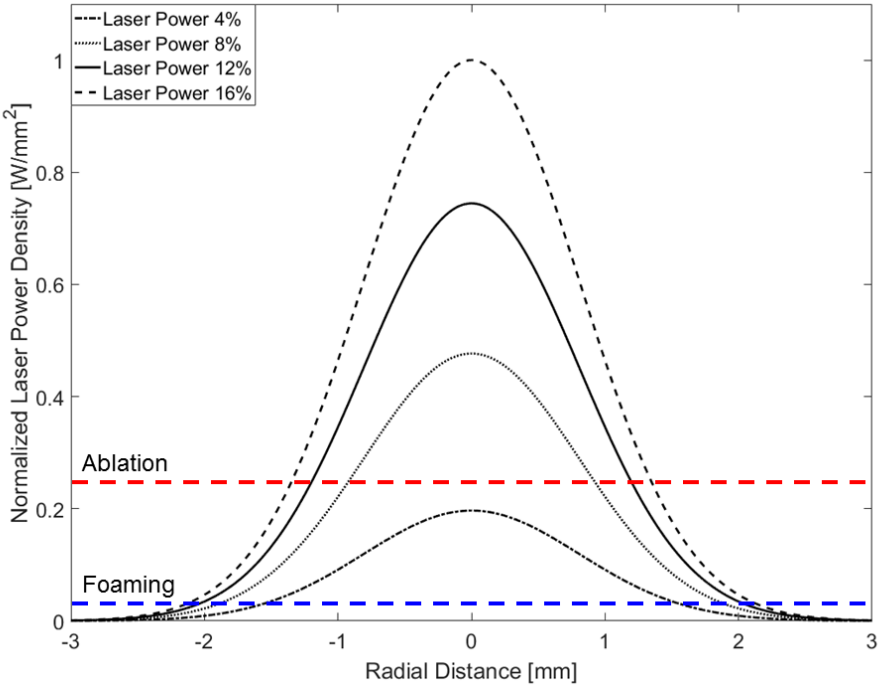

Figure 4-12. Normalized laser power density along with radial direction of laser beam

4.5. CONCLUSIONS

A finite element model has been developed to study the selective laser foaming process. The model was validated with experimental data. It has been found that once foaming occurs, the temperature increases dramatically because of the enhanced laser absorption effect of porous structure. For a fixed laser power, the depths of both ablated and foamed regions are linearly proportional to the lasing time before they reach a limit defined by the substrate thickness. Laser power has an effect on the slope of this linear trend. The diameters of the ablated and foamed regions increase rapidly at the early stage of the process and approach to a limit determined by the laser power setting. Therefore,

laser power is a more effective variable to use in order to control the diameter of the foamed and ablated regions. Laser foaming is a complex process involving heating, foaming and ablation. The FEA model developed in this study provides a useful tool to aid future development of the process.

Chapter 5. Fabrication of High Throughput Three-Dimensional Cell Culture Platform on a Compact Disc

5.1. INTRODUCTION

As mentioned above, the traditional two-dimensional (2D) cell culture has a lack of the complex and dynamic microenvironment of an ECM-like structure and it causes the cells to lose certain functionality [3]. On the other hand, three-dimensional structure such as porous polymers can provide the *in vivo*-like environment. The concept of cell culture in a 3D structure are integrated with the microfluidic channel to mimic multi-organ interaction and key physiological and pathological processes *in vivo* [13]. Thus, the 3D perfusion-based device allows a realistic 3D tissue model system for a variety of biomedical related studies, such as drug discovery. The *in-vitro* 3D tissue model systems can be utilized to improve test results via mimicking *in vivo* functions of human organ including liver metabolism [16, 17]. Recently, a 3D two-chamber tissue model system for drug studies was developed in our lab [22]. The two chambers allowed liver and brain tumor cells to reproduce *in vivo* tissue-like structures via providing a 3D environment. The effects of liver metabolism on cancer treatment drugs could be studied using the system. However, it has certain limitations for high throughput applications. The size of the 3D two chamber system should be reduced to fabricated multiple systems on one platform. Therefore, it is proposed to fabricate a micro-scale 3D tissue scaffold systems on a compact disc (CD) with selective laser foaming, as shown in Figure 5-1. Localized foamed wells will be fabricated in line and connected with micro-channels on a CD. Reservoirs for culture medium will be micro-machined on the center side and waste chambers will be positioned on the outer side. All the cell culture wells and chambers will be radially arranged in line. Cell seeding and nutrient diffusion will be assisted with the centrifugal force generated by disc rotation.

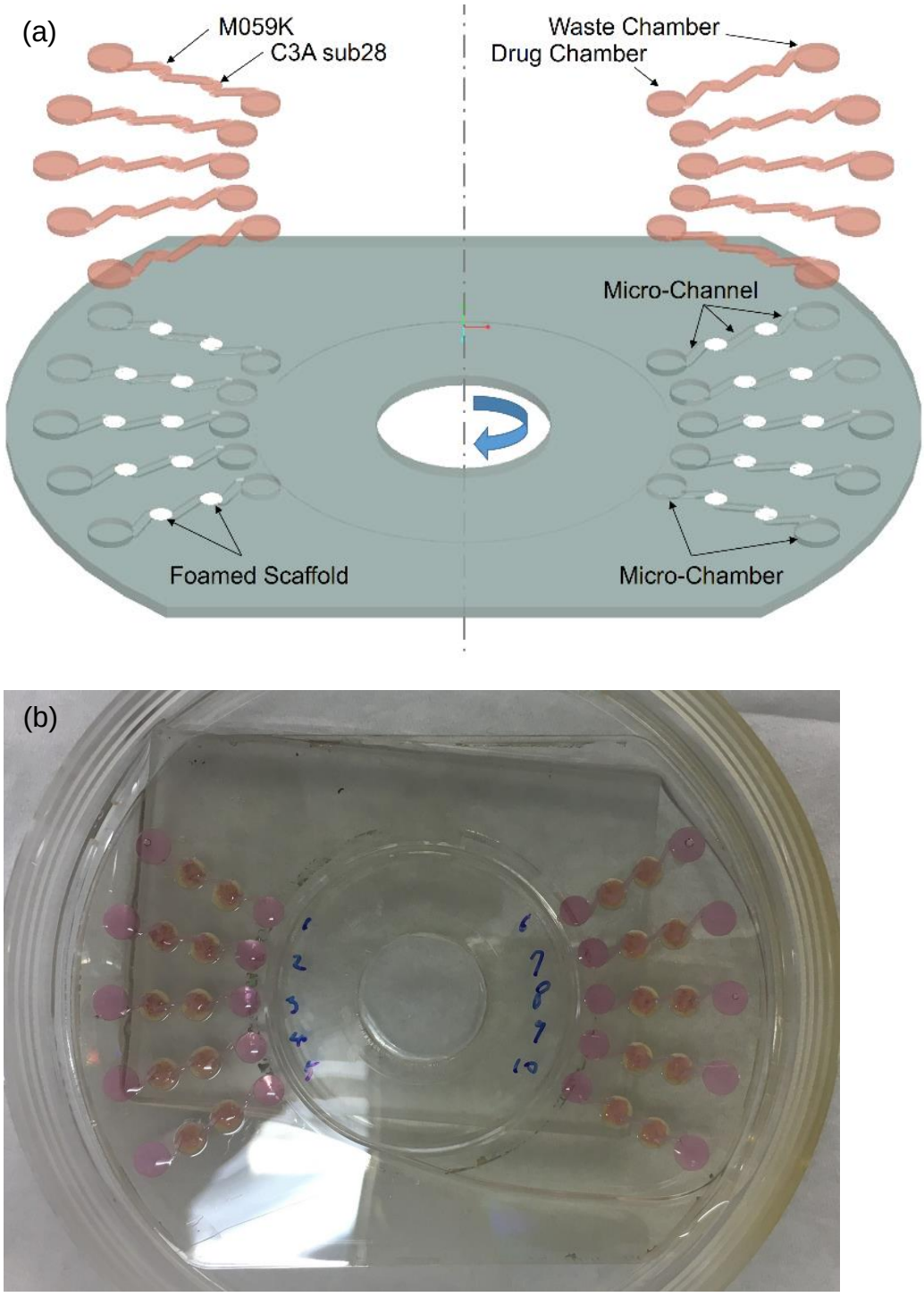

Figure 5-1. Schematic of the centrifugation-based tissue model system (a) and actual system after cell seeding (b)

A key step to create the proposed high throughput tissue model platform is to fabricate the micro-scaled tissue scaffolds on a CD, for which a newly developed selective laser foaming process is used in this study. The selective laser foaming process has been demonstrated [169] with polylactic acid (PLA), a semi-crystalline polymeric material. While PLA could be molded into CDs, in this study we proposed to use commercially available CDs for device fabrication. Commercially available CDs are made of polycarbonate (PC). As an amorphous, the gas saturation and foaming characteristic of PC are significantly different from PLA. On the other hand, the glass transition temperature of PC is 150 ºC, allowing it to be sterilized using autoclave, a benefit over both PLA and commonly used polystyrene (PS) for 3D cell culture devices.

In this chapter, we present a study of the selective laser foaming process with PC CDs. We determine the effect of process parameters including gas concentration, laser power, exposure time, pulsation, and laser energy. Two micro-chambers and micro-channels were micro-machined on the disc surfaces after laser foaming. The surface of the device was coated with polydopamine to increase hydrophilicity. The increased hydrophilicity was confirmed by measuring a contact angle. The rotation stage was developed and controlled with a stepper motor controller. It was demonstrated that the centrifugal force could accelerate diffusion in the system. The high thorough-put 3D tissue model was evaluated using human glioblastoma and hepatoblastoma cells.

5.2. EXPERIMENTS

5.2.1 Materials, cells, and chemicals

The commercially available compact disc (CD) used in this study was a business card disc acquired from Ritek (Taiwan). For the physical blowing agent, medical grade CO_2 (99.9% purity) was used in the gas sorption process and it was obtained from Airgas

Nor Pac, Inc. Dopamine-hydrochloride and Tris (tris(hydroxymethyl)aminomethane) base were purchased from Thermo Fisher Scientific (Waltham, MA).

Human brain tumor cells representing glioblastoma multiforme (GBM) (cell line M09K) were purchased from American Type Culture Collection (ATCC, Manassas, VA), and were used in the cell culture study. Human hepatoblastoma (cell line C3A-sub28) were obtained from ATCC and the cell line was generated from C3A cells for enhanced expression of CYP3A4 mRNA and CYP3A4-mediated activity at the University of Eastern Finland [186]. Dulbecco's modified Eagle medium (DMEM) with 4500 mg/L glucose, L-glutamine, sodium pyruvate, and sodium bicarbonate was acquired from Sigma–Aldrich (St Louis, Missouri). Fetal bovine serum (FBS) with endotoxin (≤ 5EU/ml) and hemoglobin (≤ 10mg/dl) was purchased from Thermo Fisher Scientific (Waltham, MA). Penicillin/streptomycin (PS) and Dulbecco's phosphate buffered saline (DPBS) was obtained from Sigma–Aldrich (St Louis, Missouri). Cell viability was qualitatively evaluated using the live/dead staining solution. The live/dead stain assay was obtained from Invitrogen Inc. (Carlsbad, CA).

5.2.2 3D scaffold platform fabrication

Polycarbonate CDs were laser-foamed via two stages of selective laser foaming as shown in Figure 5-2: CO_2 gas saturation and foaming. In the gas saturation stage, the CDs were saturated with CO_2 in a pressure vessel with a 2 MPa gas pressure for 11, 22, 33, and 44 hours at room temperature. Gas saturated samples were taken out of the pressure chamber and their weights measured to determine CO_2 concentration. CO_2-saturated CDs were mounted on a computer-controlled XYZ positioner (MAXNC 10 from MAXNC, Inc.) for laser foaming. The laser conditions in this study are shown in Table 5-1.

Table 5-1. Parameters for laser foaming of polycarbonate CD

Parameter	Value
Saturation pressure (MPa)	2
Saturation temperature (°C)	21
Saturation time (hr)	11, 22, 33, 44
Laser power (W)	0.54-33.7
Laser exposure time (s)	0.016-1
Laser pulses	1, 10

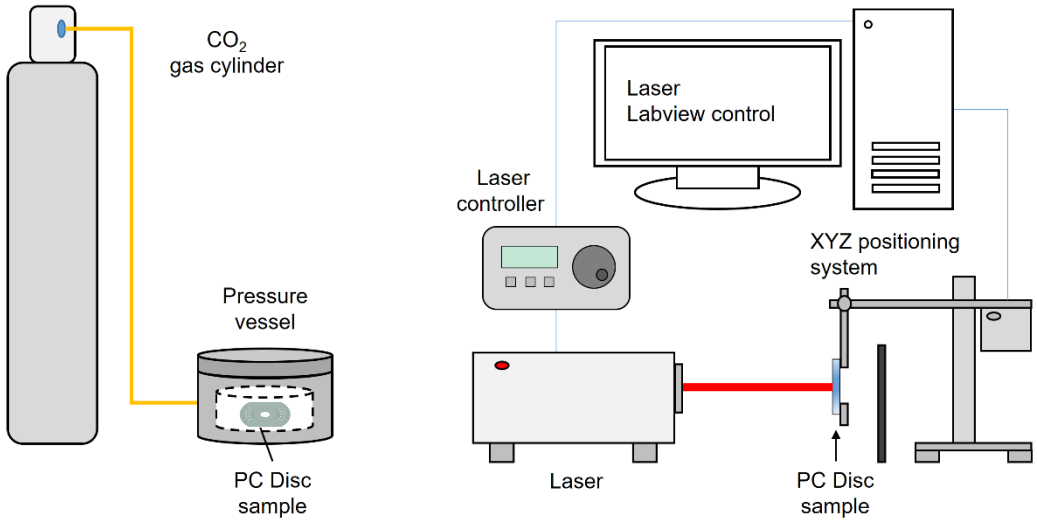

Figure 5-2. Schematics of major experiment processes [169]

For parametric study, each CD has 26 foamed spots as shown in Figure 5-6. A continuous CO_2 laser was used (Synrad Firestar v30 from Synrad, Inc., WA). The wavelength of the laser was 10.6 μm and the beam diameter was 2.5±0.5 mm. The maximum averaged laser power that could be achieved was 35 W. A LabVIEW program

was developed to control the laser exposure time and pulse rate. A Synrad UC-2000 control unit was used to control the laser power. Laser power according to laser controller setting was measured and calibrated using laser power meter, and the result is shown in Figure 5-3. The dash lines are a curve-fitted line with an R^2 value of 0.999. The average laser power has a range from 0.54 W to 33.7 W, corresponding to a power density between 11 W/cm^2 to 686 W/cm^2, and the lasing time varied from 0.016 s to 1.00 s. Laser pulses having 50% duty cycle were generated using the LabVIEW control project, 1 pulse and 10 pulses. For a comparison of the samples, other parameters were identical.

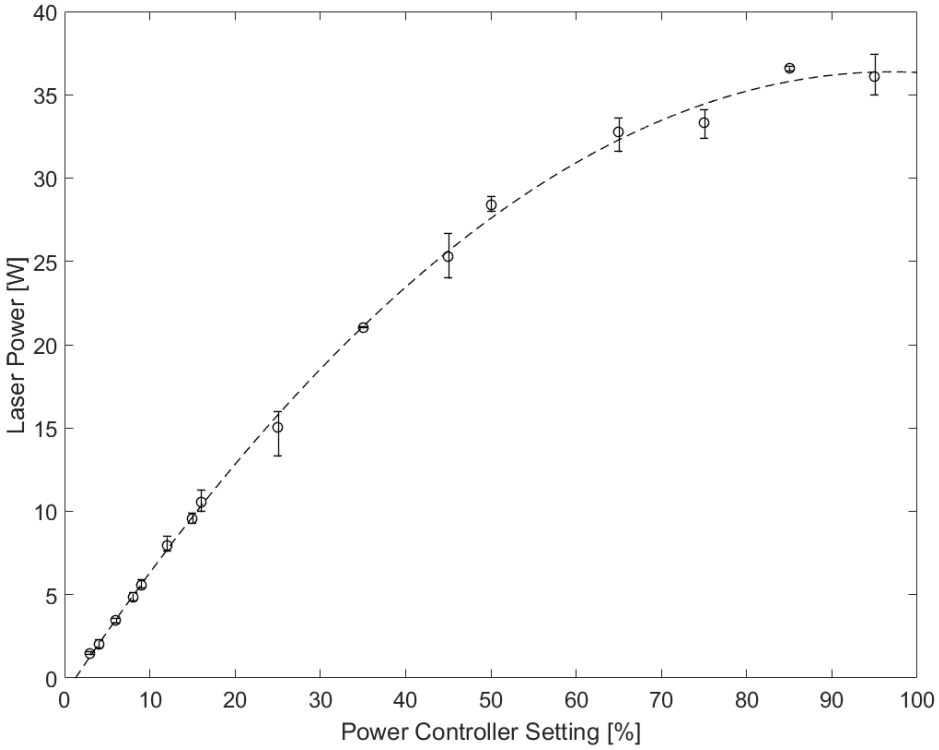

Figure 5-3. Laser power according to percentage setting of laser control unit

After the parametric study, another G-code for XYZ positioner was modified to generate aligned foamed spots as described in Figure 5-1. Foamed CDs were exposed to ambient conditions for a week to desorb the remaining CO_2. A fully open structure was

necessary for cell culturing on the foamed area. The skin layer on the foamed spot was mechanically removed. The samples were placed in liquid nitrogen for 1 min and the skin layer was cut off using a razor blade. Micro-channels and micro-chambers were micro-machined using PCB prototyping machine (cirQoid, Latvia). The machine was controlled manually via several G-codes written based on the schematics in Figure 5-1. During the machining, air is blown on drill bits (500 μm and 2 mm) to cool the bits and to remove chips.

A protective layer and a metal reflective-data layer on the back of the CDs were removed. The CDs without those layers were submerged in 100 % ethanol and sonicated to remove oil that come from the airgun while micro-machining and organic dye on the back for 1 hours using a Branson 3510 ultrasonic cleaner (Branso Ultrasonic, Danbury, CT). Then, the CD samples were rinsed with running distilled water for 1 min. The samples were dried in a vacuum oven at 35 ºC overnight before polydopamine (PDA) coating.

For polydopamine coating, 1.8 g of dopamine-HCl was dissolved in 900 ml of (tris(hydroxymethyl)- aminomethane)-hydrochloride (Tris-HCl) (10 mM, pH8.5). In order to get complete dissolution, the solution was stirred for 1 min at 850 rpm (mass concentration: 2 mg/mL) [187]. The CD samples were then quickly immersed and vertically oriented in the solution for 4 hours. During the polymerization, the solution was stirred at 400 rpm, then the polydopamine coated CDs were rinsed with deionized water thoroughly. The samples were dried in vacuum oven at 25 ºC for 1 day before sterilization and cell culturing.

5.2.3 Microstructure characterization and contact angle goniometry

The samples were freeze-fractured with liquid nitrogen for microstructure examination. The fractured foamed spots were sputter coated with gold and palladium using an EMS 500x sputter coater (Electron Microscopy Science, Hatfield, PA). The microstructure of the laser foamed samples was characterized using a JEOL NeoScope JCM-5000 (Nikon®, UK) scanning electron microscope (SEM) under 5-10 kV accelerating voltage and 0.1 nA beam current. The image processing software, ImageJ, from National Institutes of Health was used to analyze the SEM image [154]. Static water contact angles of the bare surface and the PDA coating were measured using FTÅ 200 contact angle analyzer (First Ten Ångstroms, Inc., Portsmouth, Virginia). The static sessile drop method was used to perform the measurement. Deionized water was delivered on the surfaces using a syringe controlled by FTA program and images of the droplets were taken within 3 s of placing the droplets.

5.2.4 Disc rotation stage with a humidity chamber

A chamber was fabricated to maintain humidity during rotation of our system. The humidity could not be controlled, but it maintained the maximum humidity at the room temperature by adding four Petri dishes filled with distilled water. It was made of acrylic sheets (6 mm of thickness) and the sheets were cut using P-series laser cutter (Full Spectrum Laser, Las Vegas, NV). A rotation state consists of four parts including stepper motor with spindle platter, stepper drive, Arduino Uno, and power supply. The stepper motor, stepper drive, and power supply were purchased from AutomationDirect.com Inc. (Atlanta, GA). The motor control code was based on a code in open Arduino stepper library. The setup is seen in Figure 5-4. The ration speed of the spindle platter was measured using a laser tachometer (AGPtek®, Brooklyn, NY).

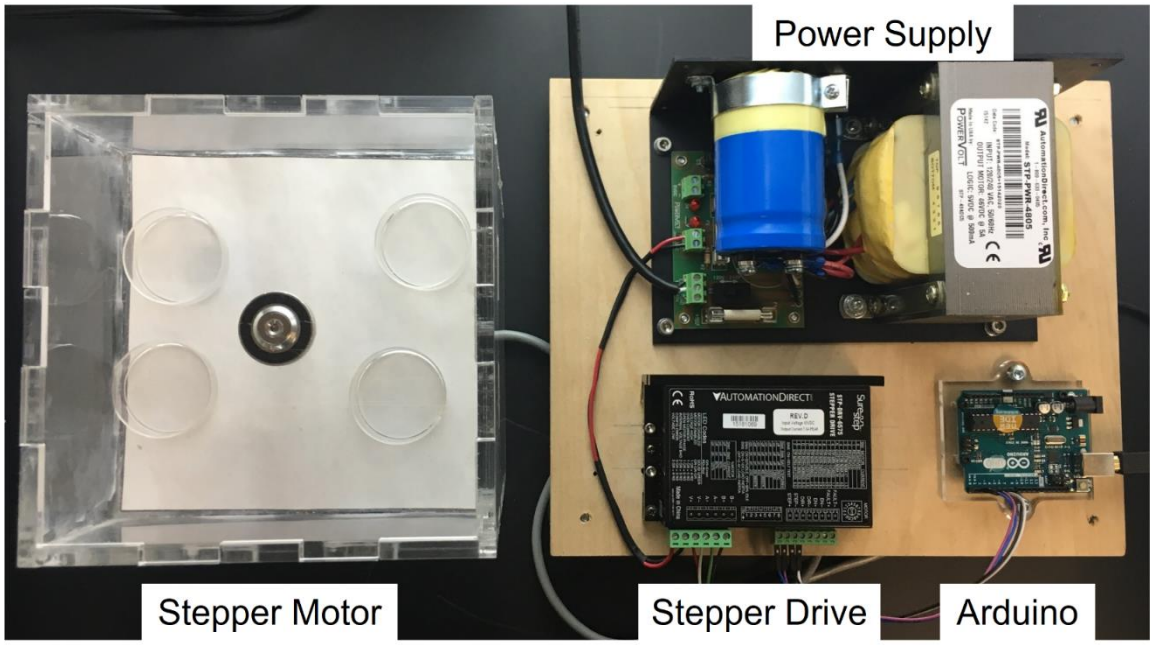

Figure 5-4. Experimental apparatus setup, rotation stage and control system

5.2.5 Sterilization and cell culture

After polydopamine coating, the samples were rinsed using distilled water several times and sterilized with 70 % ethanol for 30 min. The samples were placed in a vacuum oven at 25 ºC overnight and then exposed to ultraviolet light for 30 min. Cell culture medium (1.5 µl) was dropped on the foamed regions. The CD samples were placed on an acrylic block in a Petri-dish and 4 ml of distilled water was put in the Petri-dish to prevent dry-out of the culture medium. The samples with the cell culture medium were at 37 ºC and 5 % CO_2 for more than two days before cell seeding. The cell culture medium was made of DMEM mixed with 10% of FBS and 1% of PS. The blended solution was filtered using Stericup®/ Steritop® and a vacuum pump. The cell culture medium on the foamed areas was removed. Human brain tumor cells (M059K) and human liver cells (C3A-sub28) were seeded in the laser foamed regions as shown in Figure 5-1. After cell seeding, the samples were placed in an incubator for 2 hours in order to make cells settled on a foamed

surface. The micro-channel and micro-chambers were then filled with cell culture medium. Cell concentration was measured using a microscope and a hemocytometer.

5.2.6 Cell viability assessment

To evaluate cell viability and morphology of two different cells lines (M059K and C3A-sub28), two types of cells were stained using a live/dead viability/ cytotoxicity kit (calcein-AM and ethidium homodimer-1). The dyes were diluted with DPBS. Before cell staining, the culture medium in our system (including foamed region, micro-channel, and micro-chamber) was removed and the staining solution was added in the system. The samples were incubated for 20 minutes and then the samples were moved to two types of microscopes. Images of two different cell lines were taken using an upright fluorescent stereomicroscope (LEICA M205 FA) and an inverted fluorescence confocal microscope (LEICA SP8).

All data were analyzed and expressed as mean ± standard deviation. The statistical significance was analyzed using student's *t*-tests while comparing data pairs. A *p*-value smaller than 0.05 ($p < 0.05$) indicated that there is significant difference.

5.3. Result and Discussion

5.3.1 Effect of CO_2 concentration

Table 5-2. shows the CO_2 absorption behavior of a polycarbonate CD sample under 2 MPa gas pressure. Four different gas absorption times were chosen to determine the CO_2 gas concentration and to evaluate its effect on the porous structure. The results were in agreement with our previous experiment using other materials such as poly methyl methacrylate (PMMA) and poly lactic acid (PLA) [169, 188]. The gas concentration increases along a gradient which is determined by gas pressure. The increment of the

concentration decreases around saturation and then the CO_2 concentration in the sample reaches saturation.

Table 5-2. Gas concentration of polycarbonate CDs

Parameter	Value			
Absorption Time [hr]	11	22	33	44
Weight of CD before gas sorption [g]	5.2571	5.2612	5.6009	5.8245
Weight of CD after gas sorption [g]	5.3661	5.4198	5.7905	6.0447
Gas concentration [wt%]	2.07	3.01	3.39	3.78

The effect of gas concentration on a microstructure of laser-foaming is described in Figure 5-5. A previous study demonstrated that the pore size underneath the laser-foamed surface is mainly dependent on the blowing agent concentration [169]. In order to evaluate the effect of CO_2 concentration, all the samples were laser-foamed with the identical condition, the laser power of 25.83 W for 0.02 sec. As shown in Figure 5-5, the pore size decreases and the porous structure gets denser, as the gas saturation time (i.e., CO_2 concentration in the sample) increases. This result is consistent with bulk foaming results, where pore size is strongly affected by the saturation pressure, thus the gas concentration in the polymer sample. The difference between laser foaming and bulk foaming is that a solid skin layer will form in the bulk foaming process, whereas in laser foaming, the top surface of the foamed region has an open cell structure. The pore size in the open cell structure tends to be bigger than those underneath, indicating that the surface of the laser processed region may be molten during the foaming process. This open cell structure is needed for cell culture, since cells need openings to enter the porous structure underneath the surface.

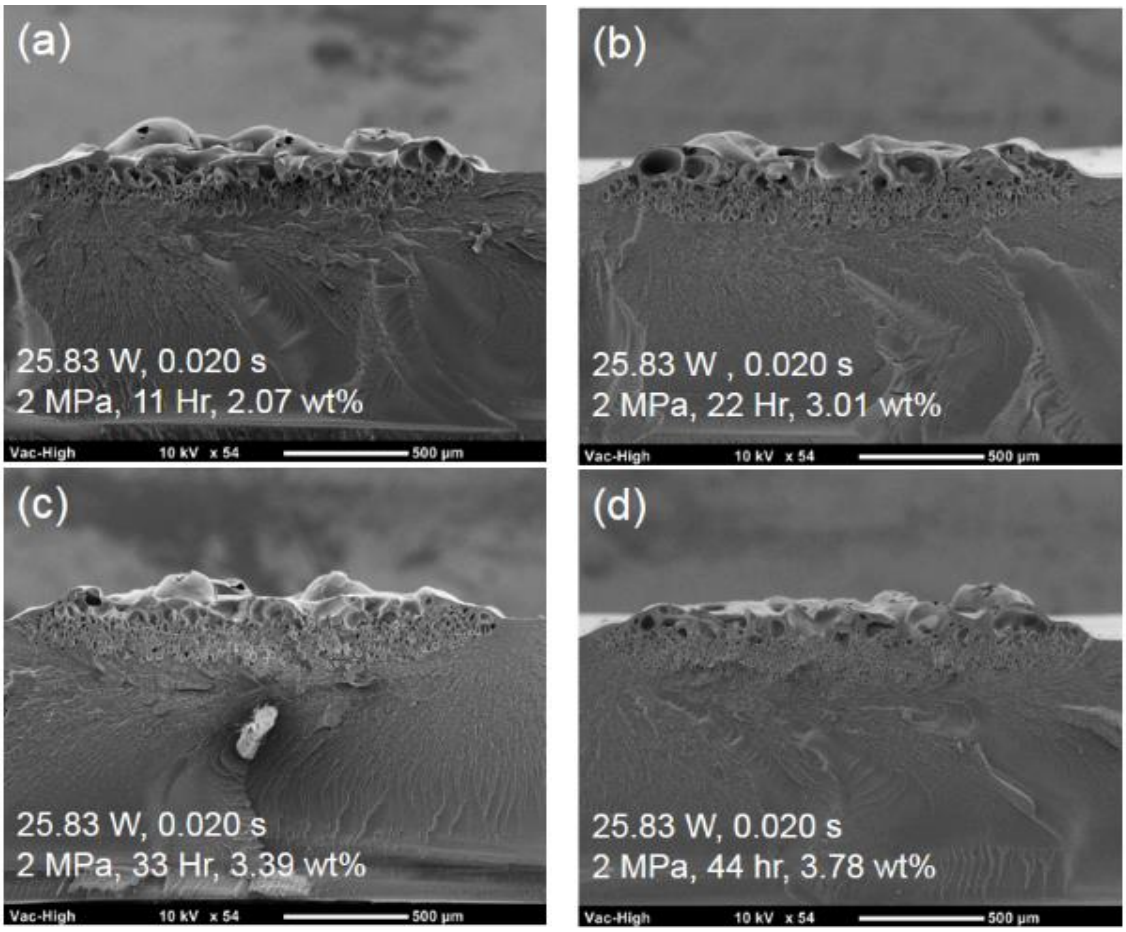

Figure 5-5. Effect of gas concentration on porous structure

5.3.2 Effects of laser foaming parameters

The effects of laser energy are shown in Figure 5-6. The numbers under the spot indicate the laser power (in percentage) and exposure time. All these spots were made with a single laser pulse. It is seen that the size of the laser-foamed region increases as the laser power and lasing time increase, i.e., the total laser energy increases. However, there are differences between the PLA and PC samples in the laser foaming process, it requires much more energy to generate inverse cone-shaped micro-wells in PC samples. In our study, the energy required is determined to be about 1.7 J on the PC sample, whereas PLA was ablated with the laser energy of 1 J. Second, there is char forming in the foamed region for PC

samples. This may be due to the fact that the ablation mechanisms differ for the two types of polymers with different chemical structures [189]. In the case of unsaturated polycarbonate, the char formation is related to the kinetic relationships between the rates of growth and removal of the charred layer. A char layer can be generated with a low laser density up to 50 W/cm^2 on PC and no char layer can be produced at higher level power densities over 200 W/cm^2. This is because the rate of its formation is equal to or less than the rate of ablation by sublimation [190]. However, gas-saturated polycarbonate showed a different characteristics. The char layer was created over laser power of 200 W/cm^2. This can be explained by the fact that the gas saturation process changes the thermal and physical characteristics of the PC. The char growth rate and its properties highly depends on the thermo-physical characteristics of the material, and can be related to the morphology and characteristics of the porous structure of the char [189]. The char layer might have a negative effect on the cell culture, so the layer needs to be removed from the surface. In this study, the char layer was mechanically removed using a razor blade after a sample was frozen using liquid nitrogen. The liquid nitrogen was utilized to make the sample more brittle, so it would be easier to remove the char layer and the microstructure would have minimum damages.

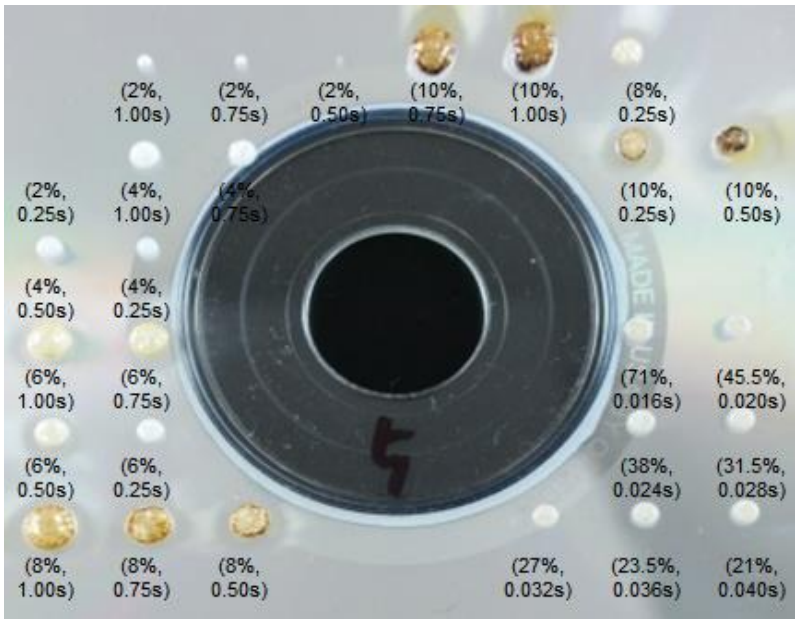

Figure 5-6. Polycarbonate CD sample after laser foaming (laser settings are below the spots). Samples were saturated for 44 hours.

Typical microstructures of the laser foamed spots are shown in Figure 5-7. The PC sample was saturated for 44 hours under 2 MPa. The resulting CO_2 concentration was 3.78 wt%. The laser foaming parameters are shown at the bottom right-corner of each image. Figure 5-7(b) represents a preferable microstructure than Figure 5-7(a), since the open cell structure is more uniform. In addition, sizes of the open cell structures have a range from 100 μm to 300 μm which are a range of optimum pore sizes reported [191-196] As a result, more laser energy may be beneficial for PC scaffold fabrication. However, too much energy could generate a charred surface, which would need an extra step (a mechanical removal) to remove. From the SEM image analysis of all the experimental cases conducted in this study, the energy required to generate an inverse cone-shaped well in the selective laser foaming process was determined to be 1.7 J.

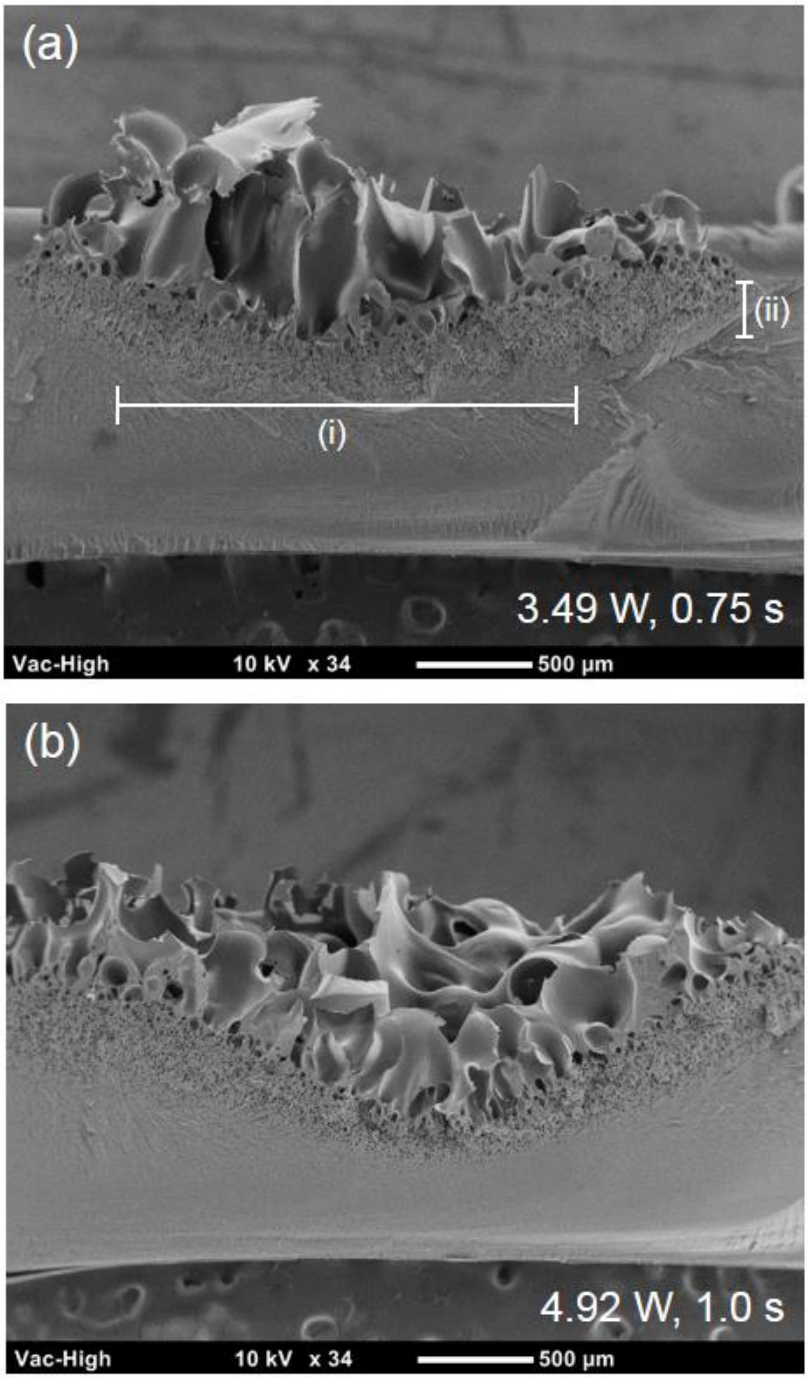

Figure 5-7. Effects of laser parameters on inverse cone-shaped well. (i) diameter, (ii) depth.

As the laser power and lasing time increase, the diameter and depth of the well also increase. The overall volume of the inverse cone-shaped well was calculated using diameter and depth defined in Figure 5-7(a). The relationship between the laser energy and the volume of the well is shown in Figure 5-8. The relationship exhibits two proportional increasing trends. This is because the laser intensity has a Gaussian distribution, so different laser powers have an effect on the laser diameter. Therefore, the higher the laser power, the stiffer the gradient in the relationship. In other words, higher power laser ablates the material faster. The overall relationship between the laser energy and volume of the well (3.48 W and 4.92 W) can be analyzed using Figure 5-8. The relationship exhibits an exponentially increasing trend, which may be due to the effect of nonlinear heating caused by the generation of a porous structure.

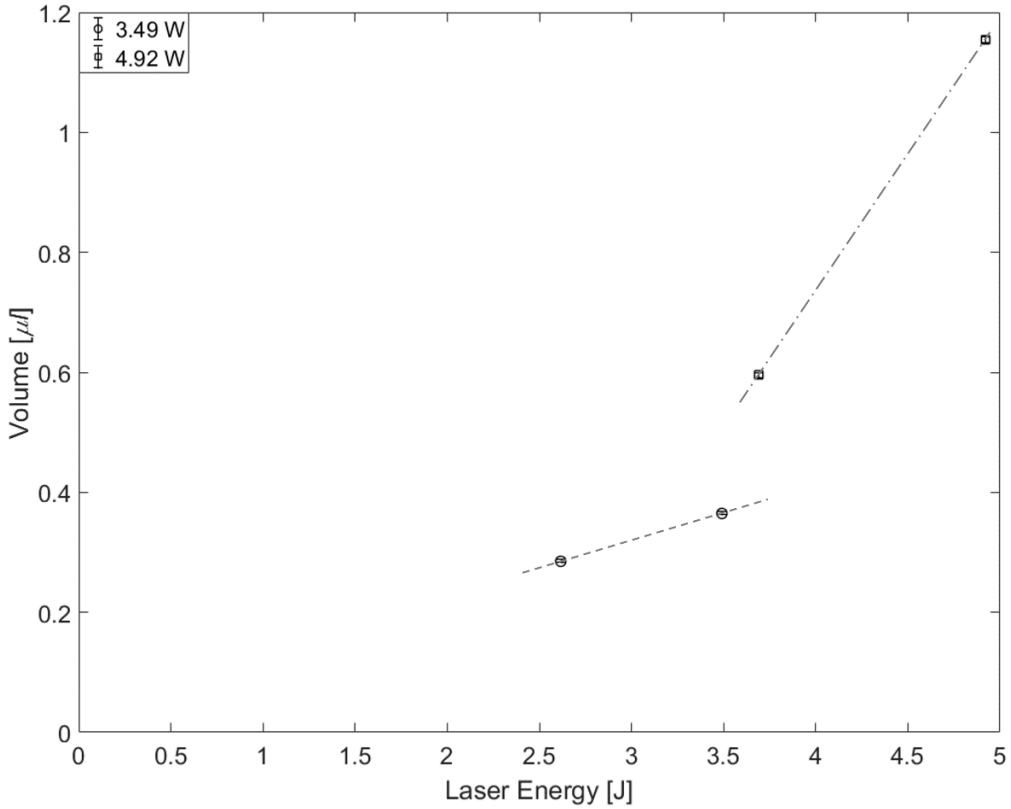

Figure 5-8. Relationship between laser energy and the volume of the laser generated well

5.3.3 Effects of laser power

The effect of laser power is shown in Figure 5-9. For comparison, the total laser energy is fixed and the laser power was changed from 5 W to 20 W. A single pulse laser was used. It can be seen that the lower power setting generated a larger scaffold volume. However, the large volume came from a large bubble that formed in the surface of the scaffold. The foamed layer was also thicker and the pore sizes bigger. Figure 5-10 also describes the effect of laser power on diameter, depth, and volume of the laser generated well. There is no noticeable difference in depth. On the other hand, the diameter of the well increases as the laser power gets higher. As I mentioned, this is because higher laser power results in a larger laser beam size. Therefore, the volume of the laser generated well increases according to laser power although they have the same laser energy.

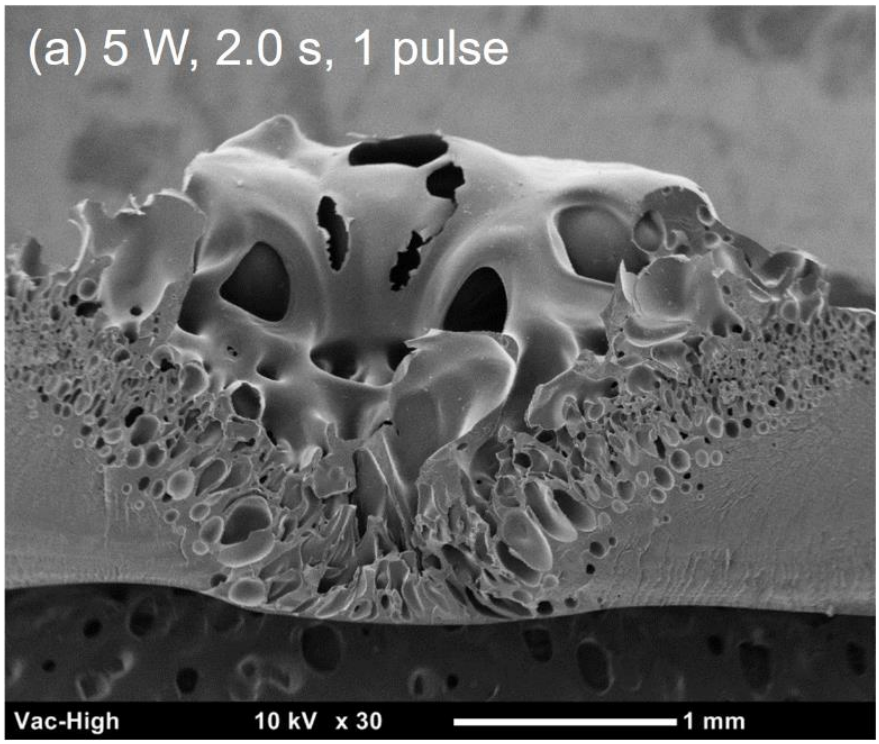

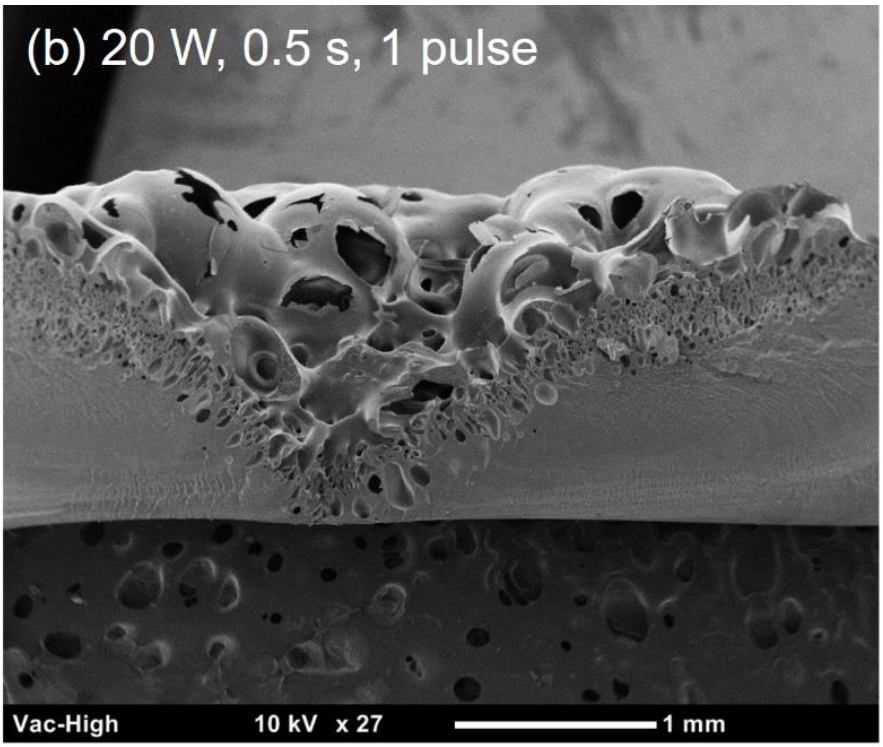

Figure 5-9. Effects of laser power on geometry of laser generated well

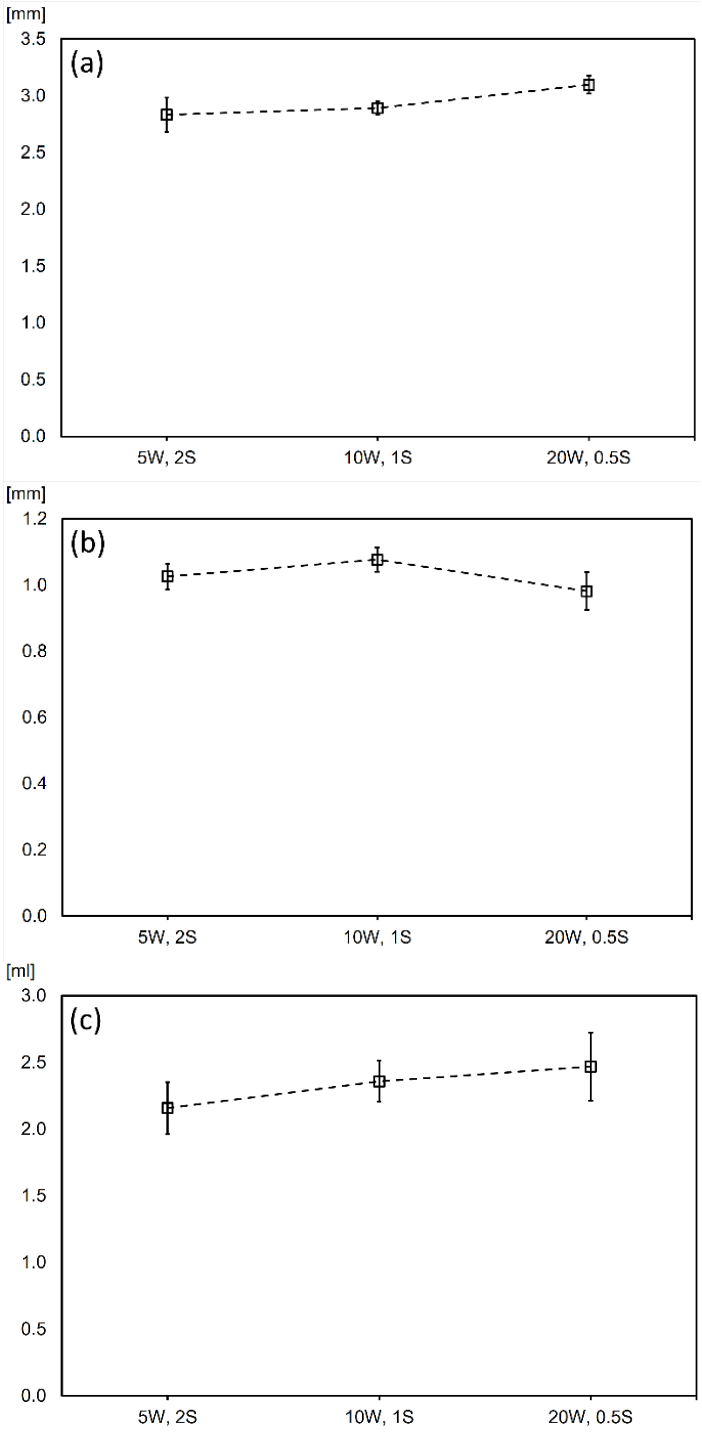

Figure 5-10. Parametric study with the same laser energy level (a) diameter of laser generated well, (b) depth of laser generated well, and (c) volume of laser generated well

5.3.4 Effects of lasing pattern

In order to compare samples fabricated using different laser pulses, the laser parameters were controlled to generate either 1 or 10 pulses. Both cases have identical laser power and total lasing time. The total laser energy is the same, 10 J (5 W of laser power and 0.5 second of lasing time), for the two different laser patterns. However, the lasing time was divided into 10 intervals for generation of 10 pulses. Each cycle has a 50% duty cycle. Figure 5-11 shows the pulse effect on the geometry of the laser ablated well. The diameter, depth, and volume of the well are similar, which stems from the fact that all the samples were laser-foamed with the same energy level. However, the wells fabricated with 10 pulses were slightly smaller. This is due to the fact that longer total lasing time gives more time for heat to dissipate instead of generating a porous structure.

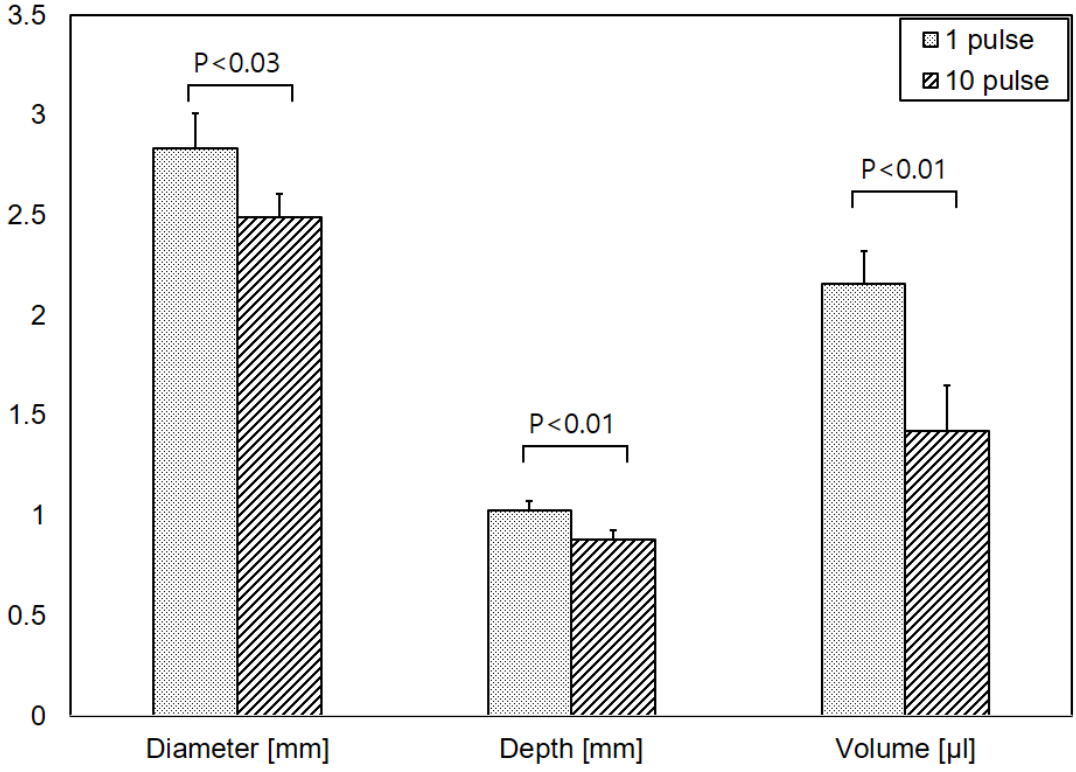

Figure 5-11. Effects of laser pattern on geometry of laser generated well

5.3.5 Surface treatment

The system in this study is an open one including a laser foamed spot, micro-channel and micro-chamber. Higher hydrophilicity than pipet surface is necessary to put the cell culture medium in the system. Various methods have been tested and the polydopamine (PDA) coating was finally chosen. This is because it could be done by an easy and quick procedure [197]. In addition, the coating can be applied to both hydrophilic and hydrophobic surfaces [198]. The PDA layer can serve as a platform for covalent immobilization of several serum adhesive proteins [199, 200]. The sample having our cell culture systems were coating with the PDA for 4 hours. The hydrophilicity was evaluated by measuring contact angles of the bare surface and the PDA coating. Figure 5-12 shows contact angles of those surfaces and the angle is decreased after the PDA coating from 75º to 60 º. The results are consistent with the data of Dr. Cho's study [187], and prove that the PDA coating makes the surface of the sample more hydrophilic.

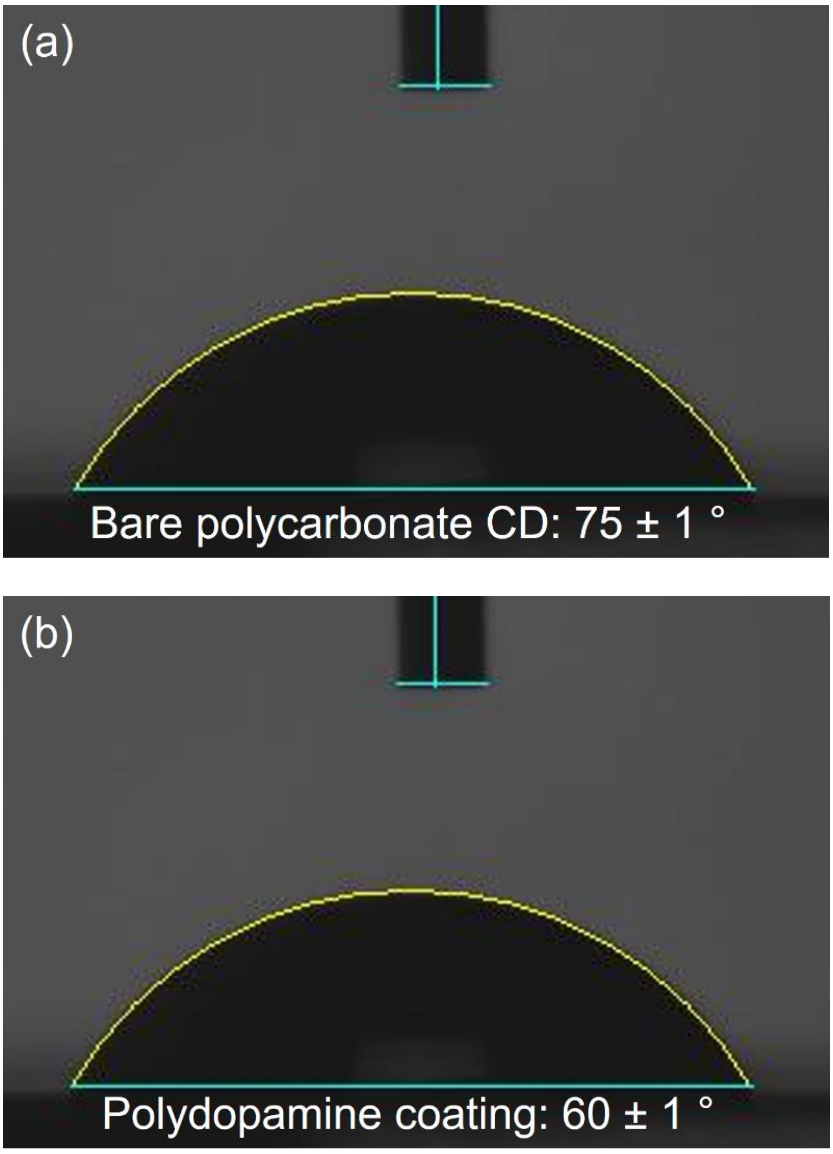

Figure 5-12. Static contact angle of bare polycarbonate CD and PDA coating

5.3.6 Effect of centrifugal force on diffusion

The effect of centrifugal force generated by disc rotation was described in Figure 5-13. Food coloring was diluted in distilled water (4 %) and 2 μl of the diluted coloring was dropped in the drug chamber. In order to minimize evaporation, a sample without rotation was placed on a block in a Petri dish having 4 ml of distilled water. On the other hand, the sample with rotation was placed on the spindle platter in a humidity chamber. Diffusion in the system driven by concentration differences between the drug chamber and the waste chamber can be accelerated by centrifugal force [109-111]. The high throughput device in this study will be rotated to assist the nutrient or drug diffusion across the foamed spots on which cells will be seeded. This is because it is required for a certain amount of time for cells to interact with chemicals used for drug study. In this manner, it is preferable that the diffusion is slow in a stationary condition and it is accelerated with the rotation of the CD system. The result in Figure 5-13 shows the agreement with the purpose of our design. The coloring was diffused to the second foamed spot within 10 minutes under 60 rpm of rotation, although it could reach only the first foamed spot after 2 hours without rotation. In 60 rpm rotation, it is not necessary to discuss damages of cells because it occurs in a high speed over 1200 rpm [201].

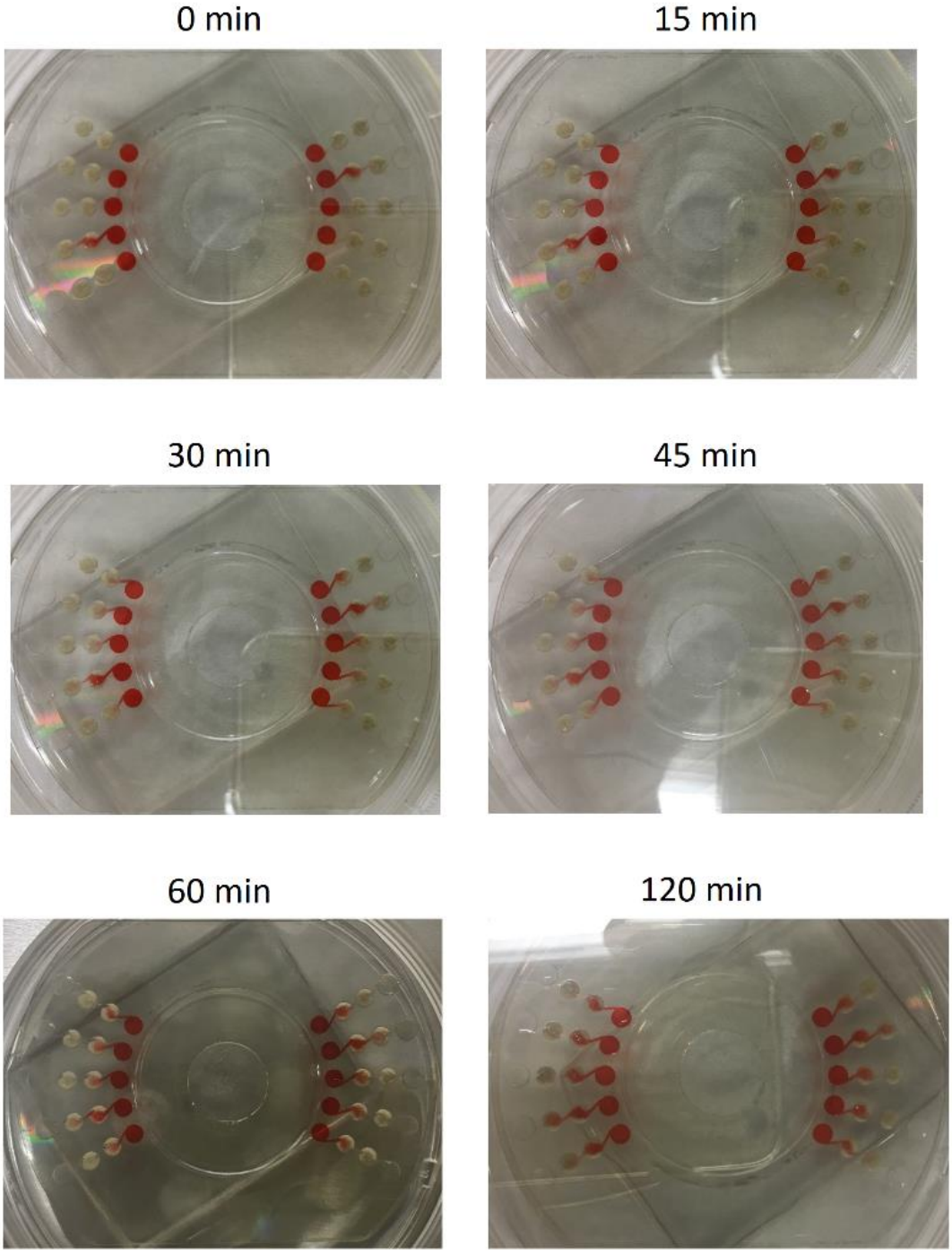

Figure 5-13 (a). Diffusion test without rotation

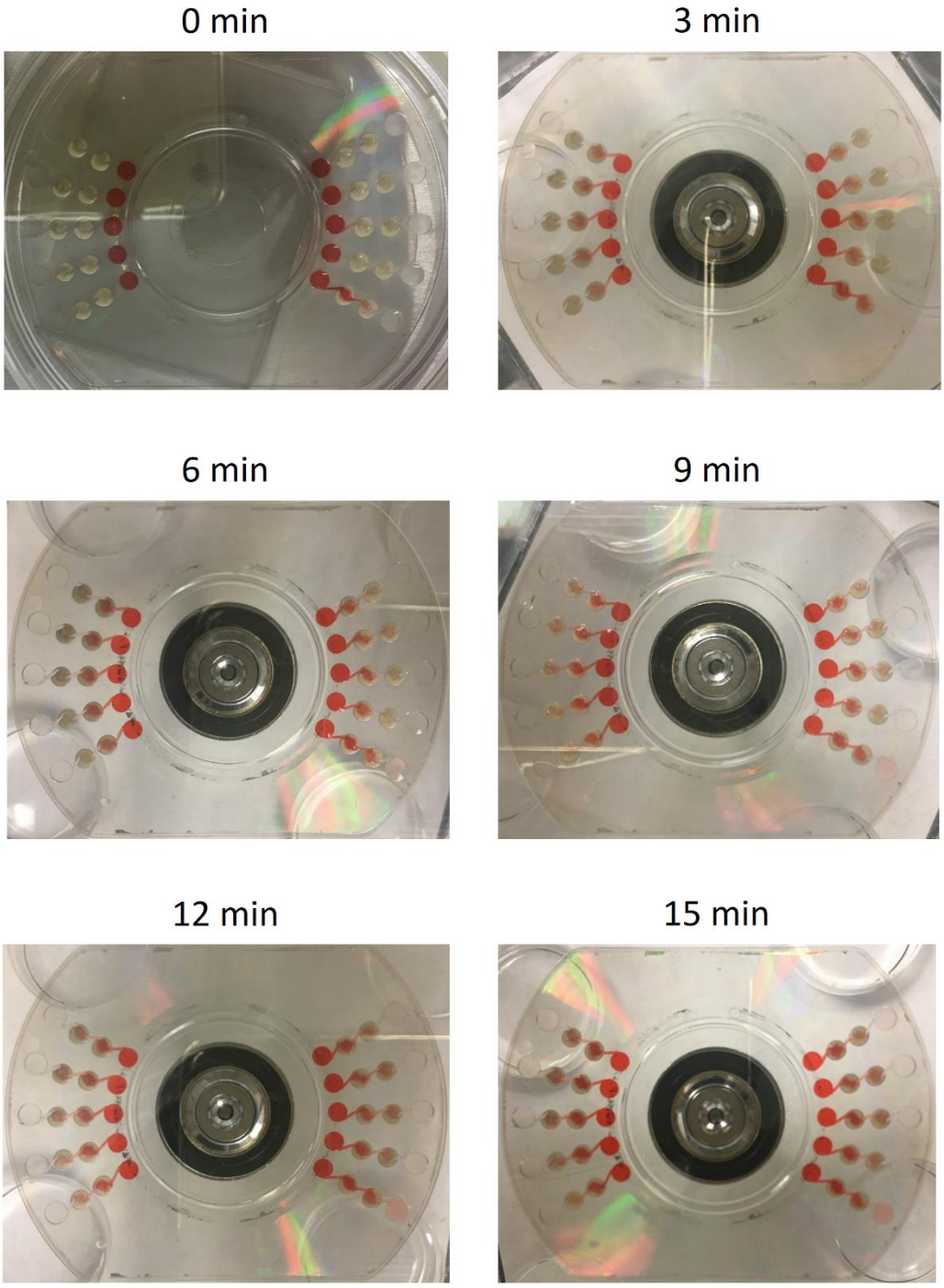

Figure 5-13 (b). Diffusion test 60 rpm of rotation speed

5.3.7 Cell culture results

The C3A-sub28 and M059K cells were cultured on a foamed chamber, separately. Cells after live/dead staining are shown in Figure 5-14. Polycarbonate scaffold was also stained by the staining kit, so the depth of an open pore can be estimated by focusing an upright microscope. The range of the depth is from 150 ± 0.5 μm to 250 ± 0.5 μm. More cells are attached on the bottom of the pore. This is because the cells were settled down and moved downward due to gravity, and small pores underneath the surface might be beneficial for cell adhesion on the bottom of the open pore [202].

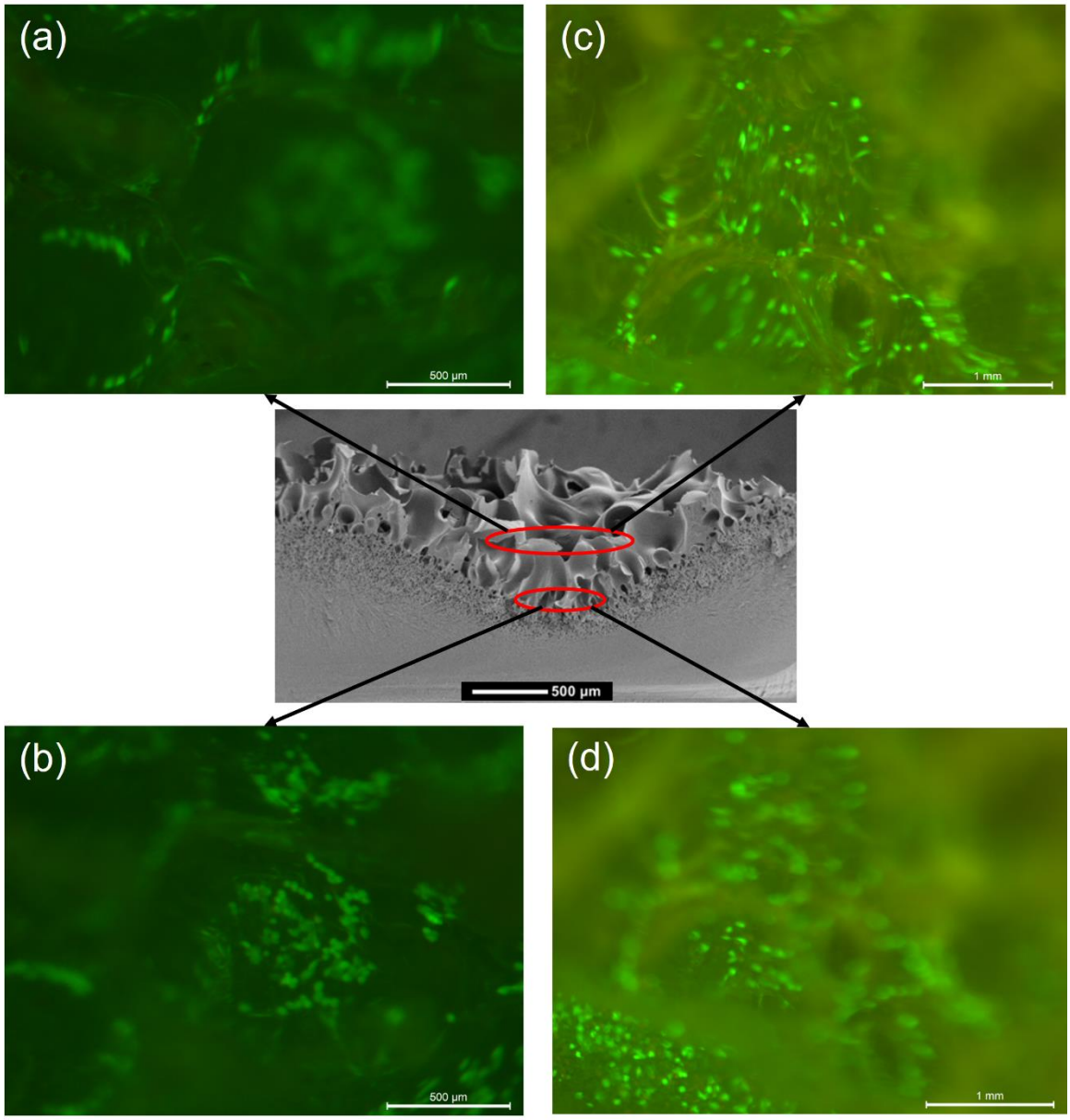

Figure 5-14. Depth of foamed hole and cell attachment after 13 hours of cell seeding (a-b) C3A sub28 cells and (c-d) M059K cells (982500 cells/ml for C3A sub28 and 1170000 cells/ml for M059K)

Figure 5-15 shows the fluorescence images of cells after 24 hour cell culturing. The left column represents C3A-sub 28 cells (Figure 5-15(a) and (c)) and the right column show GBM cells (Figure 5-15(d) and (f)). The 1st, 2nd, and 3rd rows show the characteristics of cell morphology after 24 hours, 48 hours, and 72 hours. It is observed that both cell lines maintained high viability. It is seen that the cells began to aggregate each other and to form organoid structures. In order to demonstrate the cell aggregation better, 3D images were taken using the confocal microscope with Z-stacking. Figure 5-16 clearly depicts the cell aggregation inside the open pore structure. Currently, using a 3D cell culture system is a fast growing experimental approach due to better mimicking of an *in vivo* environment [203]. In addition, the effects of anticancer drugs were different between 2D and 3D cell culture systems [13, 204, 205]. The 3D cell culture system in this study could be suitable for drug screening study by providing a good microenvironment for cell aggregation.

For long term cell culture study, the two types of cells were seeded on laser foamed scaffold on each system, respectively. Cell concentrations in each cell solution were 10 times less than one of the previous cell culture studies in this chapter. The centration of each cell solution are shown in Figure 5-17. The cell culture medium was changed every 24 hours during the first half of cell culturing and was replaced with a new medium every 12 hours for the rest of culturing. High viability and cell aggregation was apparently observed. The long term cell culture study also supports that the scaffold in our device is feasible for cell culturing.

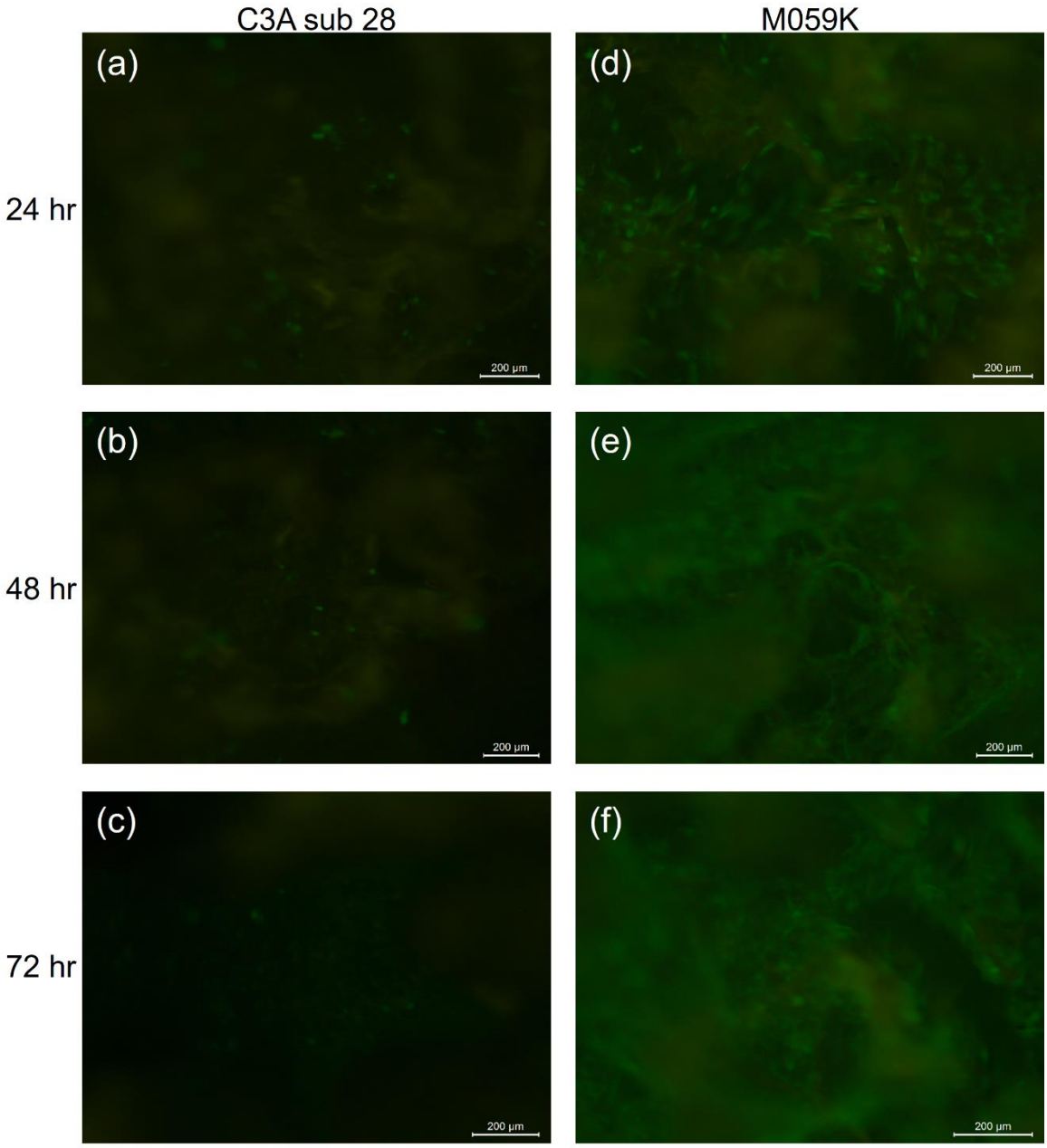

Figure 5-15 Cell morphology along with times 24 hours, 48 hours, and 72 hours (a-c) C3A sub28 cells and (d-f) M059K cells (9272500 cells/ml for C3A sub 28 and 5617500 cells/ml for M059K)

24 hours

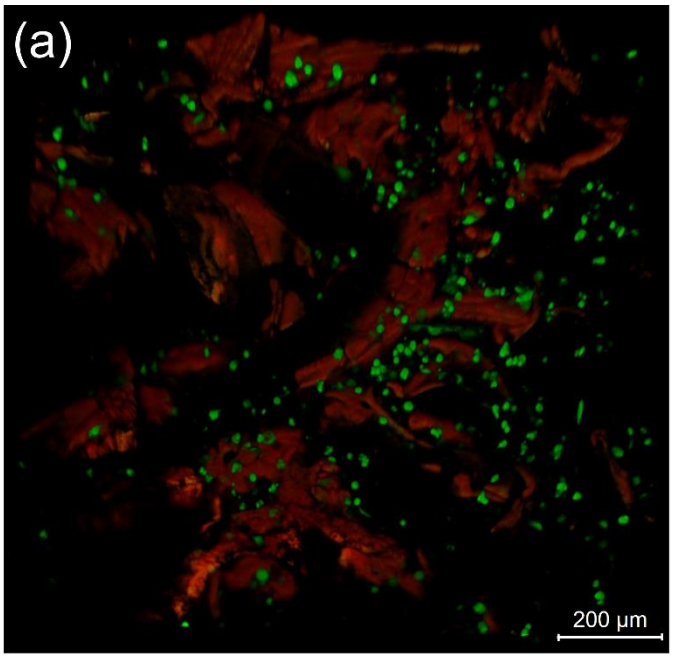

72 hours

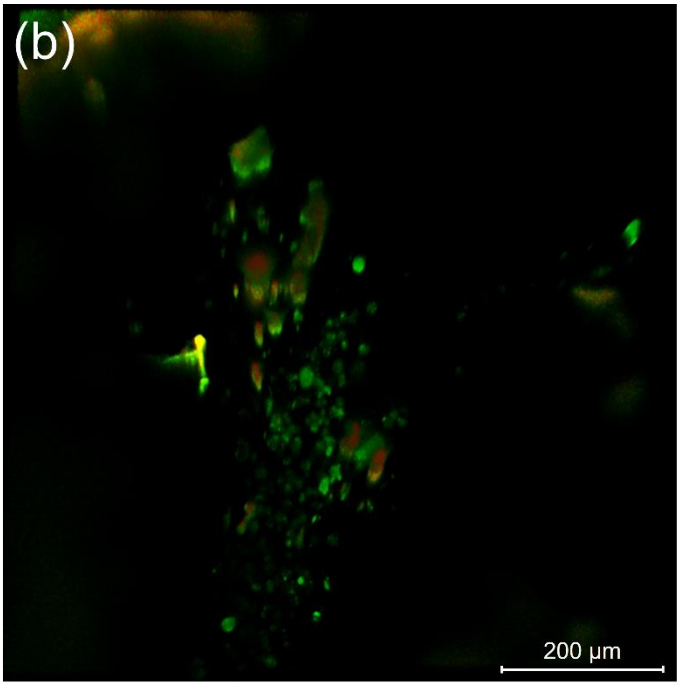

Figure 5-16. Cell morphology of C3A-sub28 cells along with times (a) 24 hours and (b) 72 hours from the confocal microscope (17635000 cells/ml)

24 hours

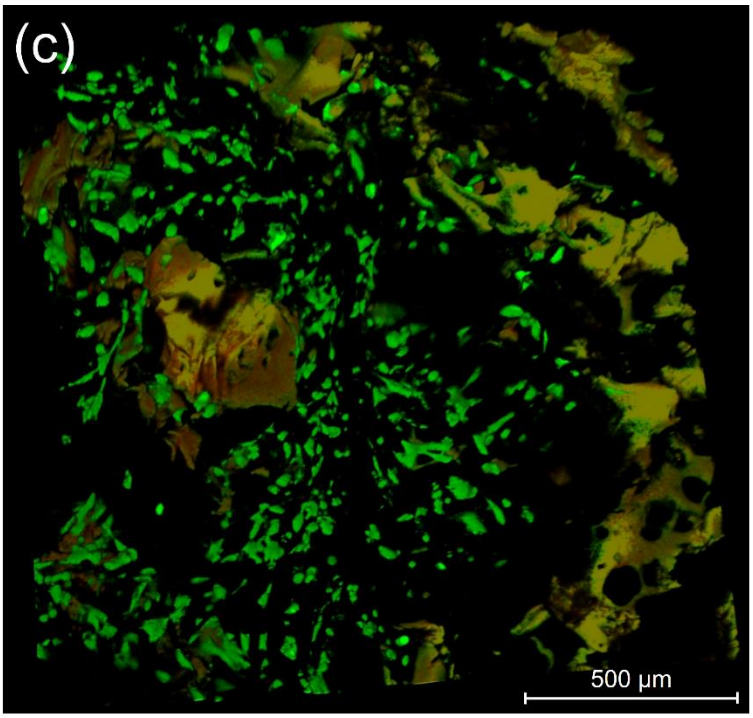

72 hours

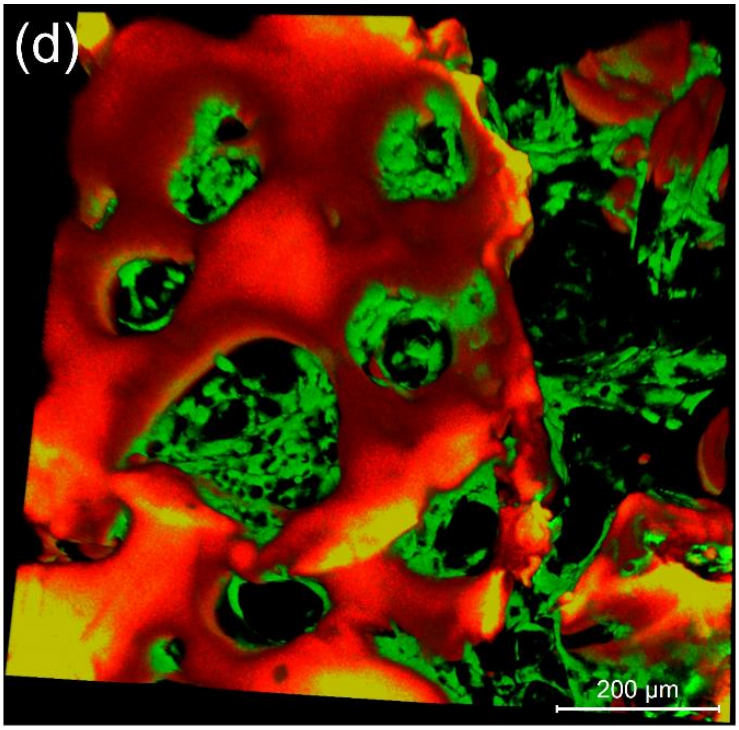

Figure 5-16. Cell morphology of M059K cells along with times (c) 24 hours and (d) 72 hours from the confocal microscope (7022500 cells/ml)

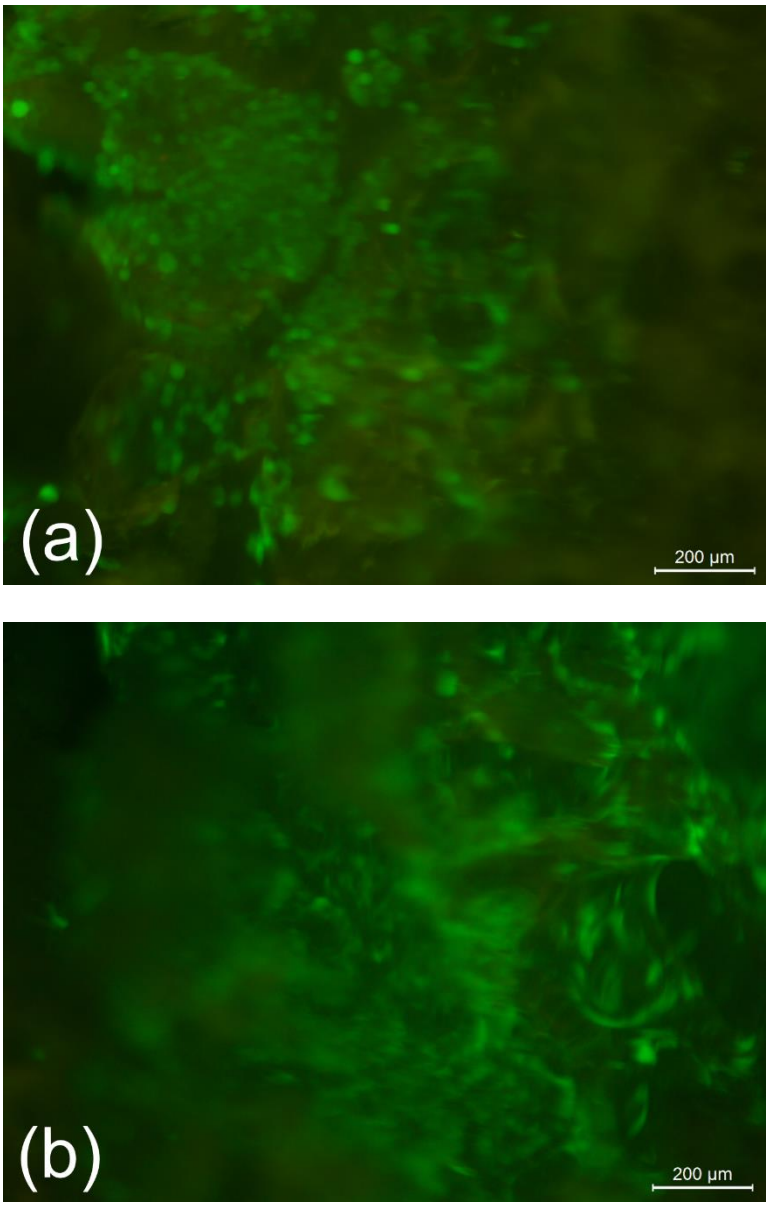

Figure 5-17 Cell morphology after 28 days cell culturing (a) C3A-sub28 (1440000 cells /ml) (b) M059K (515000 cells/ml)

5.4. CONCLUSIONS

A high throughput three-dimensional micro-scale centrifugal force driven two-chamber tissue model device was developed for drug screening study. Three-dimensional porous scaffolds were created on a commercially available CD made of polycarbonate

using selective laser foaming. Experimental studies were conducted with different saturation conditions and laser parameters. Laser foaming generated an inverse-cone shaped well with a perforated inner surface covering the porous structure. The selective laser foaming is an integration of solid state foaming and laser machining. This is because the scaffold fabricated by selective laser foaming shows the characteristics of both manufacturing methods. The size of the ablated and foamed regions is dependent on the laser power and lasing time, whereas the open pore structure and underneath pore size are a function of the gas concentration. A higher laser energy led to a larger scaffold volume; however, a higher power is more preferential due to the less nonlinear heating effect that it has by reducing the heating time. A multiple pulse laser will lead to heat dissipation to the surrounding area, such that the foam volume is reduced. The tissue model platform was accomplished with micro-machining and surface treatment, and the template consists of 10 micro-scale tissue model systems having two micro-reservoirs and two micro-scale scaffolds connected in tandem. It is seen that the diffusion in the system is accelerated by centrifugal force induced by rotation, whereas the diffusion is very slow without rotation. Two types of cells (M059K and C3A sub28) were cultured in the scaffolds separately in one system. The cells shows high viability after 72 hour culturing at 37 ºC and 5 % CO_2. The results demonstrate that the micro-scale two-scaffold tissue model platform driven by centrifugal force could provide a proper *in vitro* environment mimicking 3D ECM *in vivo*. The cells were seeded on the scaffolds with 1-2 µl, so it is very hard to define quantitative cell viability. The quantitative study for cell viability can be conducted in future.

Chapter 6. Summary and Future Work

6.1 SUMMARY

A novel fabrication process, selective laser foaming, was developed and novel high throughput porous polymer-based 3D cell culture platforms including microarray and tissue model device were developed in this study. The high throughput microarray was fabricated on PLA and a finite element model was developed to evaluate the effect of laser parameters on a porous structure on PLA. The high throughput 3D tissue model device was laser-foamed and micro-machined on a commercially available PC CD. The centrifugal force induced by rotation of the CD enhanced diffusion of nutrients across micro-chambers and micro-porous scaffolds in the device. Cell culture studies were conducted to demonstrate the biocompatibility of fabricated scaffolds in each platform.

The contributions of this work are summarized as follows.

- A novel polymer foaming technique, selective laser foaming, was developed to fabricate small size and localized tissue engineering scaffolds on a polymer chip. The effects of laser processing parameters on the morphology of the resulting porous structure were investigated, including size of the foamed volume, and pore size as functions of laser power, exposure time and CO_2 concentration. The diameter and depth of the foamed region were proportional to laser power and exposure time. The pore size decreased and the density of the pores increased as the saturation pressure increased. The 3D porous scaffolds can be fabricated with a volume on the level of a few microliters, allowing high density packing of such scaffolds on a small polymer chip.
- A finite element model was developed to study the effects of laser parameters on a porous structure. It was found that the enhanced laser

absorption of a porous structure induced a dramatic increase in temperature during foaming. For a fixed laser power, the depths of both ablated and foamed regions had a linearly proportional relationship with the lasing time. The slope of this linear trend was dependent on laser power. The diameters of the ablated and foamed regions increase rapidly at the early stage of the process and approach a limit determined by the laser power setting. Therefore, laser power is a more effective variable to use in order to control the diameter of the foamed and ablated regions.

- A novel high throughput three-dimensional micro-scale centrifugal force driven two-chamber tissue model device was developed and tested for the drug screening study. Three-dimensional porous scaffolds were laser-foamed on commercially available CD made of polycarbonate. The micro-chambers and micro-channels were fabricated using micro-machining. The hydrophilicity was enhanced using polydopamine coating. The platform consisted of 10 micro-scale tissue model systems having two micro-reservoirs and two micro-scale scaffolds connected. It was observed that the diffusion in the system is accelerated by centrifugal force generated by rotation, whereas the diffusion is very slow without rotation. Human brain tumor cells and human hepatoblastoma were cultured in the scaffolds separately in the system. The high cell viability and cell aggregation were observed after 72 hour culturing. These indicated that the device could provide a proper *in vitro* environment mimicking 3D ECM *in vivo*.

6.2 FUTURE WORK

The current research has paved the way for further study, which could include the following.

6.2.1 Anti-cancer drug study related to liver metabolism using the 3D device

The cytochrome P450 (CYP) superfamily is one of the drug metabolizing enzymes that converts drugs into their primary metabolites. CYP-mediated metabolism eliminates about 75% of drugs. Among the CYP family, CYP3A4 which is the most abundantly expressed hepatic cytochrome P450, catalyzes the oxidative metabolism of more than 60 % of marketed drugs [206, 207]. The variability of genotypes of CYPs might result in different isosyme activity and might induce the variation in drug responses among individuals [208]. The high throughput three-dimensional tissue model device in this study could be used to culture two different types of cells at the same time in one system. Various types of GBMs and the hepatoblastoma HepG2 or its derivative C3A cells could be seeded and cultured separately in the system. The drug metabolism process would be mimicked via centrifugal force induced by rotation. The experimental results could be used to further validate the suitability of the platform in this study for anti-cancer drug testing.

6.2.2 Fabrication of uniform porous structures using flattop laser beam

A uniform porous structure would be preferred in some area of tissue engineering, specifically in studies related to stem cells. In this study, it is found that a laser machined profile is dependent on the laser intensity profile. In addition, a porous structure including porosity and pore size relies on the gas concentration in a polymer sample. As shown in Figure 6-1, there are several laser intensity profiles and they could be shaped by a special apparatus, such as a flat top laser beam shaper. Wang *et al.* reported that gas concentration

is a function of the distance from a sample surface [209]. Therefore, a more uniform porous structure with a cylindrical shape could be achieved using flattop beam shaper.

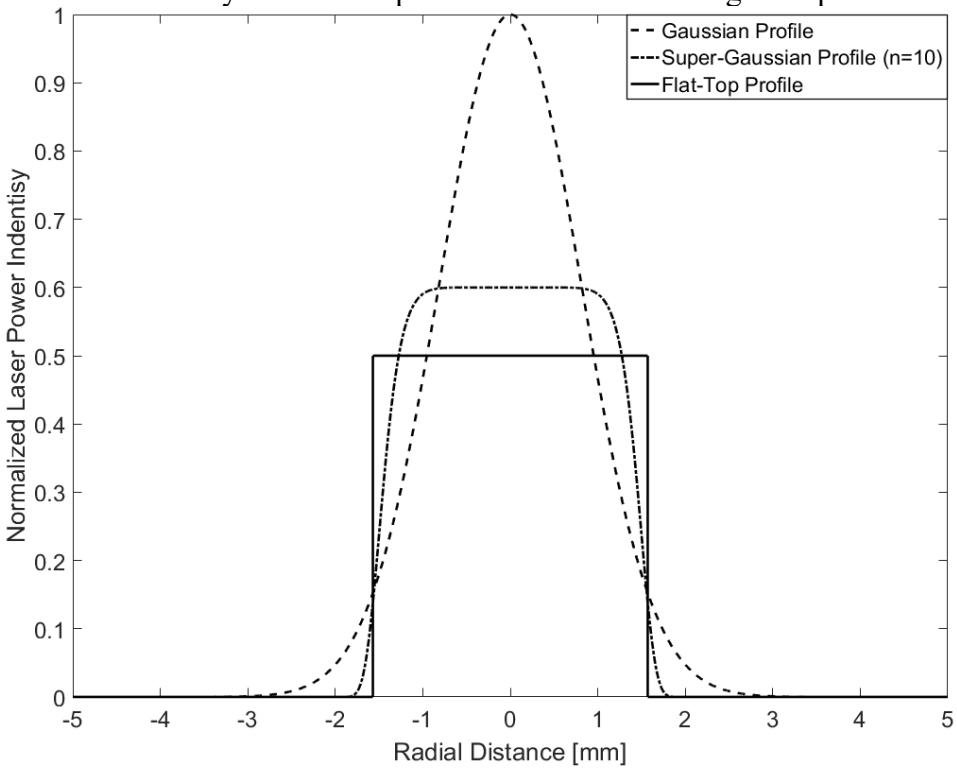

Figure 6-1 Normalized laser power intensity profiles

6.2.3 Improvement of FEA model for pore size estimation

The FEA model can be improved to estimate pore size during selective laser foaming process. It is necessary to understand intrinsic bubble growth phenomena at high temperatures. The mechanism of each process is going to be studied including nucleation, phase change, cell density, and bubble growth [210-213]. A better estimation of selective laser foaming can be achieved by applying those bubble growth mechanisms to the model in chapter 4.

6.2.4 Fabrication of micro-scale scaffolds for a denser microarray

As shown in Figure 6-2, a micro-scale scaffold can be fabricated by focusing the laser. The beam size can be controlled by adjusting the distance between the focusing lens and a target sample. It could be expected that cell morphology and cell viability in the scaffold shown in Figure 6-2 are different from those in the scaffold in this study. In addition, the laser foamed area could be reduced from millimeter-size to micrometer-size. Thus, a 3D microarray with higher volumes of scaffolds would be generated for parallel studies of tissue engineering.

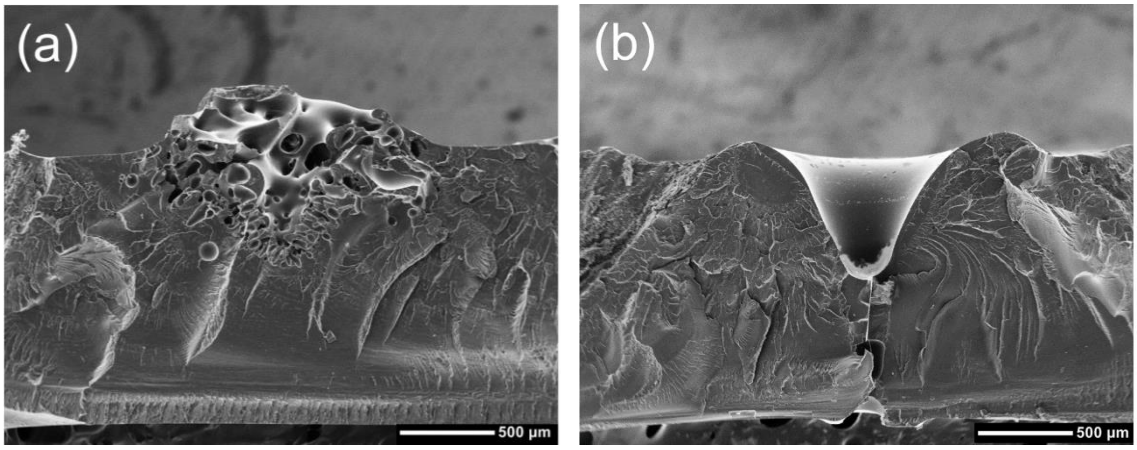

Figure 6-2 Cross-sectional images of PLA samples using focused laser (a) with gas saturation (fabricated with 2 % laser power for 1 s) (b) without gas saturation (fabricated with 2.5 % laser power for 1 s)

6.2.5 Development of a robust method for quantification of cell viability in 3D scaffolds

Both qualitative and quantitative assessments are required to evaluate biocompatibility of scaffolds. The live-dead cell staining can be used to obtain cell morphology for qualitative assessment of the biocompatibility using a upright fluorescence microscope or a confocal microscope. The quantitative evaluation can be conducted via cell viability using Alamar blue® and 3-[4,5-dimethylthiazol-2-yl]-2,5-diphenyl

tetrazolium bromide (MTT) assays. It is hard to achieve those assessments of biocompatibility of the scaffolds in Chapter 5. This results from that the scaffolds has porous structures and total volume of each scaffold is less than 2 μl. Light could be refracted passing through the porous structure. In addition, fluorescence intensity generated by enzyme activity in 2 μl of scaffolds could be too low for cell viability measurement. Therefore, a robust method to quantify cell viability in 3D scaffolds would be developed and morphology assessment could be improved by adding a drop of liquid which has the same refractive index to the polymer.

References

[1] M. McEwan, R. J. Lins, S. K. Munro, Z. L. Vincent, A. P. Ponnampalam, and M. D. Mitchell, "Cytokine regulation during the formation of the fetal–maternal interface: Focus on cell–cell adhesion and remodelling of the extra-cellular matrix," *Cytokine & growth factor reviews,* vol. 20, pp. 241-249, 2009.

[2] A. Bolshakova, O. Petukhova, L. Turoverova, D. Tentler, V. Babakov, K. Magnusson, and G. Pinaev, "Extra-cellular matrix proteins induce re-distribution of alpha-actinin-1 and alpha-actinin-4 in A431 cells," *Cell biology international,* vol. 31, pp. 360-365, 2007.

[3] A. Abbott, "Cell culture: biology's new dimension," *Nature,* vol. 424, pp. 870-872, 2003.

[4] E. Fuchs, T. Tumbar, and G. Guasch, "Socializing with the neighbors: stem cells and their niche," *Cell,* vol. 116, pp. 769-78, Mar 19 2004.

[5] M. R. Abidian, D. H. Kim, and D. C. Martin, "Conducting-Polymer Nanotubes for Controlled Drug Release," *Advanced Materials,* vol. 18, pp. 405-409, 2006.

[6] S. Simovic, D. Losic, and K. Vasilev, "Controlled drug release from porous materials by plasma polymer deposition," *Chemical communications,* vol. 46, pp. 1317-1319, 2010.

[7] M. M. Wanderley, C. Wang, C.-D. Wu, and W. Lin, "A Chiral Porous Metal–Organic Framework for Highly Sensitive and Enantioselective Fluorescence Sensing of Amino Alcohols," *Journal of the American Chemical Society,* vol. 134, pp. 9050-9053, 2012.

[8] J. Yang, G. Shi, J. Bei, S. Wang, Y. Cao, Q. Shang, G. Yang, and W. Wang, "Fabrication and surface modification of macroporous poly (L-lactic acid) and poly (L-lactic-co-glycolic acid)(70/30) cell scaffolds for human skin fibroblast cell culture," *Journal of biomedical materials research,* vol. 62, pp. 438-446, 2002.

[9] K. Rezwan, Q. Chen, J. Blaker, and A. R. Boccaccini, "Biodegradable and bioactive porous polymer/inorganic composite scaffolds for bone tissue engineering," *Biomaterials,* vol. 27, pp. 3413-3431, 2006.

[10] L. G. Griffith, "Emerging design principles in biomaterials and scaffolds for tissue engineering," *Annals of the New York Academy of Sciences,* vol. 961, pp. 83-95, 2002.

[11] A. Khademhosseini, R. Langer, J. Borenstein, and J. P. Vacanti, "Microscale technologies for tissue engineering and biology," *Proceedings of the National Academy of Sciences of the United States of America,* vol. 103, pp. 2480-2487, 2006.

[12] P.-A. Mouthuy, H. Ye, J. Triffitt, G. Oommen, and Z. Cui, "Physico-chemical characterization of functional electrospun scaffolds for bone and cartilage tissue engineering," *Proceedings of the Institution of Mechanical Engineers, Part H: Journal of Engineering in Medicine,* vol. 224, pp. 1401-1414, 2010.

[13] L. Ma, J. Barker, C. Zhou, W. Li, J. Zhang, B. Lin, G. Foltz, J. Küblbeck, and P. Honkakoski, "Towards personalized medicine with a three-dimensional micro-scale perfusion-based two-chamber tissue model system," *Biomaterials,* vol. 33, pp. 4353-4361, 2012.

[14] F. I. Carroll and R. A. Houghten, "From rapid in vitro screening to rapid in vivo screening in the drug discovery process," *Neuropsychopharmacology,* vol. 34, pp. 251-252, 2009.

[15] M. Liscovitch and Y. Lavie, "Cancer multidrug resistance: a review of recent drug discovery research," *IDrugs,* vol. 5, pp. 349-355, 2002.

[16] M. J. Powers, D. M. Janigian, K. E. Wack, C. S. Baker, D. Beer Stolz, and L. G. Griffith, "Functional behavior of primary rat liver cells in a three-dimensional perfused microarray bioreactor," *Tissue Eng,* vol. 8, pp. 499-513, Jul 2002.

[17] K. Domansky, W. Inman, J. Serdy, A. Dash, M. H. Lim, and L. G. Griffith, "Perfused multiwell plate for 3D liver tissue engineering," *Lab on a chip,* vol. 10, pp. 51-58, 2010.

[18] K. Viravaidya, A. Sin, and M. L. Shuler, "Development of a microscale cell culture analog to probe naphthalene toxicity," *Biotechnology progress,* vol. 20, pp. 316-323, 2004.

[19] J. H. Sung and M. L. Shuler, "A micro cell culture analog (μCCA) with 3-D hydrogel culture of multiple cell lines to assess metabolism-dependent cytotoxicity of anti-cancer drugs," *Lab on a chip,* vol. 9, pp. 1385-1394, 2009.

[20] M. Y. Lee, C. B. Park, J. S. Dordick, and D. S. Clark, "Metabolizing enzyme toxicology assay chip (MetaChip) for high-throughput microscale toxicity analyses," *Proceedings of the National Academy of Sciences of the United States of America,* vol. 102, pp. 983-987, 2005.

[21] E. Cukierman, R. Pankov, D. R. Stevens, and K. M. Yamada, "Taking cell-matrix adhesions to the third dimension," *Science,* vol. 294, pp. 1708-1712, 2001.

[22] L. Ma, W. Li, B. Lin, and N. Sniadecki, *Three-dimensional Cell Culture Devices for Cancer Migration and Drug Testing* vol. 73, 2012.

[23] A. G. Mikos and J. S. Temenoff, "Formation of highly porous biodegradable scaffolds for tissue engineering," *Electronic Journal of Biotechnology,* vol. 3, pp. 23-24, 2000.

[24] K. Whang, C. Thomas, K. Healy, and G. Nuber, "A novel method to fabricate bioabsorbable scaffolds," *Polymer,* vol. 36, pp. 837-842, 1995.

[25] Y. S. Nam and T. G. Park, "Biodegradable polymeric microcellular foams by modified thermally induced phase separation method," *Biomaterials,* vol. 20, pp. 1783-1790, 1999.

[26] A. G. Mikos, G. Sarakinos, S. M. Leite, J. P. Vacant, and R. Langer, "Laminated three-dimensional biodegradable foams for use in tissue engineering," *Biomaterials,* vol. 14, pp. 323-330, 1993.

[27] L. D. Harris, B.-S. Kim, and D. J. Mooney, "Open pore biodegradable matrices formed with gas foaming," 1998.

[28] B. Duan, M. Wang, W. Y. Zhou, W. L. Cheung, Z. Y. Li, and W. W. Lu, "Three-dimensional nanocomposite scaffolds fabricated via selective laser sintering for bone tissue engineering," *Acta Biomaterialia,* vol. 6, pp. 4495-4505, 2010.

[29] B. R. Ringeisen, H. Kim, J. A. Barron, D. B. Krizman, D. B. Chrisey, S. Jackman, R. Auyeung, and B. J. Spargo, "Laser printing of pluripotent embryonal carcinoma cells," *Tissue engineering,* vol. 10, pp. 483-491, 2004.

[30] C. M. Othon, X. Wu, J. J. Anders, and B. R. Ringeisen, "Single-cell printing to form three-dimensional lines of olfactory ensheathing cells," *Biomedical Materials,* vol. 3, p. 034101, 2008.

[31] G. Mapili, Y. Lu, S. Chen, and K. Roy, "Laser-layered microfabrication of spatially patterned functionalized tissue-engineering scaffolds," *Journal of Biomedical Materials Research Part B: Applied Biomaterials,* vol. 75, pp. 414-424, 2005.

[32] W. Zhang, P. Soman, K. Meggs, X. Qu, and S. Chen, "Tuning the Poisson's Ratio of Biomaterials for Investigating Cellular Response," *Advanced Functional Materials,* 2013.

[33] S. Suri, L.-H. Han, W. Zhang, A. Singh, S. Chen, and C. E. Schmidt, "Solid freeform fabrication of designer scaffolds of hyaluronic acid for nerve tissue engineering," *Biomedical microdevices,* vol. 13, pp. 983-993, 2011.

[34] C. K. Chua, K. F. Leong, and C. S. Lim, *Rapid prototyping: principles and applications*: World Scientific, 2010.

[35] K. Tan, C. Chua, K. Leong, C. Cheah, W. Gui, W. Tan, and F. Wiria, "Selective laser sintering of biocompatible polymers for applications in tissue engineering," *Bio-medical materials and engineering,* vol. 15, pp. 113-124, 2005.

[36] V. Kumar and N. P. Suh, "A process for making microcellular thermoplastic parts," *Polymer Engineering & Science,* vol. 30, pp. 1323-1329, 1990.

[37] Y. P. Handa and Z. Zhang, "A novel stress-induced nucleation and foaming process and its applications in making homogeneous foams, anisotropic foams and multilayered foams," *Cellular polymers,* vol. 19, pp. 77-91, 2000.

[38] X. Wang, W. Li, and V. Kumar, "A method for solvent-free fabrication of porous polymer using solid-state foaming and ultrasound for tissue engineering applications," *Biomaterials,* vol. 27, pp. 1924-1929, 2006.

[39] H. Wang and W. Li, "A novel 3D porous micromixer fabricated using selective ultrasonic foaming," *Journal of Micromechanics and Microengineering,* vol. 17, p. 1835, 2007.

[40] H. Wang and W. Li, "Selective ultrasonic foaming of polymer for biomedical applications," *Journal of manufacturing science and engineering,* vol. 130, p. 021004, 2008.

[41] X. Wang, W. Li, and V. Kumar, "Creating open-celled solid-state foams using ultrasound," *Journal of Cellular Plastics,* vol. 45, pp. 353-369, 2009.

[42] B. Duan and M. Wang, "Selective Laser Sintering and Its Biomedical Applications," in *Laser Technology in Biomimetics*, V. Schmidt and M. R. Belegratis, Eds., ed: Springer Berlin Heidelberg, 2013, pp. 83-109.

[43] J. M. Kanczler, S.-H. Mirmalek-Sani, N. A. Hanley, A. L. Ivanov, J. J. Barry, C. Upton, K. M. Shakesheff, S. M. Howdle, E. N. Antonov, and V. N. Bagratashvili, "Biocompatibility and osteogenic potential of human fetal femur-derived cells on surface selective laser sintered scaffolds," *Acta Biomaterialia,* vol. 5, pp. 2063-2071, 2009.

[44] F.-H. Liu, R.-T. Lee, W.-H. Lin, and Y.-S. Liao, "Selective laser sintering of bio-metal scaffold," *Procedia CIRP,* vol. 5, pp. 83-87, 2013.

[45] J. M. Williams, A. Adewunmi, R. M. Schek, C. L. Flanagan, P. H. Krebsbach, S. E. Feinberg, S. J. Hollister, and S. Das, "Bone tissue engineering using polycaprolactone scaffolds fabricated via selective laser sintering," *Biomaterials,* vol. 26, pp. 4817-4827, 2005.

[46] C. R. Deckard, "Method and apparatus for producing parts by selective sintering," ed, 1989.

[47] D. J. Odde and M. J. Renn, "Laser-guided direct writing of living cells," *Biotechnology and Bioengineering,* vol. 67, pp. 312-318, 2000.

[48] Y. Nahmias, R. E. Schwartz, C. M. Verfaillie, and D. J. Odde, "Laser-guided direct writing for three-dimensional tissue engineering," *Biotechnology and Bioengineering,* vol. 92, pp. 129-136, 2005.

[49] Y. Nahmias and D. J. Odde, "Micropatterning of living cells by laser-guided direct writing: application to fabrication of hepatic–endothelial sinusoid-like structures," *Nature protocols,* vol. 1, pp. 2288-2296, 2006.

[50] S. V. Narasimhan, R. L. Goodwin, T. K. Borg, D. M. Dawson, and B. Z. Gao, "Multiple beam laser cell micropatterning system," in *Proceedings of SPIE*, 2004, pp. 437-445.

[51] T. N. Rosenbalm, S. Owens, D. Bakken, and B. Z. Gao, "Cell viability test after laser guidance," in *Biomedical Optics 2006*, 2006, pp. 608418-608418-8.

[52] D. J. Odde and M. J. Renn, "Laser-guided direct writing for applications in biotechnology," *TRENDS in Biotechnology,* vol. 17, pp. 385-389, 1999.

[53] L. Koch, S. Kuhn, H. Sorg, M. Gruene, S. Schlie, R. Gaebel, B. Polchow, K. Reimers, S. Stoelting, and N. Ma, "Laser printing of skin cells and human stem cells," *Tissue Engineering Part C: Methods,* vol. 16, pp. 847-854, 2009.

[54] M. Gruene, A. Deiwick, L. Koch, S. Schlie, C. Unger, N. Hofmann, I. Bernemann, B. Glasmacher, and B. Chichkov, "Laser printing of stem cells for biofabrication of scaffold-free autologous grafts," *Tissue Engineering Part C: Methods,* vol. 17, pp. 79-87, 2010.

[55] L. Koch, A. Deiwick, S. Schlie, S. Michael, M. Gruene, V. Coger, D. Zychlinski, A. Schambach, K. Reimers, and P. M. Vogt, "Skin tissue generation by laser cell printing," *Biotechnology and Bioengineering,* vol. 109, pp. 1855-1863, 2012.

[56] T. Patz, A. Doraiswamy, R. Narayan, W. He, Y. Zhong, R. Bellamkonda, R. Modi, and D. Chrisey, "Three-dimensional direct writing of B35 neuronal cells," *Journal of Biomedical Materials Research Part B: Applied Biomaterials,* vol. 78, pp. 124-130, 2006.

[57] A. Doraiswamy, R. Narayan, M. Harris, S. Qadri, R. Modi, and D. Chrisey, "Laser microfabrication of hydroxyapatite-osteoblast-like cell composites," *Journal of Biomedical Materials Research Part A,* vol. 80, pp. 635-643, 2007.

[58] J. Barron, P. Wu, H. Ladouceur, and B. Ringeisen, "Biological laser printing: a novel technique for creating heterogeneous 3-dimensional cell patterns," *Biomedical microdevices,* vol. 6, pp. 139-147, 2004.

[59] J. Barron, B. Spargo, and B. Ringeisen, "Biological laser printing of three dimensional cellular structures," *Applied Physics A,* vol. 79, pp. 1027-1030, 2004.

[60] J. A. Barron, D. B. Krizman, and B. R. Ringeisen, "Laser printing of single cells: statistical analysis, cell viability, and stress," *Annals of biomedical engineering,* vol. 33, pp. 121-130, 2005.

[61] R. K. Pirlo, P. Wu, J. Liu, and B. Ringeisen, "PLGA/hydrogel biopapers as a stackable substrate for printing HUVEC networks via BioLP™," *Biotechnology and Bioengineering,* vol. 109, pp. 262-273, 2012.

[62] C. W. Hull, "Apparatus for production of three-dimensional objects by stereolithography," ed: Google Patents, 1986.

[63] W. Zhang and S. Chen, "Femtosecond laser nanofabrication of hydrogel biomaterial," *MRS bulletin,* vol. 36, pp. 1028-1033, 2011.

[64] A. Ovsianikov, A. Deiwick, S. Van Vlierberghe, M. Pflaum, M. Wilhelmi, P. Dubruel, and B. Chichkov, "Laser fabrication of 3D gelatin scaffolds for the generation of bioartificial tissues," *Materials,* vol. 4, pp. 288-299, 2011.

[65] A. Ovsianikov, A. Deiwick, S. Van Vlierberghe, P. Dubruel, L. Möller, G. Dräger, and B. Chichkov, "Laser fabrication of three-dimensional CAD scaffolds from photosensitive gelatin for applications in tissue engineering," *Biomacromolecules,* vol. 12, pp. 851-858, 2011.

[66] M. Gebinoga, J. Katzmann, U. Fernekorn, J. Hampl, F. Weise, M. Klett, A. Läffert, T. A. Klar, and A. Schober, "Multi-photon structuring of native polymers: A case study for structuring natural proteins," *Engineering in Life Sciences,* 2013.

[67] M. Göppert-Mayer, "Über elementarakte mit zwei quantensprüngen," *Annalen der Physik,* vol. 401, pp. 273-294, 1931.

[68] W. Kaiser and C. Garrett, "Two-Photon Excitation in CaF_ {2}: Eu^{2+}," *Physical Review Letters,* vol. 7, p. 229, 1961.

[69] I. Abella, "Optical double-photon absorption in cesium vapor," *Physical Review Letters,* vol. 9, p. 453, 1962.

[70] R. Gauvin, Y.-C. Chen, J. W. Lee, P. Soman, P. Zorlutuna, J. W. Nichol, H. Bae, S. Chen, and A. Khademhosseini, "Microfabrication of complex porous tissue engineering scaffolds using 3D projection stereolithography," *Biomaterials,* vol. 33, pp. 3824-3834, 2012.

[71] P. Soman, P. H. Chung, A. P. Zhang, and S. Chen, "Digital Microfabrication of User-Defined 3D Microstructures in Cell-Laden Hydrogels," *Biotechnology and bioengineering,* 2013.

[72] P. Soman, D. Y. Fozdar, J. W. Lee, A. Phadke, S. Varghese, and S. Chen, "A three-dimensional polymer scaffolding material exhibiting a zero Poisson's ratio," *Soft Matter,* vol. 8, pp. 4946-4951, 2012.

[73] P. Soman, J. W. Lee, A. Phadke, S. Varghese, and S. Chen, "Spatial tuning of negative and positive Poisson's ratio in a multi-layer scaffold," *Acta Biomaterialia,* vol. 8, pp. 2587-2594, 2012.

[74] H. Lin, D. Zhang, P. G. Alexander, G. Yang, J. Tan, A. W.-M. Cheng, and R. S. Tuan, "Application of visible light-based projection stereolithography for live cell-scaffold fabrication with designed architecture," *Biomaterials,* 2012.

[75] F. P. Melchels, J. Feijen, and D. W. Grijpma, "A review on stereolithography and its applications in biomedical engineering," *Biomaterials,* vol. 31, pp. 6121-6130, 2010.

[76] A. P. Zhang, X. Qu, P. Soman, K. C. Hribar, J. W. Lee, S. Chen, and S. He, "Rapid fabrication of complex 3D extracellular microenvironments by dynamic optical projection stereolithography," *Advanced Materials,* vol. 24, pp. 4266-4270, 2012.

[77] R. K. Pirlo, D. Dean, D. R. Knapp, and B. Z. Gao, "Cell deposition system based on laser guidance," *Biotechnology journal,* vol. 1, pp. 1007-1013, 2006.

[78] A. Ovsianikov, M. Gruene, M. Pflaum, L. Koch, F. Maiorana, M. Wilhelmi, A. Haverich, and B. Chichkov, "Laser printing of cells into 3D scaffolds," *Biofabrication,* vol. 2, p. 014104, 2010.

[79] V. Chan, P. Zorlutuna, J. H. Jeong, H. Kong, and R. Bashir, "Three-dimensional photopatterning of hydrogels using stereolithography for long-term cell encapsulation," *Lab on a chip,* vol. 10, pp. 2062-2070, 2010.

[80] P. S. Kharkar, "Two-dimensional (2D) in silico models for absorption, distribution, metabolism, excretion and toxicity (ADME/T) in drug discovery," *Current topics in medicinal chemistry,* vol. 10, pp. 116-126, 2010.

[81] M. L. Yarmush and K. R. King, "Living-cell microarrays," *Annual review of biomedical engineering,* vol. 11, p. 235, 2009.

[82] L. Y. Wu, D. Di Carlo, and L. P. Lee, "Microfluidic self-assembly of tumor spheroids for anticancer drug discovery," *Biomedical microdevices,* vol. 10, pp. 197-202, 2008.

[83] E. Mercey, P. Obeïd, D. Glaise, M.-L. Calvo-Muñoz, C. Guguen-Guillouzo, and B. Fouqué, "The application of 3D micropatterning of agarose substrate for cell culture and< i> in situ</i> comet assays," *Biomaterials,* vol. 31, pp. 3156-3165, 2010.

[84] Y.-C. Tung, A. Y. Hsiao, S. G. Allen, Y.-s. Torisawa, M. Ho, and S. Takayama, "High-throughput 3D spheroid culture and drug testing using a 384 hanging drop array," *Analyst,* vol. 136, pp. 473-478, 2011.

[85] K. L. Brouwer and R. G. Thurman, "Isolated perfused liver," *Pharm Biotechnol,* vol. 8, pp. 161-92, 1996.

[86] A. W. Wolkoff, K. L. Johansen, and T. Goeser, "The isolated perfused rat liver: preparation and application," *Anal Biochem,* vol. 167, pp. 1-14, Nov 15 1987.

[87] C. Lerche-Langrand and H. J. Toutain, "Precision-cut liver slices: characteristics and use for in vitro pharmaco-toxicology," *Toxicology,* vol. 153, pp. 221-53, Nov 16 2000.

[88] G. Neupert, R. Glockner, and D. Muller, "Immunohistochemical localization of cytochrome P450 1A1 in precision-cut rat liver slices after in vitro exposure to beta-naphthoflavone," *Exp Toxicol Pathol,* vol. 50, pp. 514-8, Sep 1998.

[89] G. Neupert, R. Glöckner, and D. Müller, "Immunohistochemical localization of cytochrome P450 1A1 in precision-cut rat liver slices after< i> in vitro</i> exposure to β-naphthoflavone," *Experimental and Toxicologic Pathology,* vol. 50, pp. 514-518, 1998.

[90] D. Müller, R. Glöckner, M. Rost, and P. Steinmetzer, "Monooxygenation, cytochrome P450-mRNA expression and other functions in precision-cut rat liver slices," *Experimental and Toxicologic Pathology,* vol. 50, pp. 507-513, 1998.

[91] M. N. Berry, A. R. Grivell, M. B. Grivell, and J. W. Phillips, "Isolated hepatocytes--past, present and future," *Cell Biol Toxicol,* vol. 13, pp. 223-33, Jul 1997.

[92] M. Vore, Y. Liu, and T. C. Ganguly, "Isolated hepatocytes," *Pharm Biotechnol,* vol. 8, pp. 115-20, 1996.

[93] L. Liu, E. L. LeCluyse, J. Liu, and C. D. Klaassen, "Sulfotransferase gene expression in primary cultures of rat hepatocytes," *Biochemical pharmacology,* vol. 52, pp. 1621-1630, 1996.

[94] E. L. LeCluyse, P. L. Bullock, A. Parkinson, and J. H. Hochman, "Cultured rat hepatocytes," in *Models for assessing drug absorption and metabolism*, ed: Springer, 1996, pp. 121-159.

[95] R. Gebhardt, J. G. Hengstler, D. Muller, R. Glockner, P. Buenning, B. Laube, E. Schmelzer, M. Ullrich, D. Utesch, N. Hewitt, M. Ringel, B. R. Hilz, A. Bader, A. Langsch, T. Koose, H. J. Burger, J. Maas, and F. Oesch, "New hepatocyte in vitro systems for drug metabolism: metabolic capacity and recommendations for application in basic research and drug development, standard operation procedures," *Drug Metab Rev,* vol. 35, pp. 145-213, May-Aug 2003.

[96] J. B. Houston and D. J. Carlile, "Prediction of hepatic clearance from microsomes, hepatocytes, and liver slices," *Drug Metab Rev,* vol. 29, pp. 891-922, Nov 1997.

[97] A. D. Rodrigues and S. L. Wong, "Application of human liver microsomes in metabolism-based drug-drug interactions: in vitro-in vivo correlations and the Abbott Laboratories experience," *Adv Pharmacol,* vol. 43, pp. 65-101, 1997.

[98] N. Meropol, "Oral fluoropyrimidines in the treatment of colorectal cancer," *European Journal of Cancer,* vol. 34, pp. 1509-1513, 1998.

[99] H. Lee, S. M. Dellatore, W. M. Miller, and P. B. Messersmith, "Mussel-inspired surface chemistry for multifunctional coatings," *Science,* vol. 318, pp. 426-430, 2007.

[100] S. H. Ku and C. B. Park, "Human endothelial cell growth on mussel-inspired nanofiber scaffold for vascular tissue engineering," *Biomaterials,* vol. 31, pp. 9431-9437, 2010.

[101] S. H. Ku and C. B. Park, "Combined Effect of Mussel-Inspired Surface Modification and Topographical Cues on the Behavior of Skeletal Myoblasts," *Advanced healthcare materials,* vol. 2, pp. 1445-1450, 2013.

[102] W.-B. Tsai, W.-T. Chen, H.-W. Chien, W.-H. Kuo, and M.-J. Wang, "Poly (dopamine) coating of scaffolds for articular cartilage tissue engineering," *Acta Biomaterialia,* vol. 7, pp. 4187-4194, 2011.

[103] S. H. Ku, J. Ryu, S. K. Hong, H. Lee, and C. B. Park, "General functionalization route for cell adhesion on non-wetting surfaces," *Biomaterials,* vol. 31, pp. 2535-2541, 2010.

[104] M. d'Ischia, A. Napolitano, A. Pezzella, P. Meredith, and T. Sarna, "Chemical and Structural Diversity in Eumelanins: Unexplored Bio-Optoelectronic Materials," *Angewandte Chemie International Edition,* vol. 48, pp. 3914-3921, 2009.

[105] Q. Ye, F. Zhou, and W. Liu, "Bioinspired catecholic chemistry for surface modification," *Chemical Society Reviews,* vol. 40, pp. 4244-4258, 2011.

[106] H. Lee, N. F. Scherer, and P. B. Messersmith, "Single-molecule mechanics of mussel adhesion," *Proceedings of the National Academy of Sciences,* vol. 103, pp. 12999-13003, 2006.

[107] Y. Ding, M. Floren, and W. Tan, "Mussel-inspired polydopamine for bio-surface functionalization," *Biosurface and Biotribology,* vol. 2, pp. 121-136, 2016.

[108] J. H. Waite and X. Qin, "Polyphosphoprotein from the adhesive pads of Mytilus edulis," *Biochemistry,* vol. 40, pp. 2887-2893, 2001.

[109] A. Eftekhari, "Diffusion of electrolytes in solution under gravitational forces," *Chemical physics letters,* vol. 381, pp. 427-433, 2003.

[110] W. J. Archibald, "The process of diffusion in a centrifugal field of force," *Physical Review,* vol. 53, p. 746, 1938.

[111] T. Mashimo, "Self-consistent approach to the diffusion induced by a centrifugal field in condensed matter: Sedimentation," *Physical Review A,* vol. 38, p. 4149, 1988.

[112] R. Gorkin, J. Park, J. Siegrist, M. Amasia, B. S. Lee, J.-M. Park, J. Kim, H. Kim, M. Madou, and Y.-K. Cho, "Centrifugal microfluidics for biomedical applications," *Lab on a chip,* vol. 10, pp. 1758-1773, 2010.

[113] T. Kawai, N. Naruishi, H. Nagai, Y. Tanaka, Y. Hagihara, and Y. Yoshida, "Rotatable Reagent Cartridge for High-Performance Microvalve System on a Centrifugal Microfluidic Device," *Analytical chemistry,* vol. 85, pp. 6587-6592, 2013.

[114] M. Madou, J. Zoval, G. Jia, H. Kido, J. Kim, and N. Kim, "Lab on a CD," *Annu. Rev. Biomed. Eng.,* vol. 8, pp. 601-628, 2006.

[115] M. Tang, G. Wang, S.-K. Kong, and H.-P. Ho, "A review of biomedical centrifugal microfluidic platforms," *Micromachines,* vol. 7, p. 26, 2016.

[116] H. HINO, S. HASHIMOTO, and T. YASUDA, "Effect of Centrifugal Force on Cell Culture," in *Proc. 18th World Multi-Conference on Systemics Cybernetics and Informatics*, 2014, pp. 132-137.

[117] N. Thomas, A. Ocklind, I. Blikstad, S. Griffiths, M. Kenrick, H. Derand, G. Ekstrand, C. Ellström, A. Larsson, and P. Andersson, "Integrated cell based assays in microfabricated disposable CD devices," in *Micro Total Analysis Systems 2000*, 2000, pp. 249-252.

[118] H. Nagai, Y. Narita, M. Ohtaki, K. Saito, and S.-i. Wakida, "A single-bead analysis on a disk-shaped microfluidic device using an antigen-immobilized bead," *Analytical Sciences,* vol. 23, pp. 975-980, 2007.

[119] K. Wang, R. Liang, H. Chen, S. Lu, S. Jia, and W. Wang, "A microfluidic immunoassay system on a centrifugal platform," *Sensors and Actuators B: Chemical,* vol. 251, pp. 242-249, 2017.

[120] O. A. Zasedateleva, A. L. Mikheikin, A. Y. Turygin, D. V. Prokopenko, A. V. Chudinov, E. E. Belobritskaya, V. R. Chechetkin, and A. S. Zasedatelev, "Gel-based oligonucleotide microarray approach to analyze protein-ssDNA binding specificity," *Nucleic Acids Res,* vol. 36, p. e61, Jun 2008.

[121] H. Tanaka, M. Hanasaki, T. Isojima, H. Takeuchi, T. Shiroya, and H. Kawaguchi, "Enhancement of sensitivity of SPR protein microarray using a novel 3D protein immobilization," *Colloids Surf B Biointerfaces,* Jan 4 2009.

[122] D. I. Stimpson, S. M. Knepper, M. Shida, K. Obata, and H. Tajima, "Three-dimensional microarray platform applied to single nucleotide polymorphism analysis," *Biotechnol Bioeng,* vol. 87, pp. 99-103, Jul 5 2004.

[123] P. Angenendt, J. Glokler, Z. Konthur, H. Lehrach, and D. J. Cahill, "3D protein microarrays: performing multiplex immunoassays on a single chip," *Anal Chem,* vol. 75, pp. 4368-72, Sep 1 2003.

[124] J. Ziauddin and D. M. Sabatini, "Microarrays of cells expressing defined cDNAs," *Nature,* vol. 411, pp. 107-10, May 3 2001.

[125] J. J. Diaz-Mochon, G. Tourniaire, and M. Bradley, "Microarray platforms for enzymatic and cell-based assays," *Chem Soc Rev,* vol. 36, pp. 449-57, Mar 2007.

[126] S. E. How, B. Yingyongnarongkul, M. A. Fara, J. J. Diaz-Mochon, S. Mittoo, and M. Bradley, "Polyplexes and lipoplexes for mammalian gene delivery: from traditional to microarray screening," *Comb Chem High Throughput Screen,* vol. 7, pp. 423-30, Aug 2004.

[127] S. N. Bailey, D. M. Sabatini, and B. R. Stockwell, "Microarrays of small molecules embedded in biodegradable polymers for use in mammalian cell-based screens," *Proc Natl Acad Sci U S A,* vol. 101, pp. 16144-9, Nov 16 2004.

[128] D. G. Anderson, S. Levenberg, and R. Langer, "Nanoliter-scale synthesis of arrayed biomaterials and application to human embryonic stem cells," *Nat Biotechnol,* vol. 22, pp. 863-6, Jul 2004.

[129] P. T. Charles, E. R. Goldman, J. G. Rangasammy, C. L. Schauer, M. S. Chen, and C. R. Taitt, "Fabrication and characterization of 3D hydrogel microarrays to measure antigenicity and antibody functionality for biosensor applications," *Biosens Bioelectron,* vol. 20, pp. 753-64, Nov 1 2004.

[130] S. Duggal, K. B. Fronsdal, K. Szoke, A. Shahdadfar, J. E. Melvik, and J. E. Brinchmann, "Phenotype and Gene Expression of Human Mesenchymal Stem Cells in Alginate Scaffolds," *Tissue Eng Part A,* Dec 30 2008.

[131] S. Ghosh, G. C. Spagnoli, I. Martin, S. Ploegert, P. Demougin, M. Heberer, and A. Reschner, "Three-dimensional culture of melanoma cells profoundly affects gene expression profile: a high density oligonucleotide array study," *J Cell Physiol,* vol. 204, pp. 522-31, Aug 2005.

[132] M. Y. Lee, R. A. Kumar, S. M. Sukumaran, M. G. Hogg, D. S. Clark, and J. S. Dordick, "Three-dimensional cellular microarray for high-throughput toxicology assays," *Proc Natl Acad Sci U S A,* vol. 105, pp. 59-63, Jan 8 2008.

[133] M. Yliperttula, B. G. Chung, A. Navaladi, A. Manbachi, and A. Urtti, "High-throughput screening of cell responses to biomaterials," *Eur J Pharm Sci,* vol. 35, pp. 151-60, Oct 2 2008.

[134] K. Cheng, Y. Lai, and W. S. Kisaalita, "Three-dimensional polymer scaffolds for high throughput cell-based assay systems," *Biomaterials,* vol. 29, pp. 2802-12, Jun 2008.

[135] B. E. Chaignaud, R. Langer, and J. P. Vacanti, *The history of tissue engineering using synthetic biodegradable polymer scaffolds and cells*, 1997.

[136] A. G. Mikos and J. S. Temenoff, "Formation of highly porous biodegradable scaffolds for tissue engineering," *Electronic Journal of Biotechnology,* vol. 3, pp. 23-24, 2000.

[137] A. G. Mikos, Y. Bao, L. G. Cima, D. E. Ingber, J. P. Vacanti, and R. Langer, "Preparation of poly(glycolic acid) bonded fiber structures for cell attachment and transplantation," *Journal of Biomedical Materials Research,* vol. 27, pp. 183-189, 1993.

[138] A. G. Mikos, G. Sarakinos, S. M. Leite, J. P. Vacanti, and R. Langer, "Laminated three-dimensional biodegradable foams for use in tissue engineering," *Biomaterials,* vol. 14, pp. 323-330, 1993.

[139] A. G. Mikos, A. J. Thorsen, L. A. Czerwonka, Y. Bao, R. Langer, D. N. Winslow, and J. P. Vacanti, "Preparation and characterization of poly (L-lactic acid) foams," *Polymer,* vol. 35, pp. 1068-1077, 1994.

[140] V. P. Shastri, I. Martin, and R. Langer, "Macroporous polymer foams by hydrocarbon templating," *Proc Natl Acad Sci U S A,* vol. 97, pp. 1970-5, Feb 29 2000.

[141] H. Lo, S. Kadiyala, S. E. Guggino, and K. W. Leong, "Poly(L-lactic acid) foams with cell seeding and controlled-release capacity," *J Biomed Mater Res,* vol. 30, pp. 475-84, Apr 1996.

[142] H. Lo, M. S. Ponticiello, and K. W. Leong, "Fabrication of controlled release biodegradable foams by phase separation," *Tissue Eng,* vol. 1, p. 15, 1995.

[143] K. Whang, C. H. Thomas, K. E. Healy, and G. Nuber, "A novel method to fabricate bioabsorbable scaffolds," *Polymer,* vol. 36, pp. 837-842, 1995.

[144] L. D. Harris, B. S. Kim, and D. J. Mooney, "Open pore biodegradable matrices formed with gas foaming," *J Biomed Mater Res,* vol. 42, pp. 396-402, Dec 5 1998.

[145] D. J. Mooney, D. F. Baldwin, N. P. Suh, J. P. Vacanti, and R. Langer, "Novel approach to fabricate porous sponges of poly(D,L-lactic-co- glycolic acid) without the use of organic solvents," *Biomaterials,* vol. 17, pp. 1417-1422, 1996.

[146] Y. S. Nam, J. J. Yoon, and T. G. Park, "Novel fabrication method of macroporous biodegradable polymer scaffolds using gas foaming salt as a porogen additive," *Journal of Biomedical Materials Research,* vol. 53, pp. 1-7, 2000.

[147] T. G. Park, "New approaches to fabricate highly porous tissue scaffolds," *fourth Asia-Pacific Conference on Medical and Biological Engineering,* 1999.

[148] D. Sparacio and E. J. Beckman, "Generation of microcellular biodegradable polymers in supercritical carbon dioxide," Las Vegas, NV, USA, 1997, pp. 422-423.

[149] S. Das, S. F. Hollister, C. Flanagan, A. Adewunmi, K. Bark, C. Chen, K. Ramaswamy, D. Rose, and E. Widjaja, "Freeform fabrication of nylon-6 tissue engineering scaffolds," *Rapid Prototyping Journal,* vol. 9, pp. 43-49, 2003.

[150] Oncolink, *http://www.oncolink.com/resources/article.cfm?c=16&s=46&ss=205&id=923*.

[151] X. Wang, *Solvent-free fabrication of porous polymer for tissue engineering applications*, 2007.

[152] D. Garlotta, "A literature review of poly (lactic acid)," *Journal of Polymers and the Environment,* vol. 9, pp. 63-84, 2001.

[153] I. Armentano, M. Dottori, E. Fortunati, S. Mattioli, and J. Kenny, "Biodegradable polymer matrix nanocomposites for tissue engineering: a review," *Polymer degradation and stability,* vol. 95, pp. 2126-2146, 2010.

[154] C. A. Schneider, W. S. Rasband, and K. W. Eliceiri, "NIH Image to ImageJ: 25 years of image analysis," *Nat Methods,* vol. 9, pp. 671-675, 2012.

[155] J. Weissmüller, R. N. Viswanath, D. Kramer, P. Zimmer, R. Würschum, and H. Gleiter, "Charge-Induced Reversible Strain in a Metal," *Science,* vol. 300, pp. 312-315, 2003/04/11/ 2003.

[156] M. J. Karnovsky, "A formaldehyde-glutaraldehyde fixative of high osmolarity for use in electron microscopy," *J. cell Biol,* vol. 27, 1965.

[157] A. Svensson, E. Nicklasson, T. Harrah, B. Panilaitis, D. Kaplan, M. Brittberg, and P. Gatenholm, "Bacterial cellulose as a potential scaffold for tissue engineering of cartilage," *Biomaterials,* vol. 26, pp. 419-431, 2005.

[158] L. Ma, C. Zhou, B. Lin, and W. Li, "A porous 3D cell culture micro device for cell migration study," *Biomedical microdevices,* vol. 12, pp. 753-760, 2010.

[159] H. Tai, M. L. Mather, D. Howard, W. Wang, L. J. White, J. A. Crowe, S. P. Morgan, A. Chandra, D. J. Williams, and S. M. Howdle, "Control of pore size and structure of tissue engineering scaffolds produced by supercritical fluid processing," *Eur Cell Mater,* vol. 14, pp. 64-77, 2007.

[160] C. Zhou, L. Ma, W. Li, and D. Yao, "Fabrication of tissue engineering scaffolds through solid-state foaming of immiscible polymer blends," *Biofabrication,* vol. 3, p. 045003, 2011.

[161] S. S. Kim, H. Utsunomiya, J. A. Koski, B. M. Wu, M. J. Cima, J. Sohn, K. Mukai, L. G. Griffith, and J. P. Vacanti, "Survival and function of hepatocytes on a novel three-dimensional synthetic biodegradable polymer scaffold with an intrinsic network of channels," *Annals of surgery,* vol. 228, p. 8, 1998.

[162] Q. Lv, K. Hu, Q. Feng, F. Cui, and C. Cao, "Preparation and characterization of PLA/fibroin composite and culture of HepG2 (human hepatocellular liver carcinoma cell line) cells," *Composites Science and Technology,* vol. 67, pp. 3023-3030, 2007.

[163] N. A. Kotov, Y. Liu, S. Wang, C. Cumming, M. Eghtedari, G. Vargas, M. Motamedi, J. Nichols, and J. Cortiella, "Inverted colloidal crystals as three-dimensional cell scaffolds," *Langmuir,* vol. 20, pp. 7887-7892, 2004.

[164] H. Wang and W. Li, "Selective ultrasonic foaming of polymer for biomedical applications," *Journal of manufacturing science and engineering,* vol. 130, pp. 020601.1-024503.5, 2008.

[165] D. W. Hutmacher, "Biomaterials offer cancer research the third dimension," *Nature materials,* vol. 9, pp. 90-93, 2010.

[166] Y. Manome, S. Mizuno, N. Akiyama, K. Fujioka, H. Saito, Y. Hataba, T. Kobayashi, and M. Watanabe, "Three-dimensional cell culture of glioma and morphological comparison of four different human cell lines," *Anticancer research,* vol. 30, pp. 383-389, 2010.

[167] M. Erguven, A. Bilir, N. Yazihan, E. Ermis, A. Sabanci, E. Aktas, Y. Aras, and V. Alpman, "Decreased therapeutic effects of noscapine combined with imatinib mesylate on human glioblastoma in vitro and the effect of midkine," 2011.

[168] J. Ock, B. T. Philpott, and W. Li, "Fabrication of Three-Dimensional Tissue Scaffold Arrays Using Laser Foaming," in *ASME 2013 International Mechanical Engineering Congress and Exposition*, 2013, pp. V02BT02A005-V02BT02A005.

[169] J. Ock and W. Li, "Fabrication of a three-dimensional tissue model microarray using laser foaming of a gas-impregnated biodegradable polymer," *Biofabrication,* vol. 6, p. 024110, 2014.

[170] J. Ock and W. Li, "Selective Laser Foaming for Three-Dimensional Cell Culture on a Compact Disc," in *ASME 2015 International Manufacturing Science and Engineering Conference*, 2015, pp. V002T03A007-V002T03A007.

[171] M. Sealya, G. Madireddya, C. Lib, and Y. Guob, "FINITE ELEMENT MODELING OF HYBRID ADDITIVE MANUFACTURING BY LASER SHOCK PEENING."

[172] J. Cheng and Y. L. Yao, "Process design of laser forming for three-dimensional thin plates," *TRANSACTIONS-AMERICAN SOCIETY OF MECHANICAL ENGINEERS JOURNAL OF MANUFACTURING SCIENCE AND ENGINEERING,* vol. 126, pp. 217-225, 2004.

[173] G. Satoh, C. Qiu, S. Naveed, and Y. L. Yao, "Strength and Phase Identification of Autogenous Laser Brazed Dissimilar Metal Microjoints," *Journal of Manufacturing Science and Engineering,* vol. 137, p. 011012, 2015.

[174] S. W. Churchill and H. H. Chu, "Correlating equations for laminar and turbulent free convection from a vertical plate," *International journal of heat and mass transfer,* vol. 18, pp. 1323-1329, 1975.

[175] M. Jamshidinia, F. Kong, and R. Kovacevic, "Numerical modeling of heat distribution in the electron beam melting® of Ti-6Al-4V," *Journal of Manufacturing Science and Engineering,* vol. 135, p. 061010, 2013.

[176] M. Lax, "Temperature rise induced by a laser beam," *Journal of applied physics,* vol. 48, pp. 3919-3924, 1977.

[177] S. Nisar, M. Sheikh, L. Li, A. J. Pinkerton, and S. Safdar, "The effect of laser beam geometry on cut path deviation in diode laser chip-free cutting of glass," *Journal of Manufacturing Science and Engineering,* vol. 132, p. 011002, 2010.

[178] M. Pyda, R. Bopp, and B. Wunderlich, "Heat capacity of poly (lactic acid)," *The Journal of Chemical Thermodynamics,* vol. 36, pp. 731-742, 2004.

[179] J. Radice, P. Joyce, A. Tresansky, and R. Watkins, "A comsol model of damage evolution due to high energy laser irradiation of partially absorptive materials," in *Excerpts from the Proceedings of the 2012 COMSOL Conference in Boston*, 2012.

[180] D. Groulx and W. Ogoh, "Solid-liquid phase change simulation applied to a cylindrical latent heat energy storage system," in *COMSOL Conference 2009*, 2009.

[181] R. M. Stephenson, *Handbook of the thermodynamics of organic compounds*: Springer Science & Business Media, 2012.

[182] X. Wang, V. Kumar, and W. Li, "Low density sub-critical CO2-blown solid-state PLA foams," *Cellular polymers,* vol. 26, pp. 11-35, 2007.

[183] X. Wang, V. Kumar, and W. Li, "Development of Crystallization in PLA During Solid-State Foaming Process Using Sub-Critical CO," *Cellular polymers,* vol. 31, pp. 1-18, 2012.

[184] M. Agarwal, K. W. Koelling, and J. J. Chalmers, "Characterization of the degradation of polylactic acid polymer in a solid substrate environment," *Biotechnology progress,* vol. 14, pp. 517-526, 1998.

[185] N. C. Nayak, Y. Lam, C. Yue, and A. T. Sinha, "CO2-laser micromachining of PMMA: the effect of polymer molecular weight," *Journal of Micromechanics and Microengineering,* vol. 18, p. 095020, 2008.

[186] J. Küblbeck, M. Reinisalo, R. Mustonen, and P. Honkakoski, "Up-regulation of CYP expression in hepatoma cells stably transfected by chimeric nuclear receptors," *european journal of pharmaceutical sciences,* vol. 40, pp. 263-272, 2010.

[187] J. H. Cho, R. Katsumata, S. X. Zhou, C. B. Kim, A. R. Dulaney, D. W. Janes, and C. J. Ellison, "Ultrasmooth Polydopamine Modified Surfaces for Block Copolymer Nanopatterning on Flexible Substrates," *ACS applied materials & interfaces,* vol. 8, pp. 7456-7463, 2016.

[188] H. Wang and W. Li, "Selective Ultrasonic Foaming of Polymer for Biomedical Applications," *Journal of Manufacturing Science and Engineering,* vol. 130, pp. 021004-021004, 2008.

[189] É. Said-Galiev and L. Nikitin, "Ablation of polymers and composites when exposed to CO2 laser radiation (review)," *Mechanics of composite materials,* vol. 28, pp. 97-114, 1992.

[190] A. Krasovskii and E. Tolstopyatov, "Use of Laser Radiation for the Formation of Polymer Films in Vacuum on the Solid Surface," ed: Poverkhnost, 1985.

[191] S. H. Oh, I. K. Park, J. M. Kim, and J. H. Lee, "In vitro and in vivo characteristics of PCL scaffolds with pore size gradient fabricated by a centrifugation method," *Biomaterials,* vol. 28, pp. 1664-1671, 2007.

[192] S. Yang, K.-F. Leong, Z. Du, and C.-K. Chua, "The design of scaffolds for use in tissue engineering. Part I. Traditional factors," *Tissue engineering,* vol. 7, pp. 679-689, 2001.

[193] C. Danielsson, S. Ruault, M. Simonet, P. Neuenschwander, and P. Frey, "Polyesterurethane foam scaffold for smooth muscle cell tissue engineering," *Biomaterials,* vol. 27, pp. 1410-1415, 2006.

[194] I. SCHWARTZ, B. P. ROBINSON, J. O. HOLLINGER, E. H. SZACHOWICZ, and J. BREKKE, "Calvarial bone repair with porous D, L-polylactide," *Otolaryngology-Head and Neck Surgery,* vol. 112, pp. 707-713, 1995.

[195] L. D. Zardiackas, D. E. Parsell, L. D. Dillon, D. W. Mitchell, L. A. Nunnery, and R. Poggie, "Structure, metallurgy, and mechanical properties of a porous tantalum foam," *Journal of biomedical materials research,* vol. 58, pp. 180-187, 2001.

[196] J. Bobyn, G. Stackpool, S. Hacking, M. Tanzer, and J. Krygier, "Characteristics of bone ingrowth and interface mechanics of a new porous tantalum biomaterial," *Journal of Bone & Joint Surgery, British Volume,* vol. 81, pp. 907-914, 1999.

[197] C.-T. Kao, C.-C. Lin, Y.-W. Chen, C.-H. Yeh, H.-Y. Fang, and M.-Y. Shie, "Poly (dopamine) coating of 3D printed poly (lactic acid) scaffolds for bone tissue engineering," *Materials Science and Engineering: C,* vol. 56, pp. 165-173, 2015.

[198] J. Yan, L. Yang, M. F. Lin, J. Ma, X. Lu, and P. S. Lee, "Polydopamine spheres as active templates for convenient synthesis of various nanostructures," *Small,* vol. 9, pp. 596-603, 2013.

[199] C. Wu, P. Han, X. Liu, M. Xu, T. Tian, J. Chang, and Y. Xiao, "Mussel-inspired bioceramics with self-assembled Ca-P/polydopamine composite nanolayer: preparation, formation mechanism, improved cellular bioactivity and osteogenic differentiation of bone marrow stromal cells," *Acta Biomaterialia,* vol. 10, pp. 428-438, 2014.

[200] X. Shi, L. Li, S. Ostrovidov, Y. Shu, A. Khademhosseini, and H. Wu, "Stretchable and micropatterned membrane for osteogenic differentation of stem cells," *ACS applied materials & interfaces,* vol. 6, pp. 11915-11923, 2014.

[201] S.-W. Lee, J. Y. Kang, I.-H. Lee, S.-S. Ryu, S.-M. Kwak, K.-S. Shin, C. Kim, H.-I. Jung, and T.-S. Kim, "Single-cell assay on CD-like lab chip using centrifugal massive single-cell trap," *Sensors and Actuators A: Physical,* vol. 143, pp. 64-69, 2008.

[202] N. Krasteva, B. Seifert, W. Albrecht, T. Weigel, M. Schossig, G. Altankov, and T. Groth, "Influence of polymer membrane porosity on C3A hepatoblastoma cell adhesive interaction and function," *Biomaterials,* vol. 25, pp. 2467-2476, 2004.

[203] M. Ravi, V. Paramesh, S. Kaviya, E. Anuradha, and F. Solomon, "3D cell culture systems: advantages and applications," *Journal of cellular physiology,* vol. 230, pp. 16-26, 2015.

[204] E. Millerot-Serrurot, M. Guilbert, N. Fourré, W. Witkowski, G. Said, L. Van Gulick, C. Terryn, J.-M. Zahm, R. Garnotel, and P. Jeannesson, "3D collagen type I matrix inhibits the antimigratory effect of doxorubicin," *Cancer Cell International,* vol. 10, p. 26, 2010.

[205] D. Loessner, K. S. Stok, M. P. Lutolf, D. W. Hutmacher, J. A. Clements, and S. C. Rizzi, "Bioengineered 3D platform to explore cell–ECM interactions and drug resistance of epithelial ovarian cancer cells," *Biomaterials,* vol. 31, pp. 8494-8506, 2010.

[206] S. Ekins, B. J. Ring, J. Grace, D. J. McRobie-Belle, and S. A. Wrighton, "Present and future in vitro approaches for drug metabolism," *Journal of pharmacological and toxicological methods,* vol. 44, pp. 313-324, 2000.

[207] J. M. Lehmann, D. D. McKee, M. A. Watson, T. M. Willson, J. T. Moore, and S. A. Kliewer, "The human orphan nuclear receptor PXR is activated by compounds that regulate CYP3A4 gene expression and cause drug interactions," *Journal of Clinical Investigation,* vol. 102, p. 1016, 1998.

[208] C. P. Martínez-Jiménez, R. Jover, M. Teresa Donato, J. V. Castell, and M. Jose Gomez-Lechon, "Transcriptional regulation and expression of CYP3A4 in hepatocytes," *Current drug metabolism,* vol. 8, pp. 185-194, 2007.

[209] H. Wang and W. Li, "A Concentration-Dependent Diffusion Model for Selective Ultrasonic Foaming," *ASME Conference Proceedings,* vol. 2007, pp. 689-695, 2007.

[210] I. Tsivintzelis, A. G. Angelopoulou, and C. Panayiotou, "Foaming of polymers with supercritical CO< sub> 2</sub>: An experimental and theoretical study," *Polymer,* vol. 48, pp. 5928-5939, 2007.

[211] L. J. Jacobs, M. F. Kemmere, and J. T. Keurentjes, "Sustainable polymer foaming using high pressure carbon dioxide: a review on fundamentals, processes and applications," *Green Chemistry,* vol. 10, pp. 731-738, 2008.

[212] J. S. Colton and N. P. Suh, "Nucleation of microcellular foam: theory and practice," *Polymer Engineering & Science,* vol. 27, pp. 500-503, 1987.

[213] H. E. Naguib, C. B. Park, and N. Reichelt, "Fundamental foaming mechanisms governing the volume expansion of extruded polypropylene foams," *Journal of applied polymer science,* vol. 91, pp. 2661-2668, 2004.